

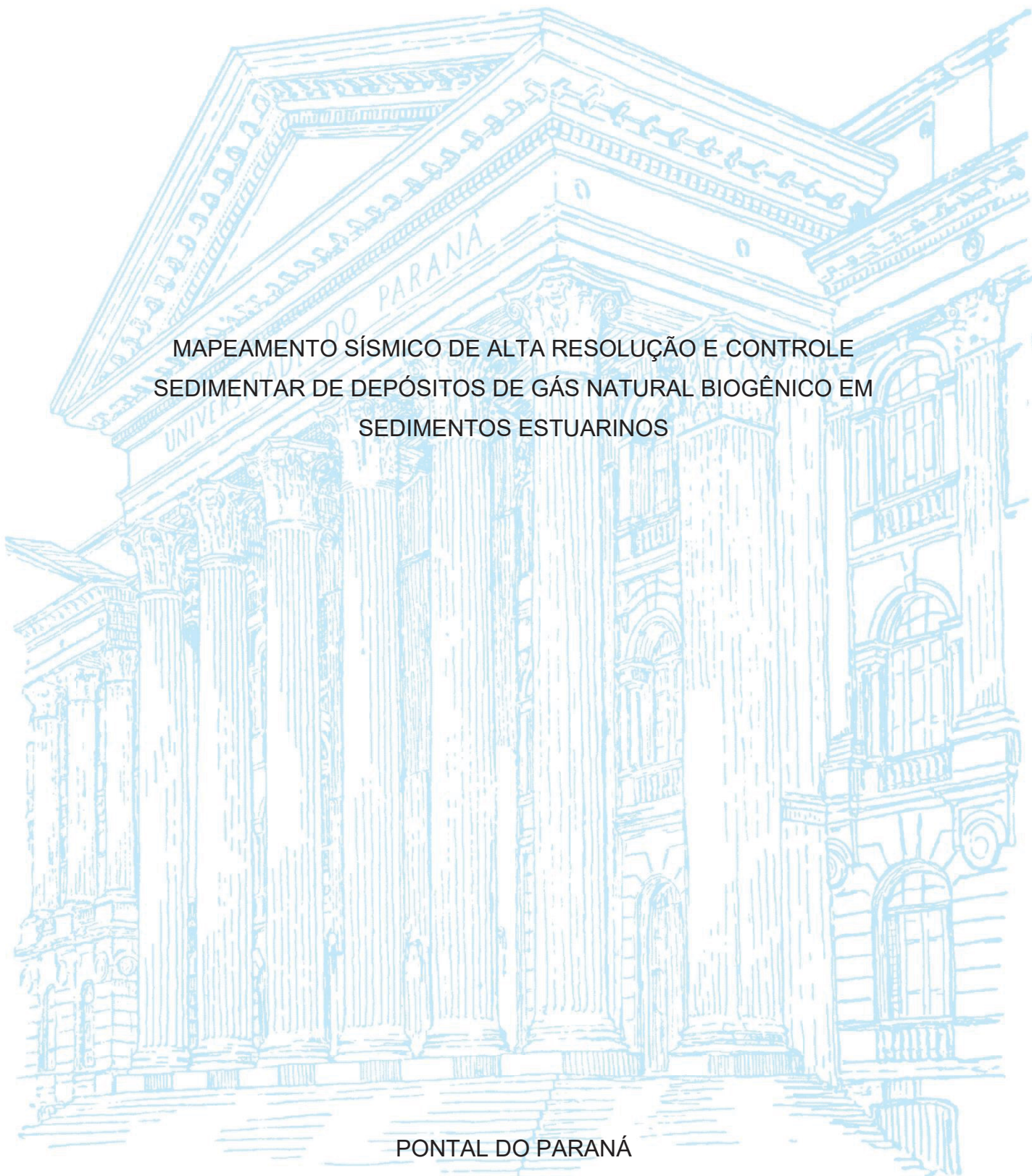
UNIVERSIDADE FEDERAL DO PARANÁ

JOÃO FERNANDO PEZZA ANDRADE

MAPEAMENTO SÍSMICO DE ALTA RESOLUÇÃO E CONTROLE
SEDIMENTAR DE DEPÓSITOS DE GÁS NATURAL BIOGÊNICO EM
SEDIMENTOS ESTUARINOS

PONTAL DO PARANÁ

2023



JOÃO FERNANDO PEZZA ANDRADE

MAPEAMENTO SÍSMICO DE ALTA RESOLUÇÃO E CONTROLE
SEDIMENTAR DE DEPÓSITOS DE GÁS NATURAL BIOGÊNICO EM
SEDIMENTOS ESTUARINOS

Tese apresentada ao curso de Pós-Graduação em Sistemas Costeiros e Oceânicos, Campus Pontal do Paraná – Setor de Estudos do Mar, Universidade Federal do Paraná, como requisito parcial à obtenção do título de Doutor em Sistemas Costeiros e Oceânicos.

Orientadora: Profa. Dra. Renata Hanae Nagai.

Coorientador: Prof. Dr. Maurício Almeida Noernberg.

PONTAL DO PARANÁ

2023

DADOS INTERNACIONAIS DE CATALOGAÇÃO NA PUBLICAÇÃO (CIP)
UNIVERSIDADE FEDERAL DO PARANÁ
SISTEMA DE BIBLIOTECAS – BIBLIOTECA DE CIÊNCIA E TECNOLOGIA

Andrade, João Fernando Pezza

Mapeamento sísmico de alta resolução e controle sedimentar de depósitos de gás natural biogênico em sedimentos estuarinos / João Fernando Pezza Andrade. – Curitiba, 2023.

1 recurso on-line : PDF.

Tese (Doutorado) - Universidade Federal do Paraná, Setor Centro de Estudos do Mar, Programa de Pós-Graduação em Sistemas Costeiros e Oceânicos.

Orientadora: Renata Hanae Nagai

Coorientador: Maurício Almeida Noernberg

1. Metano. 2. Complexo Estuarino - Lagunar de Iguape - Pranguá. I. Universidade Federal do Paraná. II. Programa de Pós-Graduação em Sistemas Costeiros e Oceânicos. III. Nagai, Renata Hanae. IV. Noernberg, Maurício Almeida. V. Título.

Bibliotecário: Leticia Priscila Azevedo de Sousa CRB-9/2029



MINISTÉRIO DA EDUCAÇÃO
REITORIA
UNIVERSIDADE FEDERAL DO PARANÁ
PRÓ-REITORIA DE PESQUISA E PÓS-GRADUAÇÃO
PROGRAMA DE PÓS-GRADUAÇÃO SISTEMAS COSTEIROS
E OCEÂNICOS - 40001016054P6

TERMO DE APROVAÇÃO

Os membros da Banca Examinadora designada pelo Colegiado do Programa de Pós-Graduação SISTEMAS COSTEIROS E OCEÂNICOS da Universidade Federal do Paraná foram convocados para realizar a arguição da tese de Doutorado de **JOÃO FERNANDO PEZZA ANDRADE** intitulada: **Mapeamento sísmico de alta resolução e controle sedimentar de depósitos de gás natural biogênico em sedimentos estuarinos**, sob orientação da Profa. Dra. RENATA HANAE NAGAI, que após terem inquirido o aluno e realizada a avaliação do trabalho, são de parecer pela sua APROVAÇÃO no rito de defesa.

A outorga do título de doutor está sujeita à homologação pelo colegiado, ao atendimento de todas as indicações e correções solicitadas pela banca e ao pleno atendimento das demandas regimentais do Programa de Pós-Graduação.

Pontal do Paraná, 31 de Março de 2023.

Assinatura Eletrônica
31/03/2023 11:39:34.0
RENATA HANAE NAGAI
Presidente da Banca Examinadora

Assinatura Eletrônica
31/03/2023 11:46:43.0
ANTONIO HENRIQUE DA FONTOURA KLEIN
Avaliador Externo (UNIVERSIDADE FEDERAL DE SANTA CATARINA)

Assinatura Eletrônica
20/04/2023 23:13:08.0
ARTHUR AYRES NETO
Avaliador Externo (UNIVERSIDADE FEDERAL FLUMINENSE)

Assinatura Eletrônica
01/04/2023 18:01:37.0
HUMBERTO MAROTTA RIBEIRO
Avaliador Externo (55003236)

AGRADECIMENTOS

Agradeço à minha orientadora Prof^a. Dr^a. Renata Hanae Nagai pela amizade, por todo o suporte intelectual e pelos importantes conselhos e ensinamentos. Agradeço também o Prof. Dr. Till Hanebuth pela amizade e por me acolher em sua casa e por todos os outros inúmeros suportes que me providenciou nos EUA.

Agradeço ao INPE, em especial ao Dr. Plinio Alvalá e ao MSc. Willian Ferreira do Laboratório de Pesquisa em Biogeoquímica Ambiental (LAPBio) pelo suporte e ajuda nas análises de amostras de gás. Agradeço também à equipe do LabPaleo² pela amizade e ajuda no campo e nas análises das amostras. Agradeço ao prof. Dr. Luiz Carlos Cotovicz Junior pelo suporte intelectual no Cap. III. Agradeço ao meu coorientador Prof. Dr. Mauricio Noernberg.

Agradeço minha família e amigos.

Agradeço à Coordenação de Aperfeiçoamento de Pessoal de Nível Superior - Brasil (CAPES) - Código de Financiamento 001 pela bolsa durante o doutorado, ao Conselho Nacional de Desenvolvimento Científico e Tecnológico (CNPQ) pelo suporte financeiro através do projeto “Panorama Histórico e Perspectivas Futuras Frente à Ocorrência de Estressores Químicos Presentes no Complexo Estuarino de Paranaguá (EQCEP) Edital MCTIC/CNPq 21/2017 (processo n ° 441265/2017-0), e ao programa CAPES-PRINT pela bolsa e oportunidade de estudar nos EUA (processo 88887.571227/2020-00).

*"Our passion for learning is our
tool for survival."*

Carl Sagan

RESUMO

O gás metano é um dos principais gases do efeito estufa, porém suas fontes e sumidouros ainda não são totalmente compreendidas. Entre elas os sistemas estuarinos se destacam pois são locais de deposição de uma grande quantidade de matéria orgânica vindo dos continentes a qual é degradada por microrganismos formando, em última instância, o metano. O trabalho tem como objetivo o gás metano presente nos sedimentos estuarinos. Dois sistemas foram estudados: O Complexo Estuarino de Paranaguá (CEP) – Paraná / Brasil – e o Delta Santee (DS) – Carolina do Sul / EUA. Dados de sísmica de alta resolução foram utilizados para mapear a presença de bolhas de metano presentes nos sedimentos desses ambientes devido seu alto contraste de impedância acústica e reverberação do sinal acústico. Os dados acústicos foram utilizados também para entender a dinâmica do gás dentro da coluna sedimentar através de reconhecimento de diferentes tipos de assinaturas sísmicas do gás. Os resultados mostraram que o acúmulo de gás é dinâmico dentro da coluna sedimentar na qual é possível reconhecer estruturas de migração. Amostras sedimentares foram coletadas em ambos os ambientes, sendo que no CEP as amostras são limitadas a superfície enquanto no SD foram adquiridos testemunhos sedimentares que alcançaram, e em alguns casos ultrapassaram, os acúmulos de gás na coluna sedimentar. Análises granulométricas e de matéria orgânica foram realizadas para caracterização sedimentar da região com e sem presença de bolhas. No DS foram realizadas a descrição dos testemunhos e cálculo de porosidade. Os dados indicaram que as facies sedimentares, em especial as facies reconhecidas por unidades sísmicas, não são suficientes para explicar a variação espacial do gás nos estratos sedimentares, tendo em vista que as propriedades sedimentares medidas aqui não apresentam diferença significativa entre as regiões com e sem gás. O trabalho investiga também a influência dos acúmulos de gás raso na quantidade de metano dissolvido na água e seu fluxo para a atmosfera. Amostras de água superficial e de fundo, bem como amostra de ar atmosférico e de fluxo, foram adquiridos no CEP. Os dados indicaram que não existe uma diferença significativa de concentração de metano entre as regiões com e sem acúmulo de gás metano. Os resultados indicaram também que o CEP possui pouco metano dissolvido e é um estuário de baixo índice de emissão de metano.

Palavras-chave: Gás metano, gás raso em sedimentos, sistemas estuarinos, Complexo Estuarino de Paranaguá, Delta Santee.

ABSTRACT

Methane gas is one of the main greenhouse gases, but its sources and sinks are still not fully understood. In this context, estuarine systems stand out because they are places of deposition of a large amount of organic matter coming from the continents, which is degraded by microorganisms, ultimately forming methane. The work aims to investigate methane gas present in estuarine sediments. Two systems were studied: the Paranaguá Estuarine Complex (PEC) - Paraná/Brazil - and the Santee Delta (SD) - South Carolina/USA. High-resolution seismic data were used to map the presence of methane bubbles in the sediments of these environments due to their high contrast of acoustic impedance and acoustic signal reverberation. Acoustic data were also used to understand the gas dynamics within the sedimentary column through recognition of different types of seismic signatures of the gas. The results showed that the gas accumulation is dynamic within the sedimentary column in which it is possible to recognize migration structures. Sedimentary samples were collected in both environments, in the PEC the samples are limited to the surface while in the SD were acquired sedimentary cores that reached, and in some cases surpassed, the gas accumulations in the sedimentary column. Granulometric and organic matter analyzes were performed to characterize the sedimentary region with and without the presence of bubbles. In the SD, the description of the cores and porosity calculation were performed. The data indicated that the sedimentary facies, especially the facies recognized by seismic units, are not sufficient to explain the spatial variation of the gas in the strata, considering that the sedimentary properties measured here show little or no variation between the regions with and without gas. The work also investigates the influence of shallow gas accumulations on the amount of methane dissolved in water and its flow into the atmosphere. Surface and bottom water samples, as well as atmospheric and flow samples, were acquired at the PEC. The data indicated that there is no significant difference in methane concentration between regions with and without methane gas accumulation. The results also indicated that CEP has small amounts of dissolved methane and is an estuary with low methane emission.

Keywords: Methane gas, gas-charged sediments, estuarine systems, Paranaguá Estuarine Complex, Santee Delta.

RESUMO EM LINGUAGEM ACESSÍVEL

O metano é um gás importante para o clima do nosso planeta, sendo ele um dos principais gases que geram o aquecimento global. Porém, ainda não compreendemos completamente como é sua dinâmica ao redor do globo. Esse trabalho investiga o metano que é formado na lama do fundo dos estuários. Dois estuários foram estudados: O Complexo Estuarino de Paranaguá (CEP), no Paraná – Brasil, e o Delta Santee (DS), na Carolina do Sul – EUA. Para mapear o gás metano foi utilizado ondas de som que refletem nas bolhas de gás presas na lama. O resultado do mapeamento mostrou diferentes formatos desses depósitos de gás no CEP indicando que ele é dinâmico, se movimentando em alguns locais e preso em outros. Amostras da lama também foram coletadas nas regiões com e sem o gás. Os resultados indicaram que não existe uma diferença significativa entre essas amostras. O trabalho investigou também a influência desses depósitos de bolhas na quantidade de metano dissolvido na água e seu escape para a atmosfera. Para isso foram coletadas amostras de água e de ar, além de usar câmaras flutuantes para medir as emissões de metano. Os resultados indicaram que a quantidade de metano na água e sua emissão para a atmosfera não parece estar correlacionada com esses depósitos de bolhas. Os dados indicaram também que o CEP é um estuário com baixa quantidade de metano na água e baixa emissão para a atmosfera.

Highlights:

- Gás metano biogênico formado nos sedimentos de estuários
- Geração, migração e acúmulo de gás metano em sedimentos inconsolidados
- Acúmulo e decomposição de matéria orgânica em estuários
- Gás metano no Complexo Estuarino de Paranaguá

LISTA DE FIGURAS

CAPÍTULO I

- Fig. 1: The Paranaguá Estuarine Complex bathymetric map, and Pleistocene evolution, with the position of the seismic lines analyzed in this study.....23
- Fig. 2: Intrasedimentary gas seismic signatures observed in the Paranaguá Estuarine Complex classified with a 2-9 kHz CHIRP source and their acoustic characteristic. The scale of all images is 5 m x 100 m.....26
- Fig. 3: Location map of the different intrasedimentary gas seismic signatures observed in the Paranaguá Estuarine Complex (seismic data acquisition lines in black) and surficial sediment (0 – 3 cm) mud content (silt + clay) distributions. Black contour in color lines indicate gas presence under less than 1.5 m of sediment cover. Near distance analysis graphic represents the closest distance between shallow gas accumulation (< 1.5 m), comprising the BS and portions of the ABS and ABD marked by the black contour.....27
- Fig. 4: Chirp (2-9 kHz) seismic profiles in the Paranaguá zone (P1, P2, P3; see Fig. I.1 for location) showing gas accumulation seismic signatures (TP, BS, ABS, ABD) and the two seismic units (SU1, SU2) separated by a regional reflector (RH). Detailed zoom images (a, b, c with 10 x 500m scale) indicate a gas accumulation baseline change, paleochannel (Ch), and downlap termination. TP - Turbidity pinnacles; BS - Black shadow; ABS - Acoustic blanking with a sharp top; ABD - Acoustic blanking with diffuse top.....29
- Fig. 5: Chirp (2-9 kHz) seismic profiles in the Antonina zone (A1, A2; see Fig. I.1 for location) showing gas accumulation seismic signatures (BS, ABD) and the two seismic units (SU1, SU2) separated by a regional reflector (RH). Detailed zoom image indicates a stratigraphic window with a shallow basement. BS - Black shadow; ABD - Acoustic blanking with diffuse top.....30
- Fig. 6: Evolution model of shallow gas migration and accumulation, showing the changes between seismic gas signatures and their relationship with the relative permeability between sedimentary layers. The gas migrates from the source as turbidity pinnacles (a); the pinnacles head encounter a low permeability layer and start to accumulate (b); the gas accumulates forming an acoustic blanking with a sharp top (c); eventually, the gas seeps to the low permeability layer forming pinnacles (d); again the heads of pinnacles encounter a sealing layer, and de gas start to accumulate (e); this time the sealing layer has low trapping efficiency and thus the gas slowly seeps when it accumulates forming an acoustic blanking with diffuse top signature (f); heterogeneities in the sealing layer permits turbidity pinnacles locally formation (g); the pinnacles reach the sediment-water interface and can accumulate as a black shadow or seeps to the water column (h); finally, the gas slowly seeps from the black shadow to the water column (i). Note that the model above has only two sedimentary layers for didactic means. In the PEC the amount of layers capable of retaining the gas, and their relative permeability, varies locally.....36
- Fig. 7: PEC sedimentary facies evolution (based on Lessa et al. 1998) and the gas-charged sediments recognized in this work.....39

CAPÍTULO II

- Fig. 1: The Santee River Delta with the two study areas: The North Santee Bay and the Alligator Creek. Black lines indicate the seismo-acoustic survey coverage.....46
- Fig. 2: The North Santee Bay study area. a) Location of the sub-bottom echosounder lines (black lines), core sites (blue dots), and gas-charged deposits (red lines); b) A closer view on the most extensive gas zone at the southern margin of the bay chosen for the NSB1 and NSB2 core sites; c) Echosounder profile with gas signatures and cores; d) A closer view on the gas signature and cores position.....48
- Fig. 3: North Santee Bay sediment cores (a) NSB1 and (b) NSB2 showing the free-gas bubbles detected through the transparent PVC pipes and separated in three sizes; Organic matter content (TOC) in percentage (%); Porosity in percentage (%); Mean grain size (μm); Clay-silt-sand contents.....50
- Fig. 4: The Alligator Creek study area. a) Location of the sub-bottom echosounder lines (black lines), sediment core sites (blue dots), and gas-charged deposits (red lines); b) A closer view on the stratigraphy window chosen for Core AC2 and nearby gas zone chosen for Cores AC1 and AC3; c) Sub-bottom profile with gas signatures and core sites; d) A closer view on the gas signature and cores locations.....53
- Fig. 5: Alligator Creek sediment cores (a) AC12, (b) AC2, and (c) AC3 showing the gas bubbles recognized in the cores through the transparent PVC pipes and separated in three sizes; Organic matter content (TOC) in percentage (%); Porosity in percentage (%); Mean grain size (μm) Clay-silt-sand content.....55
- Fig. 6: Correlation of Total Organic Carbon (TOC) and Dry Bulk Density of the lithologic units (color bar, top to bottom colors represent units sequence) retrieved in the sedimentary cores.....59

CAPÍTULO III

- Fig. 1: Map of the Paranaguá Estuarine Complex (PEC) with the sampling sites and the seismic lines interpreted for the presence of gas (based on Pezza Andrade et al., 2021). Mean grain size distribution from Paladino et. al., 2022.....66
- Fig. 2: Sampling sites temperature ($^{\circ}\text{C}$) and salinity vertical profiles during the sampling campaign (September 27 and 28, 2021 from 9 am to 3 pm).....72
- Fig. 3: Comparison between CH_4 water-atmosphere flux of this study and diverse estuaries in Europe (Upstill-Goddard and Barnes, 2016), Australia (Rosentreter et al., 2018), and India (Rao and Sarma, 2016).....75
- Fig. 4: Comparison between CH_4 water-atmosphere flux of this study and diverse estuaries in Europe (Upstill-Goddard and Barnes, 2016), Australia (Rosentreter et al., 2018), and India (Rao and Sarma, 2016).....81

LISTA DE TABELAS

CAPÍTULO II

Tab. 1: Studied sediment cores (ID; see Fig. xx 2 and 4 for core sites), geographic coordinates, water depth, sediment recovery, shallower depth of bubble occurrence and depth of gas signature in the seismic data.....49

Tab. 2: P values of the Mann-Whitney comparison of porosity, TOC, clay, silt, and sand contents between core sections with and without bubbles presence. Significant differences occur when $p < 0.05$ (bold values).....52

CAPÍTULO III

Tab. 1: PEC's near-surface and near-bottom water dissolved oxygen concentration (DO, mg/L), and surface sediments (0-3 cm) gran size (sand, silt, and clay percentages), organic matter content (OMC), and calcium carbonate (CaCO₃) content.....71

Tab. 2: Seismic gas signatures interpretations, average concentrations (\pm SD) of dissolved CH₄, average water-atmosphere fluxes calculated and with floating chambers (\pm SD) with minimum and maximum values. Sites with no floating chamber samples (NS) or with no validated results (NR) are indicated.....73

Tab. 3: Comparison between CH₄ concentrations, physical and chemical variables of the water and sediments measured near-surface (ns) and near-bottom (nb) in the sites within and without BS zones in the Paranaguá Estuarine Complex. Analysis of variance (ANOVA) were used for comparison of normal distribution data and Kruskal-Wallis test for comparison between data that fail in normality test.....74

Tab. 4: Pearson correlation matrix for near-surface (ns) and near-bottom (nb) dissolved CH₄ concentrations, and physical and chemical variables of the water and sediments measured in the Paranaguá Estuarine Complex.....76

LISTA DE ABREVIATURAS E SIGLAS

ABD – Acoustic blanking with diffuse top

ABS – Acoustic blanking with sharp top

AC – Alligator Creek

AOM – Anaerobic oxidation of methane

BS – Black Shadow

CEP – Complexo Estuarino de Paranaguá

CH₄ – Metano

DO – Dissolved Oxigene

DS – Delta Santee

MTZ – Maximum turbidity zone

NSB – North Santee Bay

OMC – Organic matter content

PEC – Paranaguá Estuarine Complex

SD – Santee Delta

SU – Seismic unit

TOC – Total carbon content

TP – Turbidity pinnacle

SUMÁRIO

INTRODUÇÃO	15
OBJETIVO E HIPOTHESES	17
DELINEAMENTO DA TESE	17
CAPÍTULO I – Shallow gas high-resolution seismic signatures in a subtropical estuary	19
Introduction.....	20
Settings.....	21
Materials and method.....	23
Results.....	24
Discussion.....	30
Conclusion.....	39
CAPÍTULO II - Distribution and sedimentary control of shallow gas accumulation in the Santee River Delta marsh (South Carolina, U.S.A.)	41
Introduction.....	42
Settings.....	44
Materials and method.....	46
Results.....	48
Discussion.....	56
Conclusion.....	60
CAPÍTULO III - Influence of sedimentary shallow gas on methane concentrations and emissions in a subtropical estuary	62
Introduction	63
Settings.....	65
Method.....	67
Results.....	70
Discussion.....	76

Conclusion.....	83
CONSIDERAÇÕES FINAIS.....	84
REFERENCIAS.....	86

INTRODUÇÃO

O metano, constituído por um carbono e quatro hidrogênios (CH₄), é um gás nobre e o hidrocarboneto mais leve e mais abundante na atmosfera. O CH₄ tem meia-vida de 9 anos na atmosfera com um complexo caminho de oxidação que afeta os radicais ozônio e hidroxila na troposfera (Hartmann et al., 2013). Além disso, o CH₄ é o segundo gás de efeito estufa mais importante depois do gás carbônico (CO₂), com um potencial de aquecimento global 28 vezes maior em um horizonte de 100 anos (Ciais et al., 2013). A concentração do CH₄ na atmosfera quase triplicou desde a Revolução Industrial (Stocker et al., 2013).

O gás metano encontrado na natureza pode ter origem biótica ou abiótica. O CH₄ abiótico é formado por reações químicas relacionadas a processos magmáticos ou interações gás-água-rocha (Etiope & Schoell, 2014); enquanto o CH₄ biótico é gerado a partir da alteração da matéria orgânica por processos termogênicos ou biogênicos. O CH₄ termogênico é gerado na coluna sedimentar em profundidades e temperaturas elevadas ao longo de milhões de anos, sendo associado a formação de outros hidrocarbonetos (Horsfield & Rullkotter, 1994; Rooney et al., 1995). Enquanto o CH₄ biogênico é formado por decomposição microbiana (Gang & Jiang, 1985; Rice & Claypool, 1981). Mais de 85% das emissões anuais de metano são produzidas biogenicamente por metanogênese em diversos ambientes (Reeburgh, 2007; Valentine et al., 2004). Os oceanos emitem entre 10 e 30 Tg CH₄ yr⁻¹ (Kirschke et al., 2013), onde cerca de 75% dessa quantidade é associada as zonas costeiras (Bange, 2006).

Entre esses ambientes, os sistemas estuarinos se destacam por serem locais de grande aporte e acúmulo de matéria orgânica provinda dos continentes. A geração, acúmulo, escape e impacto do metano formado nesses ambientes têm sido foco de diferentes estudos (p.e., Borges & Abril, 2012; Rao & Sarma, 2016; Rosentreter et al., 2018; Upstill-Goddard & Barnes, 2016). Por meio de dados acústicos, grandes depósitos de gás raso foram mapeados em sistemas estuarinos ao redor do mundo como no Mar Báltico (Jaśniewicz et al., 2019; Thießen et al., 2006; Tóth et al., 2014), Mar Mediterrâneo (Lastras et al., 2004; Vardar & Alpar, 2016), Mar da China (G. Lee et al., 2014; Zhang & Lin, 2017), Atlântico Norte (Brothers et al., 2012; Cauchon-Voyer et al., 2008; Garcia-Gil et al., 2002) e Atlântico Sul (Bravo et al., 2018) incluindo trabalhos no Brasil (Delavy et al., 2016; Felix & Mahiques, 2013; Frazão & Vital, 2007; Pezza Andrade et al., 2021; Weschenfelder et al., 2016). Porém, a variabilidade espacial dos depósitos de gás na

coluna sedimentar dentro desses sistemas, bem como sua migração dentro da coluna sedimentar e escape, ainda está em debate.

Algumas características sedimentares são necessárias para que ocorra a metagênese e o acúmulo de bolhas de gás na coluna sedimentar em ambientes costeiros e estuarinos, como por exemplo: altas taxas de sedimentação (Sobek et al., 2012); elevado conteúdo de matéria orgânica (Rice, 1993); e baixa permeabilidade para retenção do CH₄ gerado (Katsmans, 2019). No entanto, ainda não se sabe qual é o limiar dessas características e como elas se relacionam para que ocorra a saturação do CH₄ e nem como suas variações em diferentes escalas espaciais afetam o e o acúmulo de bolhas. Além disso, a distribuição espacial dos depósitos de gás dentro dos sistemas estuarinos pode ser complexa, apresentando diferentes formas e profundidades, e normalmente, limites abruptos dentro da coluna sedimentar. Ademais, não se sabe qual é a influência desses depósitos nas concentrações de CH₄ na coluna d'água e nas emissões de sistemas estuarinos. O avanço do conhecimento nesse sentido é necessário para promover uma maior compreensão das emissões dos ambientes estuarinos e sua influência no balanço global do metano. Além disso, essa compreensão é necessária para prever o impacto das alterações antropogênicas nas emissões de CH₄ desses ambientes.

Os estuários apresentam uma ampla variação nas emissões de CH₄ e nas concentrações deste no sedimento e na água (Rao & Sarma, 2016; Upstill-Goddard & Barnes, 2016; Weschenfelder et al., 2016, Sturm et al., 2016), devido, principalmente, por diferentes graus de impactos antropogênicos no sistema (Borges & Abril, 2012; Myllykangas et al., 2019 Rosentreter et al.). Tendo isso em vista, o presente trabalho investiga a formação de gás natural em dois sistemas estuarinos distintos: O Complexo Estuarino de Paranaguá e o Delta Santee. O Complexo Estuarino de Paranaguá (CEP) é um estuário subtropical possuindo 551,8 km² de superfície de corpo d'água com 136 km² de planície de maré e 295,5 km² adicionais de áreas inundadas com vegetação (Noernberg et al., 2006). O CEP é um dos maiores estuários do Brasil e vêm sofrendo alterações antropogênicas substanciais e danosas para o meio ambiente e para o bem-estar humano da região. O Delta Santee (DS) é um delta de energia mista com uma área de aproximadamente 100 km², localizado na Carolina do Sul, é o único delta fluvial da costa leste dos Estados Unidos (Hughes et al., 1995). O delta é alimentado pelo rio Santee, que flui 160 km até o Oceano Atlântico Norte, sendo um sistema fluvial de drenagem do Piemonte e o segundo maior rio ao longo da costa leste dos EUA. Similar ao CEP, o DS

sofreu várias modificações antropológicas (Long, 2020) mudando drasticamente a descarga de água doce e o fluxo de sedimentos do rio Santee (McCarney-Castle et al., 2010).

OBJETIVO E HIPOTHESES

O objetivo geral da presente tese é investigar a variabilidade espacial dos depósitos de bolhas de gás metano, sua correlação com parâmetros sedimentares e sua influência na quantidade de metano dissolvido na coluna d'água e seu fluxo para atmosfera. Para isso, o presente estudo investiga as seguintes hipóteses:

- i. As assinaturas sísmicas do gás e as unidades sísmicas observadas em dados acústicos proporcionam informações sedimentares e indicam a origem e migração do metano nos substratos estuarinos.
- ii. Os limites, tanto verticais como horizontais, dos acúmulos de gás na coluna sedimentar, apresentam variação litológica e/ou de parâmetros sedimentares.
- iii. Os depósitos de bolhas de metano localizados no limite sedimento-água influenciam a quantidade de metano dissolvido na coluna d'água e do fluxo para a atmosfera de um sistema estuarino.

DELINEAMENTO DA TESE

A presente tese foi estruturada em três capítulos em formato de artigo científico:

O Cap. I intitulado “*Shallow gas high-resolution seismic signatures in a subtropical estuary*”, publicado na revista *Geo-Marine Letters* (ISSN 1432-1157; IF 2,267; Qualis CAPES A2), aborda a hipótese i da tese e aplica dados sísmicos e sedimentares na caracterização da presença de acúmulo de gás raso no CEP.

O cap. II intitulado “*Distribution of and sedimentary control on shallow gas accumulation in the Santee River Delta marsh (South Carolina, U.S.A.)*” aborda a hipótese ii da tese e conta com dados sísmicos e testemunhos sedimentares para caracterização do controle sedimentar na formação do gás metano. Pretende-se publicar

esse capítulo na revista *Estuarine, Coastal and Shelf Science* (ISSN 0272-7714; IF 3,229; Qualis CAPES A2).

O Cap. III intitulado “*Influence of sedimentary shallow gas on methane concentrations and emissions in a subtropical estuary*” aborda a hipótese iii da tese e conta com dados de metano dissolvido na coluna d’água e o fluxo de metano para atmosfera do CEP. Pretende-se publicar esse capítulo na revista *Estuaries and Coasts* (ISSN 1559-2731; IF 3.246; Qualis CAPES A2).

CAPÍTULO I

Shallow gas high-resolution seismic signatures in a subtropical estuary

Assinaturas sísmicas de alta resolução de gás raso em um estuário subtropical

Authors: J. F. Pezza Andrade¹; M. A. Noernberg¹; R. H. Nagai¹.

¹ Federal University of Paraná, Campus Pontal do Paraná - Center for Marine Studies, Brazil.

Geo-Marine Letters (2021) 41:38 - <https://doi.org/10.1007/s00367-021-00705-8>. (ISSN 1432-1157; IF 2,267; Qualis CAPES A2)

Abstract

High-resolution seismic surveys were carried out at the Paranaguá Estuarine Complex (Southern Brazil) to map the intrasedimentary shallow gas. The seismic signatures representing gas accumulation were separated according to the upper gas boundary characteristics in acoustic blanking with sharp top, acoustic blanking with diffuse top, turbidity pinnacles, and black shadows (gas accumulation at the water/sediment boundary). The main source of the gas has been recognized here as Pre-Holocene continental deposits. These deposits were capped by a seismic unit interpreted as a regressive mud deposited over the last 5,000 years. This seismic unit is quite heterogeneous, the gas being trapped in its different internal layers. Each gas signature represents the efficiency of the sealing layer and has specific locations and burial depths. The results point to different phases of gas migration along with the sedimentary layers. Thus, we proposed a gas migration and accumulation model based on acoustic data and sedimentary inferences within the Paranaguá Estuarine Complex.

Keywords: Paranaguá Estuarine Complex; gas seismic signatures; biogenic gas; methane.

Resumo

Levantamentos sísmicos de alta resolução foram realizados no Complexo Estuarino de Paranaguá (sul do Brasil) para mapear o gás raso intrassedimentar. As assinaturas sísmicas que representam o acúmulo de gás foram separadas de acordo com as características do limite superior do gás em branqueamento acústico com topo abrupto, branqueamento acústico com topo difuso, pináculos de turbidez e sombras negras (acumulação de gás no limite água/sedimento). A principal fonte do gás foi reconhecida aqui como depósitos continentais do Pré-Holoceno. Esses depósitos foram cobertos por uma unidade sísmica interpretada como uma lama regressiva depositada nos últimos 5.000 anos. Esta unidade sísmica é bastante heterogênea, estando o gás aprisionado nas suas diferentes camadas internas. Cada assinatura de gás representa a eficiência da camada de vedação e possui localizações e profundidades específicas. Os resultados apontam para diferentes fases de migração de gás junto com as camadas sedimentares.

Assim, propusemos um modelo de migração e acumulação de gases baseado em dados acústicos e inferências sedimentares no Complexo Estuarino de Paranaguá.

Palavras-chave: Complexo Estuarino de Paranaguá; características sísmicas de gás; gás biogênico; metano.

1 Introduction

Intrasedimentary gas accumulation in marine and coastal environments has been recognized in seismic records for decades (Emery and Hoggan 1958; Schubel 1974; Taylor 1992). The presence of shallow gas in seismic data can totally or partially mask the stratigraphical information (Judd and Hovland 1992). Within unconsolidated sediments, gas may accumulate in extensive areas in estuaries and bays (García-Gil et al. 2002; Baltzer et al. 2005; Felix and Mahiques 2013; Delavy et al. 2016a), lagoons (Baltzer et al. 2005; Klein et al. 2005; Weschenfelder and Corrêa 2018), and shallow marine regions (Okyar and Ediger 1999; Missiaen et al. 2002; García-García et al. 2007).

Gas in sediments can derive from biogenic processes, as a product of organic matter microbial decomposition (Rice and Claypool 1981; Gang and Jiang 1985), or thermogenic degradation (Rice and Claypool 1981; Horsfield and Rullkotter 1994). The latter is associated with petroleum generation, mainly developed during the catagenesis and metagenesis stages (Horsfield and Rullkotter 1994; Rooney et al. 1995). In marine environments, methane (CH₄) is the main gas produced by biogenic decomposition (Claypool and Kaplan 1974; Floodgate and Judd 1992) and during the post-mature metagenesis thermal stage (Horsfield and Rullkotter 1994), which differs from biogenic methane through a heavier methane carbon isotope ratio (Rice and Claypool 1981; Rooney et al. 1995).

The biogenic processes are the primary source of gas accumulation in coastal environments (Lee et al. 2005; García-García et al. 2007; Visnovitz et al. 2015; Vardar and Alpar 2016), normally associated with a shallow basement (García-Gil et al. 2002; Missiaen et al. 2002; Weschenfelder and Corrêa 2018). While thermal gas production needs high temperatures and considerable burial depths (Schoell 1988; Horsfield and Rullkotter 1994; Littke et al. 1999), methanogens microorganisms survive at temperatures between 0-75°C (Zeikus 1977; Gang and Jiang 1985). Biogenic gas production can occur immediately after the sediment deposition in inland water bodies (Gang and Jiang 1985). However, in marine and coastal environments, the presence of sulfate inhibits the production close to the sediment/water boundary, whereas it may occur under the sulfate

reduction zone (Nikaido 1977; Rice and Claypool 1981). High rates of CH₄ generation require abundant organic matter, high sedimentation rate, and enough interstitial space for methanogens ($\pm 1 \mu\text{m}$) (Missiaen et al. 2002; García-García et al. 2007). Also, accumulation requires a sealing layer, generally associated with fines and compact sediments (Rogers et al. 2006). In the right conditions, the biogenic methane can accumulate in large amounts and is responsible for more than 20% of the world's discovered gas reserves (Rice and Claypool 1981).

Methane is the second most important greenhouse gas after carbon dioxide (CO₂), with 28 times global warming potential over one hundred years (Ciais et al., 2013). Still, there is uncertainty in the estimates of its natural sources and sinks and how its variations can affect the growth rate of atmospheric CH₄ (Borges et al., 2016). Although some studies estimate the CH₄ flux from coastal gas-charged sediments to the atmosphere via immediate water plumes and pockmarks (Judd et al. 1997; Dimitrov 2002; García-Gil et al. 2002), there is insufficient knowledge about methane dynamics within unconsolidated sediments.

Natural gas-charged sediments are recognizable in seismic records by an abrupt decrease of acoustic velocity with possible phase inversion and signal reverberation through bubble resonance (Gorgas et al. 2003; Baltzer et al. 2005). The gas can appear in various shapes and geometries in seismic profiles, classified into distinct gas signatures. The seismic gas signatures are related to different accumulation and seepage types. Their distribution and features can explain the sedimentary structures and their characteristic (García-Gil et al. 2002; Baltzer et al. 2005; García-García et al. 2007).

The present paper aims to map and describe seismic gas signatures in the Paranaguá Estuarine Complex (PEC) and discuss their dynamics linked to the regional stratigraphy. This study suggests a gas migration and accumulation model based on acoustic data. It is important to incorporate information about the gas dynamics within unconsolidated sediments, seismic gas signatures, and stratigraphic meanings. Also, we indicate and discuss the possible source of the shallow gas and the sedimentary unit that acts as a sealing.

2 Settings

The PEC is a microtidal subtropical estuary system located in the Paraná state, southern Brazil (Fig. I.1). The system comprises two main water bodies, Paranaguá Bay and Laranjeiras Bay. The estuarine complex has a 551.8 km² water body surface with 136

km² of tidal flat and 295.5 km² of vegetated flooded areas (Noernberg et al., 2006). The PEC mean depth is 5.4 m, and the maximum depth is around 33 m at the mouth zone (Fig. I.1) (Lana et al. 2001). This estuarine system is partially stratified with asymmetric tides (Knoppers et al. 1987). The tidal range is about 2.7 m, and the maximum flood and ebb-tidal current is about 1.2 m/s and 1.4 m/s, respectively (Lamour et al. 2007). The tide intrusion is about 12.5 km (Lana et al. 2001) with a tidal prism of 1.34 km³, and the freshwater flow rate is about 200 m³/s (Lessa et al. 1998).

The estuarine system is embedded in a coastal plain bordered by the Serra do Mar mountain range. The Serra do Mar mountain range, which reaches over 1500 m (Lana et al. 2001), displays steep slopes and has high erosive potential (Noernberg, 2001). West of Paranaguá city, the estuary morphology is characterized as a drowned, narrow, incised paleo-valley (Fig. I.1). To the east of Paranaguá city, it comprises a wide coastal plain (Fig. I.1). The coastal plain is composed of a sand barrier with at least two generations of beach/dunes ridge progradation, forming a late Pleistocene and a Holocene strand plain (Lessa et al. 2000; Angulo 2004). These sedimentary facies were formed during the two transgressive/regressive cycles related to the last sea-levels maximum at Pleistocene and mid- to late-Holocene (Angulo and Suguio 1995; Lessa et al. 2000). Since the last one, the sea level gradually decreased by 3.5 meters (Angulo and Lessa 1997).

Continental deposits associated with the Alexandra formation occur in low isolated hills (Angulo 2004) and may comprise, with their reworked material (Bigarella et al. 1978), the substrate for Pleistocene and Holocene sedimentation within the PEC (Lessa et al. 1998, 2000). The Alexandra formation comprises Miocene arkosic sands and muds with lesser gravels and clays (Angulo and Suguio 1995). Sedimentary facies were interpreted as braided channels, dense underwater flows, and gravitational flow deposition, suggesting a depositional system of alluvial fans associated with small aqueous bodies (Angulo 2004). The crystalline basement under the coastal plain is reached at depths of about 50 m landward and about 100 m close to the shoreline (Lessa et al. 2000). Also, gravimetric data investigation along the shoreline indicates a maximum depth of 160 m (Castro et al. 2008). Under the estuarine system, Lessa et al. (1998) suggested a shallower depth of the basement, between 20 to 30 m, corroborated by several small rocky islands within the PEC.

The paper by Lessa et al. (1998) is the only publication about the stratigraphic evolution of the PEC. Using seismic data and several core samples, the authors interpreted four Holocene sedimentary units overlying a pre-Holocene fluvial and continental deposit

(Alexandra formation and their reworked material) (Fig. I.1). According to the authors, the sea-level rise resulted in a transgressive mud deposit, probably associated with a low-energy estuary funnel environment, followed by transgressive sand. The sand unit overlaid a Tidal Ravinement Surface (Catuneanu 2006), which eroded almost completely the transgressive mud west of Paranaguá. The subsequent highstand system tract includes a regressive mud, which comprises most of the recent superficial sediments in the central zone of the estuary, and regressive sand restricted to the estuary head. Noteworthy, the authors did not mention the presence of gas. However, they recognized non-penetration seismic signal layers, which were tentatively interpreted in different ways.

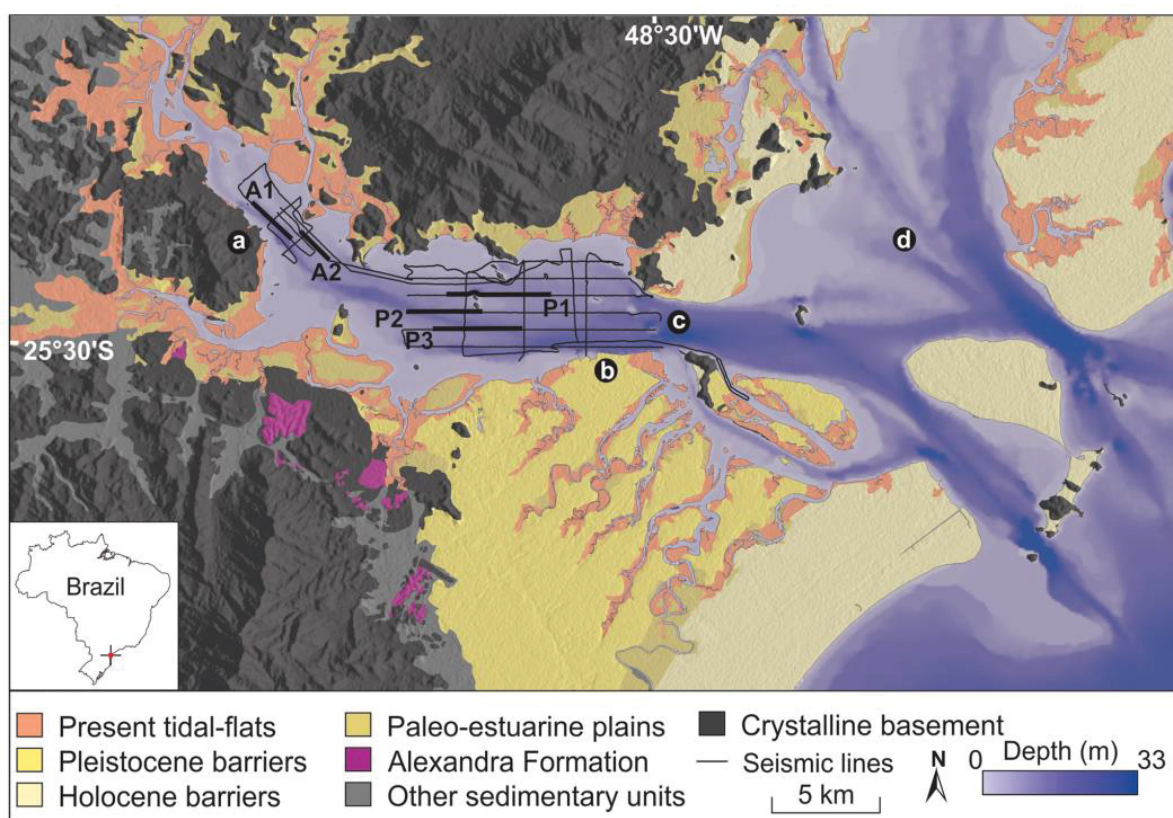


Fig. 1: The Paranaguá Estuarine Complex bathymetric map, and Pleistocene evolution (based on Lessa et al., 2000), with the position of the seismic lines analyzed in this study (P1, P2, P3 in Fig. II.4; A1, A2 in Fig. II.5). a – Antonina city; b – Paranaguá city; c – Paranaguá Bay; d - Laranjeiras Bay.

3 Materials and method

Shallow, high-resolution seismic records were acquired in two PEC zones, using two CHIRP seismic sources (Meridata Finland Ltd) with different frequencies range 2-9 kHz and 10-18 kHz. A total of 157 km of the acquisition was collected over a three-day

survey, one in April and two in July 2019 (Fig. 1). Data were processed and interpreted with the Meridata MDPS software. The time to depth conversion was made with a sound velocity of 1500 m/s for both water and sediments; thus, depth in images is approximate. Vertical mean resolution is about seven cm for the lower frequency and three cm for the high frequency. The facies were primarily classified with the lowest frequency of the CHIRP source (Fig. 2) due to its higher penetration in the sediment layers. Although the characterization was done mainly with the 2-9 kHz frequency, the 10-18 kHz CHIRP source was used to assist in the mapping and characterizing the facies and stratification.

Superficial sediment samples were performed with a Van Veen Grab sampler in about fifty PEC locations (Fig. 3). For grain size analysis, 2g of sediment was separated from each sample. Afterward, decarbonization was performed with 10% hydrochloric acid (HCl) and the removal of organic matter with 10% hydrogen peroxide (H₂O₂). Grain-size analyses were then performed with a Malvern Mastersizer 2000 through laser diffraction. The data were processed with the Sysgran 3.2 Software (Camargo 2006), later separated by the mud content (silt and clay) (Fig. I.3). Because these analyses were initially carried out in another research project, organic matter content data for these samples is not available. However, other studies show that, in the PEC, fine sediments generally have a higher organic matter content (Cattani, 2012).

Near-distance analyses were performed in the ArcMap software to ascertain the relationship of the bottom sediments with shallow gas (<1.5 m). Initially, the surface sediment samples acquired with a maximum distance of 200 m from the seismic lines were separated. Then, the distance between these samples the gas accumulation covered by a sedimentary layer less than 1.5 m was analyzed. The 1.5 m value was picked due to a good statistical correlation between the shallow gas presence and fines content in the Arousa estuary (Diez et al. 2007). Finally, the results were plotted on a graph of distance versus mud content.

4 Results

At the PEC, the gas signatures found were classified as acoustic blanking (AB) (Judd and Hovland 1992; Lee et al. 2005; Lodolo et al. 2012; Visnovitz et al. 2015; Weschenfelder et al. 2016; Jaśniewicz et al. 2019), black shadow (BS) (Baltzer et al., 2005; Delavy et al., 2016; Felix and Mahiques, 2013; Klein et al., 2005; Weschenfelder et al., 2016), and turbidity pinnacles (TP) (Delavy et al., 2016; Felix and Mahiques, 2013;

Iglesias and García-Gil, 2007; Klein et al., 2005; Weschenfelder et al., 2016) (Fig. I.2). Together, these gas accumulation facies cover 60 km of the studied area, comprising a total of 38% of the seismic profiles (Fig. I.3).

The uppermost portion of the estuary, the Antonina zone, presents a gas signature sector, where the BS facies is on the sides, and the AB facies is frequent in the central portion (Fig. I.3). In the Paranaguá zone, gas accumulation is mainly concentrated in the central region, where the gas accumulation represents different gas seismic facies types along the seismic lines (Fig. I.4). However, it is still possible to recognize different gas accumulation sectors in this zone (Fig. I.3). The seaward limit of the gas is evident, enabling us to recognize the gas accumulation boundaries in all seismic lines east of the Paranaguá city (Fig. I.3).

4.1 Acoustic blanking (AB) with sharp (ABS) or diffuse top (ABD)

The AB facies was separated according to the type of reflection at the top, which were either sharp (ABS) or diffuse (ABD) (Fig. I.2). ABD facies are the most common in the surveyed area, more than 30 km of total extension, with a maximum continuous extension of 6300 m and a minimum of 15 m (Fig. I.3). This facies have a poorly defined top, although it is possible to recognize the gas front (Fig. I.4 and I.5). It was recognized in water depths ranging from 1.6 m to 16.7 m, with sedimentary coverage between 0.7 m and 6.2 m. This facies covers a large part of the surveyed south and southeast region in the Paranaguá zone and the central and northern regions in the Antonina zone (Fig. I.3). In the Antonina zone, the gas is shallower, with an average sediment cover of about 1.4 m, while in Paranaguá, the average sediment cover is two times thicker. Also, except for BS, the shallower portion of the gas (<1.5 m of sedimentary cover) found in the study area is predominantly comprised of the ABD seismic signature (Fig. I.3).

ABS facies have a well-defined, flat or inclined top. This facies is characterized by an enhanced reflector that completely masks the data below. ABS facies is frequent in the Paranaguá zone, mainly in the basin center (Fig. I.3). It is usually associated with turbidity pinnacles, fitted between the pinnacles (P1 in Fig. I.4) or on their lateral limits, and in conjunction with the ABD facies. This facies covers 8761 m of the seismic profiles, having a minimum extension of 5 m and a maximum of 768 m (Fig. I.3). The ABS facies are under 2.2 m to 10.3 m of water and a sediment layer between 0.8 m and 8.5 m with a mean value of 4 m. Like ABD, the ABS is much shallower within the sediments in the Antonina zone than in Paranaguá, with an average difference of more than 4 m sediment

cover between them. Also, there are locations where the ABS signatures are shallower in the Antonina zone than 1.5 m in the sedimentary layer.

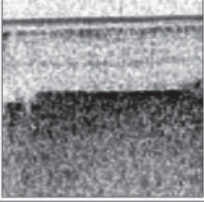
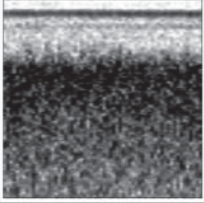
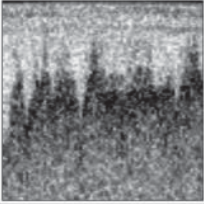
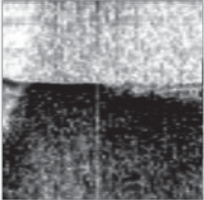
Gas accumulation types		Gas seismic signatures	Description
Acoustic Blanking	Sharp Top (ABS)		High to moderate amplitude with well-defined flat or dipping top. Completely masking the data below.
	Difuse Top (ABD)		High to moderate amplitude with poorly defined top. Completely masking the data below
Turbidity Pinnacles (TP)			High to moderate amplitude, cone shaped pinnacles with varying dimensions. Generally found as a set with tens of centimeters to a few meters between the pinnacles top and bottom .
Black Shadow (BS)			High amplitude associated with multiples, completely masking the data. Located at the sediment/water boundary, however, it may have portions covered by thin sedimentary layers

Fig. 2: Intrasedimentary gas seismic signatures observed in the Paranaguá Estuarine Complex classified with a 2-9 kHz CHIRP source and their acoustic characteristic. The scale of all images is 5 m x 100 m.

4.2 Turbidity pinnacles (TP)

TP covers about 12 km from the surveyed area. It can be found in isolation or large groups, reaching extensions of almost 1 km (Fig. I.3 and 4). TP is often associated with changes in the depth of the gas accumulation, related to the change of the gas sealing layer (Fig. I.4a), and may also be between ABS and ABD facies (P2 in Fig. I.4). This gas feature is rare in the Antonina zone and concentrated in the Paranaguá zone center (Fig. I.3). The TP facies appears in all depths, deeper than 8 m, and reaching the sediment/water limit.

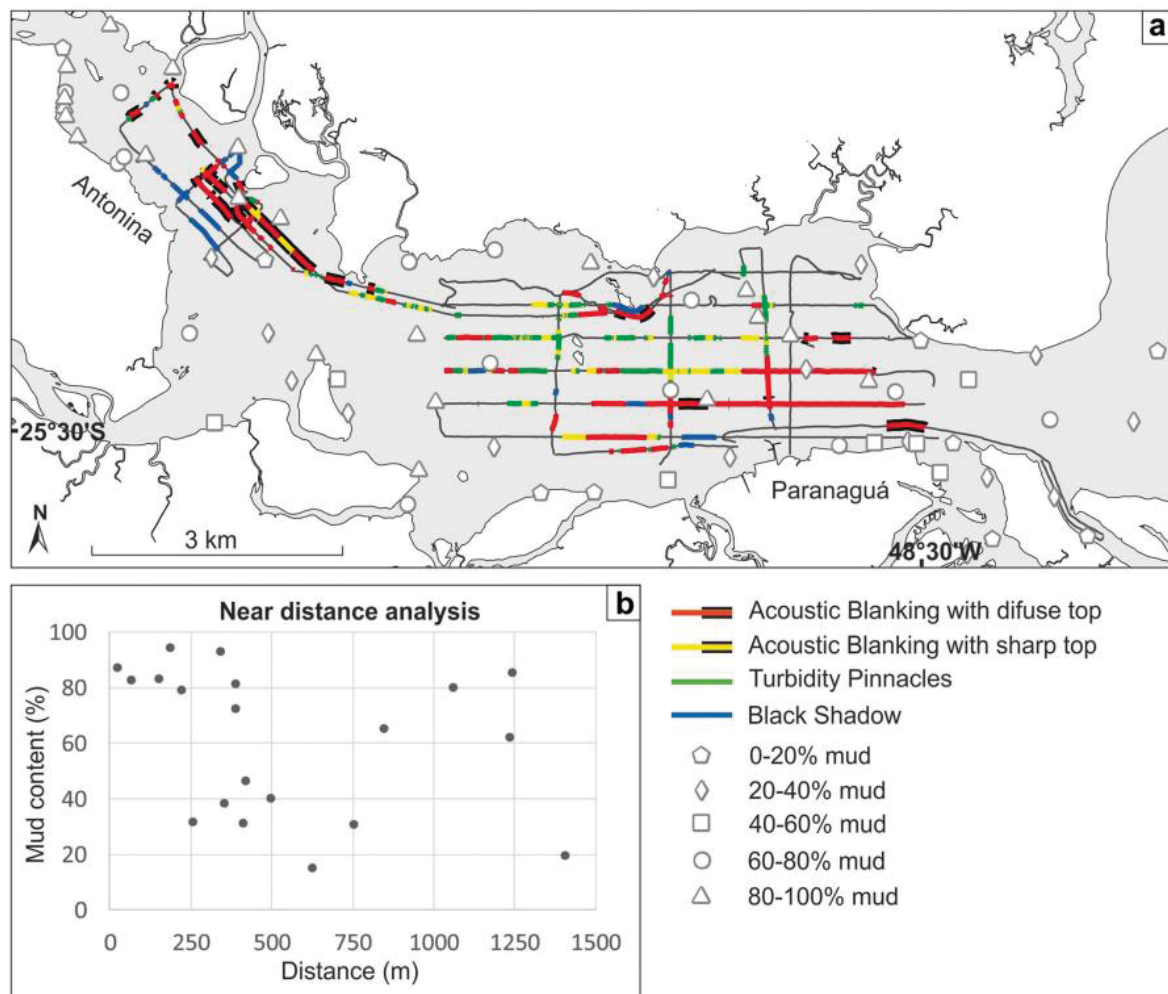


Fig. 3: Location map of the different intrasedimentary gas seismic signatures observed in the Paranaguá Estuarine Complex (seismic data acquisition lines in black) and surficial sediment (0 – 3 cm) mud content (silt + clay) distributions. Black contour in color lines indicate gas presence under less than 1.5 m of sediment cover. Near distance analysis graphic represents the closest distance between shallow gas accumulation (< 1.5 m), comprising the BS and portions of the ABS and ABD marked by the black contour.

4.3 Black shadow (BS)

BS facies cover 8272 m of the seismic profiles, with a maximum length of 1044 m and a minimum of 59 m (Fig. I.3). A strong reflector characterizes the BS facies almost in the contact between water and sediment located at depths between 2.3 m and 14.2 m. (Fig. I.2). The difference between the BS and ABS types of gas accumulation is that, in the former, it is generally not possible to recognize the sealant sediment layer between the gas accumulation and the water column. The BS sealing layer is less compact than the

ABS sealing layer due to the absence of the sediment weight. Additionally, most of the BS facies shows the presence of cloudy turbidity (García-Gil et al. 2002) of lesser or greater intensity (P2 and P3 in Fig. I.4), indicating possible seeps to the water column.

The most extensive BS is at the edge of the surveyed area (Fig. I.3). In the Paranaguá zone, this facies is usually associated with other gas accumulation types (Fig. I.4). On the other hand, in the Antonina zone, the BS facies covers much of the southwest region, appearing in isolation of other gas accumulation types (Fig. I.3). In this location, the crystalline basement appears to be shallow (Fig. I.5a). Similarly, a BS in the north margin of the Paranaguá zone also presents close to the shallow basement, inferred by the proximity of a rocky island (Fig. I.3).

4.4 Bottom sediments

Grain size analysis indicates that the PEC bed is predominantly composed of silt with varying amounts of clay and sand. Generally, the mud content decreases towards estuarine margins (Fig. I.3). Overall, surveyed regions with subsurface gas present surficial sediment with more than 60% of mud. This pattern has an exception at the north of Paranaguá city, where, above the ABD facies surface, sediments present 30.7% of mud (rhombus symbol north to Paranaguá city in Fig. I.3), here the gas is covered by a sediment layer of about 3 m thickness.

The presence of gas shallower than 1.5 m correlates with the sampled sites with the highest concentration of mud, between 80-100% (Fig. I.3). Graphical analyses also showed that the sample locations closest to gas shallower occurrences than 1.5 m necessarily have a high mud content (Fig. I.3b). However, a high concentration of fines does not necessarily indicate the presence of shallow gas (Fig. I.3b). Two sampling sites, at the northwest part of the Antonina zone and at the southeastern part of the Paranaguá zone, with more than 80% of mud on seismic lines without subsurface gas were recognized (Fig. I.3a), more than 1000 m away from shallow (<1.5 m) gas accumulation (Fig. I.3b). There are also two locations, at the southeast of the Paranaguá zone and at the southeast of the Antonina zone, where the samples closer to the gas accumulation have a mud content of less than 40% (fig. I.3). However, there are seismic lines in which the presence of gas has not been recognized (Fig I.3).

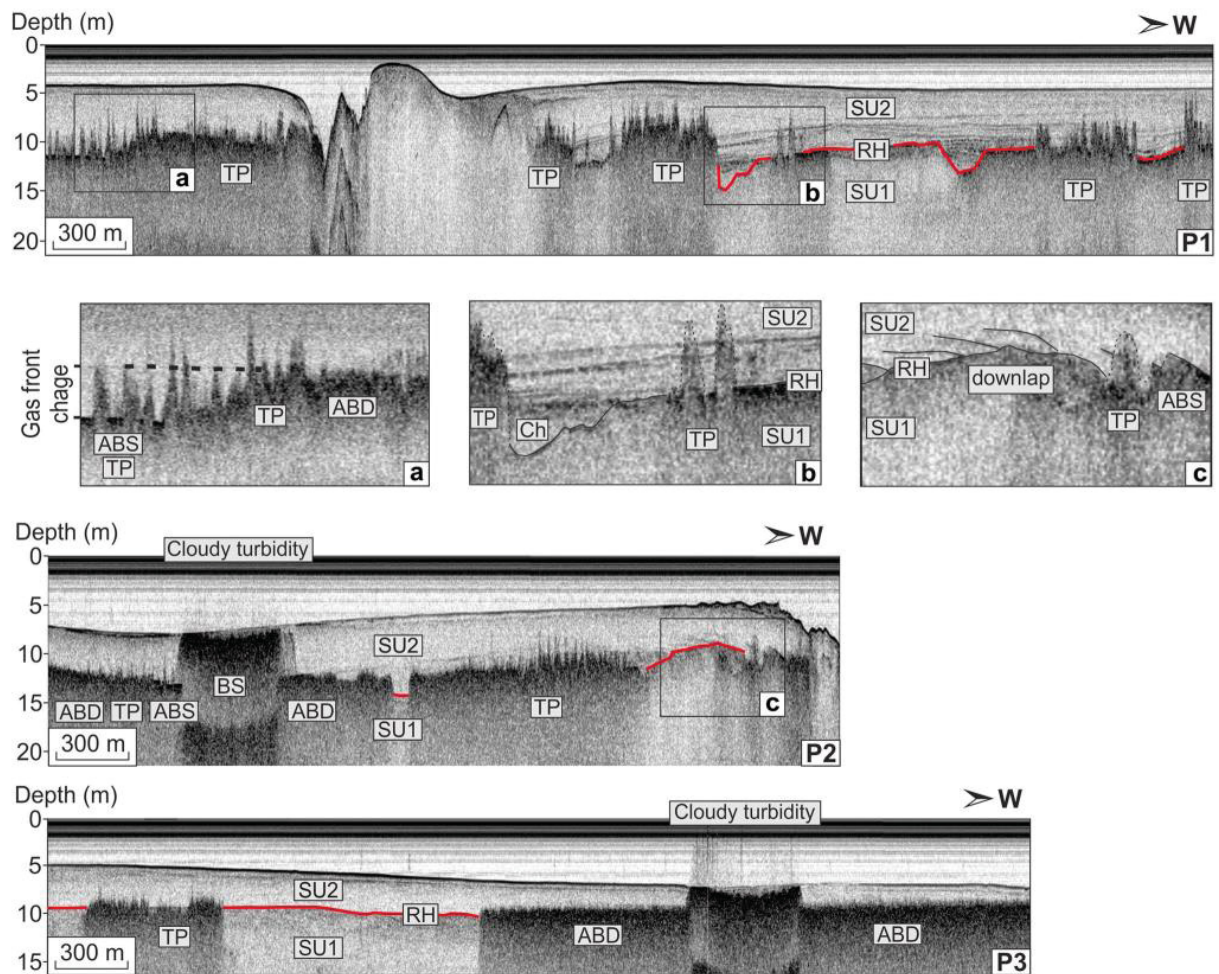


Fig. 4: Chirp (2-9 kHz) seismic profiles in the Paranaguá zone (P1, P2, P3; see Fig. I.1 for location) showing gas accumulation seismic signatures (TP, BS, ABS, ABD) and the two seismic units (SU1, SU2) separated by a regional reflector (RH). Detailed zoom images (a, b, c with 10 x 500m scale) indicate a gas accumulation baseline change, paleochannel (Ch), and downlap termination. TP - Turbidity pinnacles; BS - Black shadow; ABS - Acoustic blanking with a sharp top; ABD - Acoustic blanking with diffuse top.

4.5 Stratigraphy

Although the PEC gas features cover more than a third of the surveyed area, it is possible to recognize some stratigraphic characteristics. A regional horizon (RH) is recognized in most stratigraphic windows (P1 in Fig. I.4 and A2 in Fig. I.5). This horizon represents an irregular relief with numerous paleochannels (P1 in Fig. I.4).

The RH separates two distinct seismic units. The oldest unit (SU1) has no distinguishable reflectors (Fig. I.4), or in some places, reflectors with a chaotic pattern (Fig. I.5). Above this horizon, the seismic unit (SU2) presents flat or slightly wavy internal reflectors. In the distal portion of the Paranaguá zone, the internal reflectors of

SU2 show progradation over RH (Fig. I.4c). In the Antonina zone, there are places with the absence of SU1 where it is possible to observe direct contact of the basement with the SU2 unit (Fig. I.5a). No tectonic structure, such as faults or folds, has been recognized in the acoustic data.

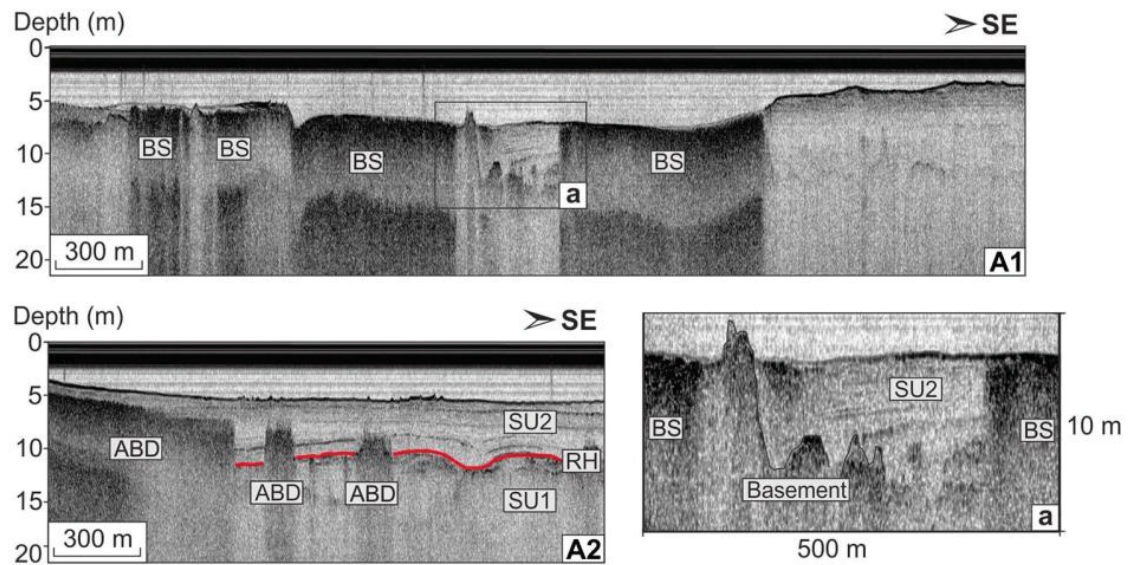


Fig. 5: Chirp (2-9 kHz) seismic profiles in the Antonina zone (A1, A2; see Fig. I.1 for location) showing gas accumulation seismic signatures (BS, ABD) and the two seismic units (SU1, SU2) separated by a regional reflector (RH). Detailed zoom image indicates a stratigraphic window with a shallow basement. BS - Black shadow; ABD - Acoustic blanking with diffuse top.

5 Discussion

5.1 High-resolution seismic gas signatures

Four types of seismic gas signatures were observed at the PEC, with unique spatial distribution and depth. As mentioned before, in the coastal plain adjacent to the study area, wells reached the crystalline basement at depths of about 50 m (Lessa et al., 2000), hindering the possibility of thermogenic gas generation (Rice and Claypool, 1981). Thus, even though this study did not perform a chemical analysis of the gas (i.e., isotopic measurements), it is highly probable that PEC gas-charged sediments result from organic matter degradation by biogenic activity.

There are several terminologies for the different seismic signatures caused by gas accumulation. However, these terminologies are often confusing, having several names for similar seismic signatures, or even the opposite, the same names for different seismic signatures (Weschenfelder, 2018). For example, despite the consensus to separate gas

accumulation signatures in acoustic blankets and acoustic curtains through their format and lateral extension (Taylor 1992; García-Gil et al. 2002; Klein et al. 2005; Vardar and Alpar 2016), there is a discrepancy as to the type of the top of the gas occurrence. Acoustic curtains are smaller, with a concave shape, while the blankets are flatter and cover large areas. However, some works indicate that acoustic curtains have a main top reflector and blankets have a diffuse top, without the presence of a strong reflector (Taylor 1992), or conversely, where the curtain has a less sharp upper gas boundary (García-Gil et al. 2002; Frazão and Vital 2007). More usually, works indicate that both have a high amplitude reflector at the top (Baltzer et al. 2005; Vardar and Alpar 2016; Weschenfelder et al. 2016).

The separation of the curtain and blanket facies was not used here, as this separation does not seem to imply different properties from the type of gas accumulation, such as gas quantity by volume or a different permeability of the sealing layer. These properties are better related to the upper boundary seismic signature of gas accumulations (Taylor 1992; García-Gil et al. 2002). The facies extensions are best seen through maps (as Fig. I.3) and the different shapes of the gas curtain – box (Weschenfelder et al. 2016; Weschenfelder and Corrêa 2018); Chevron (García-Gil et al. 2002; Frazão and Vital 2007); convex (García-Gil et al. 2002); or mushroom (Karisiddaiah et al. 1993). This feature characterizes either the sealing layer topography or of the lateral decrease in seismic wave speed caused by the gas (García-Gil et al. 2002), which can also occur on the sides of the acoustic blanket and other gas accumulation types ("pull-down"; Judd and Hovland, 1992; Lee et al., 2005; Vardar and Alpar, 2016).

Gas accumulation types were classified here mainly in terms of their top, in sharp (ABS), diffuse (ABD), and highly diffuse (TP). Black shadows were also separated for their unique characteristics. Each seismic signature represents a specific feature of the gas accumulations in the sediments. The different seismic signatures and their depths and locations provide information on the stages of migration and accumulation of shallow gas in the PEC (Fig. I.6), discussed later in this paper (section 5.2). It is worth to highlight that the seismic signatures found in this work refer to the presence of shallow intra-sedimentary gas observed in a shallow bay. This gas is trapped by a Holocene sedimentary unit with a high content of fines and imaged by CHIRP type acoustic source (2-9 kHz and 10-18 kHz). Therefore, the seismic signatures associated with gas accumulation from different coastal environments with other environmental parameters

(water depth, gas depth, sediment background) or acquired with other seismic sources can vary considerably from those presented here.

5.1.1 Acoustic blanking (AB) with sharp (ABS) or diffuse top (ABD)

We interpret the difference between ABS and ABD gas accumulation type due to the efficiency of the sealing layer. This efficiency is represented by the permeability contrast of the source and sealing layer (García-Gil et al. 2002) and gas (Taylor 1992). The results showed that ABS facies is, on average, at greater buried depths. This aspect highlights the importance of pressure for forming this facies, as greater depths accentuate sediment compaction, decreasing the permeability of the sealing layer (Nooraiepour et al. 2019). The sealing layer can retain the gas for a longer time, increasing the gas concentrations. The amount of gas can increase up to a limit, after which gas seeps into the low permeability sealing layer, generating pinnacles (Fig. I.4a and I.6d). This aspect explains the almost absence of ABS facies at the Antonina zone and its presence at the Paranaguá zone center, where gas is observed in greater depths. Also, sealing layer efficiency in the Antonina zone should be lower due to a minor mud content caused by the tapered morphology and the fluvial influence. Despite this difference, both ABS and ABD facies portray high gas accumulation, sufficient to mask the acoustic data (>30 ml/L; Whelan et al., 1977).

Additionally, at the PEC, ABS facies are smaller and less common than ABD facies (Fig. I.3). This indicates that the lowest permeability layers are rarer to form and do not reach large extensions, probably due to the heterogeneity of compaction (possible sediment reworking or bioturbation) and grain-size (similar to the existing surface of the estuary).

5.1.2 Turbidity pinnacles (TP)

TP facies indicate an upward migration of the gas without an efficient and relatively homogeneous sealing layer. Due to this characteristic, TP can be found at any depth in the sedimentary strata. The heads of TP facies may eventually find a low permeability layer, where the gas will accumulate (Fig. I.6b and I.6e) until the forming of acoustic blanking facies (Fig. I.4a and I.6). When associated with ABS facies, TP may indicate a rupture in the sealing layer (Fig. I.4a and I.6d). In contrast, when associated with ABD facies, a less common association in the study area, TP must indicate a differentiated gas migration, probably associated with the difference in the amount of gas

or heterogeneities of the sealing layer. When close to the sediment-water interface, the TP gas front can be trapped, forming BS gas accumulation type or, supposedly, the gas should seep into the water column (Fig. I.6h).

Most TP facies were found in the Paranaguá zone center, being scarce in Antonina (Fig. I.3). In the latter, gas accumulation occurs at shallower depths, and, thus, gas accumulation must be portrayed as other gas seismic signatures closest to the surface or reached the water column (Fig. I.6h). This pattern is explained by the lower efficiency of the sealing layer in Antonina.

5.1.3 Black shadow (BS)

The BS facies represents the last stage of gas trapping within unconsolidated sediments (Fig. I.6). The close to the surface in situ gas production hypothesis (Baltzer et al. 2005) does not apply here due to the influence of sulfate-rich seawater (Nikaido 1977; Rice and Claypool 1981; Gang and Jiang 1985). However, we cannot exclude the possibility of gas generation locally near the lower limit of the sulfide reduction zone, which can migrate to the sediment-water boundary.

Noteworthy, the BS facies were located even at small depths, little more than 2 m. Therefore, the hydraulic pressure is not a limiting factor for the formation of the BS. Also, it is impossible to observe the thickness of the sealant sediment layer, implying that this layer is very thin or, more likely, being passed through. Thus, we argue that grain-size must be the main factor that allows or hampers the creation of BS, not being able to have significant bioturbation or reworking of the superficial sediments. The dependence on grain-size may explain the maximum BS facies size observed in this work. Worth noting that there is substantial heterogeneity in the bottom sediments (Fig. I.3).

In PEC, regions where the basement is shallow, gas accumulates as BS, and no other gas seismic signature is observed. We suggest that these regions have a thinner seal layer or layers, so it is easier for the gas to migrate upward and concentrate at the sediment/water boundary. If the BS facies does not have an active gas source, it should disappear over time due to the gas seepage to the water column. In this sense, BS facies are probably not stable seismic signatures. In the Paranaguá zone, where BS facies is associated with other facies, it may be increasingly charged with gas from below. In the Antonina zone, upward gas migration must be at an advanced stage (Fig. I.6g), probably due to a thinner seal layer.

5.2 Shallow gas migration and accumulation within unconsolidated sediments in PEC

The gas migration and accumulation processes are dependent on the gas concentration, pressure gradient, and porosity of the surroundings, which controls the gas migration velocity (Zhou et al. 2018). Due to the strong sedimentary heterogeneity in the PEC, at least in the Holocene unit west of Paranaguá city (Lessa et al. 1998), the estuary is a great natural laboratory to observe different gas migration features, which these driving forces are locally variable. Also, there is no evidence of neotectonics or faults in the sedimentary layers in the PEC region. In the absence of a significant impermeable structural trap, the gas generated within PEC unconsolidated and mostly flat sediment layers should be in constant and slow movement by diffusion and advection. Therefore, the types of gas signatures found at different depths may indicate phases of migration and gas accumulation from its source to the water column associated with differential sedimentary properties

The CH₄ seepage to the water column and eventually to the atmosphere is little known, as the current works are restricted to recognizing gas plumes in the water column or pockmarks (Judd et al. 1997; Dimitrov 2002; García-Gil et al. 2002). Borges et al. (2016) reported high CH₄ concentrations in surface waters of the Belgian coastal zone associated with the presence of shallow gas in sediments. However, in that region, no plumes or pockmarks were recognized, but noises were reported in the water column close to the seabed (Missiaen et al. 2002). Similarly, noises were recognized in the PEC, mainly above BS. These noises may indicate a methane gas seepage, a minor version of the cloudy turbidity recognized in the water column (P2 and P3 in Fig. I.4)(García-Gil et al. 2002).

Along these lines, we propose a migration and accumulation model from the source to the water column of shallow gas in the PEC (Fig. I.6), which might apply to other coastal environments. First, the gas seeps from the source layer, migrating upward in the form of pinnacles (Fig. I.6a). Eventually, this gas encounters layers with low permeability that trap the gas. When the pinnacles 'head' encounters these layers, the gas begins to accumulate (Fig. I.6b, e) and starts to present an acoustic blanking seismic signature. Depending on the trapping efficiency of the sealing layer, the gas is completely trapped, generating an ABS signature (Fig. I.6c), or it can slowly escape into the sealing layer as it accumulates, forming an ABD signature (Fig. I.6f). In the PEC, the layers with the greatest trapping efficiency are found in greater depth, but the sequence of the layers

may vary locally, also the quantity of sealing layers. In both cases, the gas accumulating below the sealing layer can present lateral migration, causing an abrupt lateral limit (Fig. I.6b, c, e, f). When the gas is effectively trapped (ABS), it accumulates to a limit when local “breaks” occur in the sealing layer, again forming pinnacles (Fig. I.6d), which can also be formed in less efficient sealing layers (Fig. I.6 g). Finally, when the gas reaches the sediment-water interface, it can be exhumed to the water column or accumulate one last time, forming the BS (h), where the gas should eventually leak (Fig. I.6 i). A small amount of upper sedimentary layers in-situ local gas production cannot be ruled out. However, it should follow the same migration and accumulation patterns mentioned above.

The gas occurring in the PEC sediments consists of biogenic methane due to the basement configuration, but it is impossible to differentiate and quantify the current in-situ production and the deep gas migration. Thus, through the current PEC data, the temporal variation of the gas contained in the sediments and its seepage to the water column is unknown. Continuous acoustic surveys should be employed to observe temporal or seasonal variations of the gas accumulation in sediments to recognize the gas dynamics' time scale and the influence of its in-situ production. Analyzes of the methane concentration in the sediments and water would also be relevant for the possible quantification of the PEC methane contribution to the atmosphere. This would contribute to more robust estimatives of gas seepage in estuarine and coastal environments, currently underestimated (Borges et al. 2016).

5.3 Bottom sediments

The PEC bottom sediments are heterogeneous concerning mud content (Fig. I.3), probably due to the presence of several distributary channels (Fig. I.1). West of Paranaguá city, bottom sediments are associated with the top of the regressive mud (Lessa et al. 1998). Sediment core analyses indicate that the fines content of the regressive mud ranges from 30% to 91%, and the organic matter content ranges from 2.2% to 20% (Lessa et al. 1998), indicating that sedimentary heterogeneity seen in the bottom sediments is also present in all SU2. In PEC, bottom sediments with a high content of fines are related to a higher organic matter content (Cattani, 2012). There is no gas accumulation downstream of the Paranaguá zone, where sandy bottom sediments (Lamour et al. 2004) are associated with a transgressive sand layer (Lessa et al. 1998).

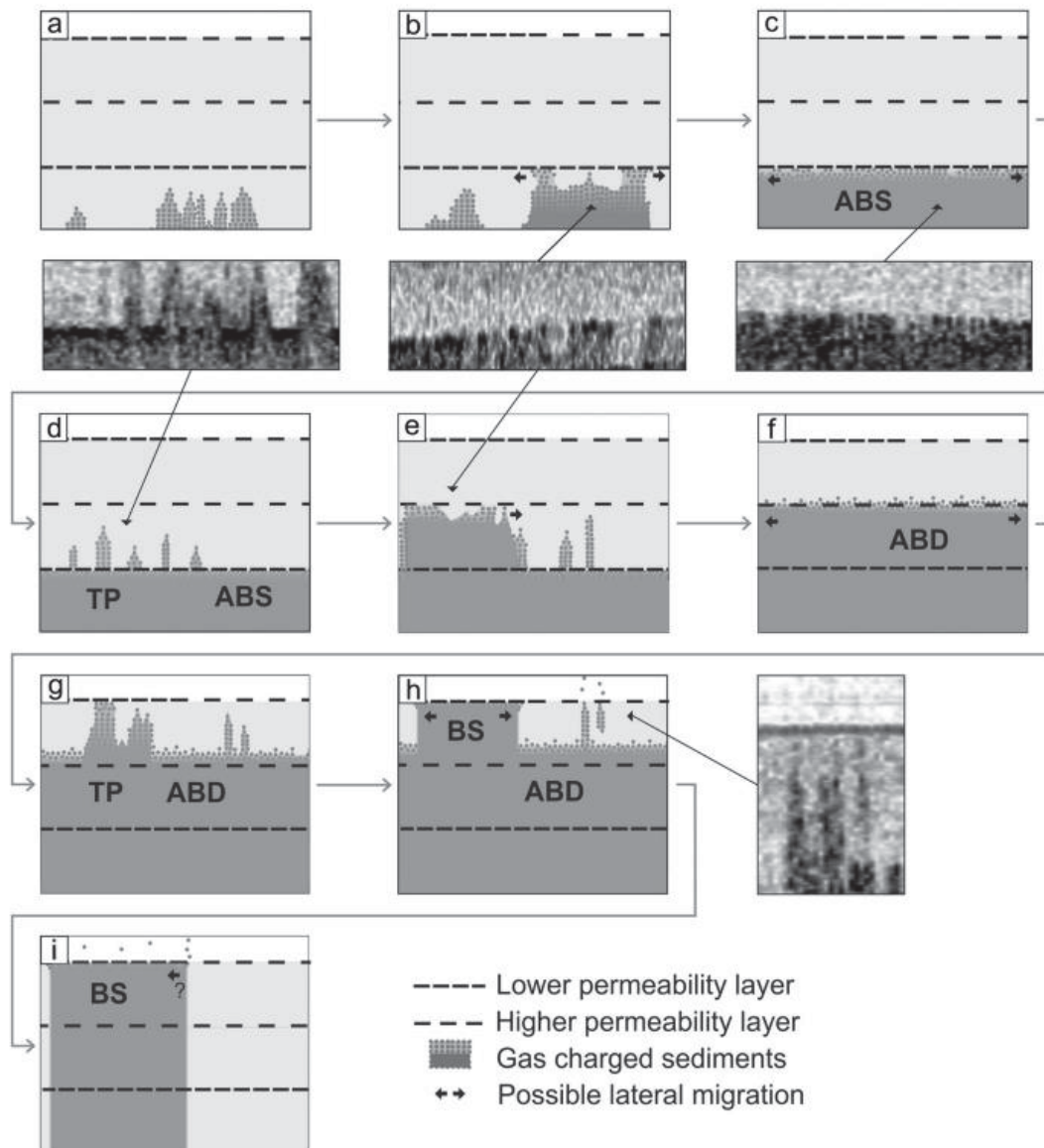


Fig. 6: Evolution model of shallow gas migration and accumulation, showing the changes between seismic gas signatures and their relationship with the relative permeability between sedimentary layers. The gas migrates from the source as turbidity pinnacles (a); the pinnacles head encounter a low permeability layer and start to accumulate (b); the gas accumulates forming an acoustic blanking with a sharp top (c); eventually, the gas seeps to the low permeability layer forming pinnacles (d); again the heads of pinnacles encounter a sealing layer, and de gas start to accumulate (e); this time the sealing layer has low trapping efficiency and thus the gas slowly seeps when it accumulates forming an acoustic blanking with diffuse top signature (f); heterogeneities in the sealing layer permits turbidity pinnacles locally formation (g); the pinnacles reach the sediment-water interface and can accumulate as a black shadow or seeps to the water column (h); finally, the gas slowly seeps from the black shadow to the water column (i). Note that the model above has only two sedimentary layers for didactic means. In the PEC the amount of layers capable of retaining the gas, and their relative permeability, varies locally.

Some studies showed that shallow gas accumulation in bays could be related to the mud content of bottom sediments (García-Gil et al. 2002; Diez et al. 2007; Jensen and Bennike 2009). In the PEC, the presence of gas shallower than 1.5 m seems to have a strong correlation with a high mud content in surficial sediments (Fig. I.3). On the other hand, samples with a high mud content in the PEC do not necessarily indicate the presence of gas (Fig. I.3b). This observation reinforces the idea that the presence of mud close to the bottom decreases permeability and traps gas from below and does not consist of a gas source.

The occurrence of the BS facies is dependent on a low permeability (Fig. I.6h). Thus, it is related to the bottom sediments' mud and sand contents (Merckelbach and Kranenburg 2004; Nooraiepour et al. 2019). The sample with low mud content close to the BS (rhombus symbol south of Antonina zone in Fig. I.3) may indicate that the bottom sand content increase defines the southern limit of this facies.

We state that gas below 1.5 m of sediment does not correlate with the bottom sediments due to the variation of the sedimentary facies in depth. Although samples over the region with a gas presence generally have greater than 60% mud content, there are very few sampling sites in this region. The high mud content in the center of the basin is correlated with the Holocene regressive mud and not necessarily with gas presence in the subsurface.

5.4 Stratigraphy

The gas accumulated in marine and coastal environments interspersed in sediments causes a significant effect on the geoaoustic behavior (Weschenfelder et al., 2016). In this study, over one-third of the acoustic data obtained in the PEC was covered by gas-associated features. Still, we recognized two very distinct seismic units (SU1 and SU2) separated by an RH reflector. The RH shows several paleochannels and high amplitude.

The oldest pre-Holocene unit (SU1) is here interpreted as continental deposits formed during low sea-level conditions (Fig. I.7), the Alexandra Formation (Angulo 1995; Lessa et al. 1998). This formation has high mud contents and is characterized by deposits interpreted as debris flows (matrix-supported conglomerates), mudflows, or even small swamps (Angulo 1995, 2004). The characteristics of the chaotic seismic pattern recognized in this unit can be associated with debris flows, which have large sparse blocks observed in the Alexandra Formation portion (Angulo 1995, 2004). Similarly, the

transparent seismic pattern can be associated with mudflows (muds and sandy muds). However, this study does not include wells to confirm these assumptions. This unit represents the main source of gas, at least in the Paranaguá zone, where it is possible to observe the TP coming out of this unit (P1 in Fig. I.4). Also, the RH reflector in the vicinity of TPs that appear to leave SU1 has a greater amplitude than gas-free regions (P1 in Fig. I.4), indicating a possible enhanced reflection related to discrete gas accumulation that usually occurs in the edges of more evident gas accumulations (Iglesias and García-Gil, 2007; Judd and Hovland 1992). However, we cannot discard the hypothesis of a small amount of gas generation in some mud layers of the SU2.

The youngest unit (SU2) represents a prograding sedimentary body. Considering Lessa et al. (1998) work, this unit should represent Holocene regressive muds deposited over the last 5000 years (Fig.7). These authors recognized this unit directly with continental deposits or with a sandy layer associated with transgressive marine sand (Fig. I.7). According to Lessa et al. (1998), the contact between these two facies results from a transgressive tidal ravine and tidal diastem associated with the estuary tapering (Fig.7). We believe that the HR reflector represents this erosion surface (Fig. I.7) with tidal channels (Fig. II.4b). The SU2 unit is highly heterogeneous, seen through the bottom sediment samples (Fig. I.3) and previous studies (Lessa et al. 1998). Changes in bottom water currents due to freshwater outflow and climatic oscillations, or other oceanographic forcings over the past millennia, have resulted in layers with different physical properties (internal reflectors in SU2 Fig. I.4 and I.5). These layers, observed in SU2, are responsible for trapping the biogenic-derived gas (Fig. I.7). The gas slowly migrates within the SU2 (TP), accumulating in the lower permeability layers (ABD and ABS), until it reaches the sediment-water interface, where, if the right conditions exist, the gas may be trapped one last time (BS) (Fig. I.6). At the same time, gas trapping by SU2 is corroborated by the absence of gas east of Paranaguá city, where regressive muds are absent (Fig. I.7)(Lessa et al. 1998). Also, in some SU2 mud layers rich in organic matter, a small amount of gas can be generated, following the same migration pattern and accumulation mentioned above.

In the Antonina zone, the gas is trapped closer to the sediment-water interface. This shallower gas may be due to a smaller sealing efficiency in internal sedimentary SU2 layers or in-situ generation of gas close to the water column. A smaller water depth and a thin SU2 unit in this region generate low gravitational pressure. With less pressure, the efficiency of the sealing layer decreases, and the gas is more easily saturated in sediment

porewater (Abegg and Anderson 1997; Lee et al. 2005). Also, the Antonina zone probably has lower efficient sealing layers due to the different environmental settings. This zone has greater fluvial influence, where coarser sediments derived directly from the fluvial course are deposited, increasing its permeability (Nooraiepour et al. 2019). Another explanation is that the gas source in the Antonina zone is shallower, associated with SU2 muddy layers deposited when the sea level was at its maximum at the mid-Holocene (Angulo et al. 2006). The crystalline basement appears to be shallower in the Antonina zone, and it is possible to see the contact between the SU2 unit and the basement (Fig. I.5a). However, possibly the SU1 unit was preserved in the basement troughs, which is not visible in seismic due to the gas presence. Other studies indicated that the source of shallow gas is associated with pre-Holocene units preserved in paleo-valleys (Judd et al. 1997; García-Gil et al. 2002; Weschenfelder et al. 2016). The basement locations close to the gas accumulation (A1 in Fig. I.5) may indicate lateral migration (Fig. I.6h).

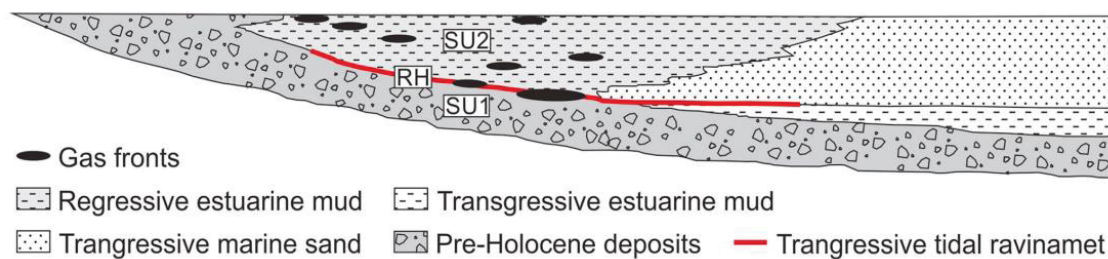


Fig. 7: PEC sedimentary facies evolution (based on Lessa et al. 1998) and the gas-charged sediments recognized in this work.

6 Conclusion

High-resolution seismic surveys were carried out at the Paranaguá Estuarine Complex to analyze intrasedimentary gas accumulation and seismic signatures. The seismic signatures were separated into acoustic blanking with a diffuse top (ABD) or sharp top (ABS), turbidity pinnacles (TP), and black shadow (BS). These features represent distinct gas accumulation types associated with the efficiency of the sealing layer relative to the permeability and gas concentration. As the gas is in constant and slow migration in unconsolidated, mostly flat, sediments layers, seismic gas signatures in the PEC are unstable. Hence, a model of gas migration and accumulation, and its seismic signatures is proposed for the PEC (Fig. I.6).

In PEC, the main gas source is associated with the pre-Holocene continental deposits of SU1 unit. While Holocene regressive muds, unit SU2, trap the gas and may have some local layers generating small amounts of biogenic gas. This unit is highly heterogeneous with layers of low permeability that trap the gas at different levels.

Although we cannot determine the gas migration time scale, this work indicates intra-sedimentary shallow gas dynamics in coastal environments. We suggest that future work may include continuous seismic surveys to monitor gas accumulation types within sediments and the evaluations of CH₄ in the water column. Which would improve our understanding of gas dynamics and gas seepage from coastal environments, and help to unravel the role of estuarine biological methane production on our planet's climate.

Acknowledgments

The authors would like to thank the Brazilian National Council for Scientific and Technological Development (CNPq) for the financial support through the project “Historical overview and future perspectives regarding the occurrence of chemical stressors present in the Paranaguá Estuarine Complex” approved in Edital MCTIC / CNPq 21/2017 (process n ° 441265/2017-0). Thanks, are also due to the Brazilian Coordination for Improvement of Higher Education (CAPES) for the research grants and to the Center for Marine Studies of the Federal University of Paraná for the infrastructure.

References

- In the end of this document -

CAPÍTULO II

Distribution and sedimentary control of shallow gas accumulation in the Santee River Delta marsh (South Carolina, U.S.A.)

Authors: J. F. Pezza Andrade¹, T. J. J. Hanebuth², R. H. Nagai¹

Potential Coauthors: Josh H. Long^{2,3}

¹ Campus Pontal do Paraná - Center for Marine Studies, Federal University of Paraná, Pontal do Sul, Paraná, Brazil.

² Department of Marine Science, Coastal Carolina University, Conway, South Carolina, U.S.A.

³ US Geological Survey, Reston, Virginia, U.S.A.

To be submitted: *Estuaries and Coasts* (ISSN 1559-2731; IF 3.246; Qualis CAPES A2)

Abstract

The presence of sedimentary deposits rich in free gas (bubbles) in estuarine systems strata is recognized worldwide. However, the factors that control the sediment-dependent spatial distribution of the shallow gas within these environments are poorly understood. The main objective of this study is to map gas-charged sediments in the Santee River Delta (central South Carolina, U.S.A.) and investigate its spatial and sub-bottom appearance variability. High-resolution seismic data, physical (grain size and porosity), and chemical (organic matter content) properties, were analyzed on five sedimentary cores taken from two different marsh environments: a widened estuarine river bay (North Santee Bay/NSB) and a marsh creek system (Alligator Creek/AC). The seismic data shows that deposits hosting abundant free-gas are sparsely distributed in the NSB, where data indicate that the sedimentary facies succession restrict the gas accumulation, with a high free-gas concentration in channels around a sand shoal due to the concentration of organic-rich muds deposits. We speculate that sediment permeability has a main role in this case. AC strata, in contrast, contain gas bubbles that are concentrated at a certain depth horizon within the sediment column, but their distribution does not show an obvious dependence on sedimentary parameters that can explain its stratigraphy appearance. We speculate in the latter case that reactivity of organic matter and sedimentation rate along the young seismic unit controls the stratigraphy windows in the creek.

Keywords: Santee Delta; high-resolution seismic; biogenic gas; gas-charged sediments.

Resumo

A presença de depósitos sedimentares ricos em gás livre (bolhas) em estratos sedimentares de sistemas estuarinos é reconhecida mundialmente. No entanto, os fatores

sedimentares que controlam a distribuição espacial do gás raso dentro desses ambientes são pouco compreendidos. O principal objetivo deste estudo é mapear sedimentos carregados de gás no delta do rio Santee (Carolina do Sul, EUA) e investigar sua variabilidade espacial de sub-fundo. Dados sísmicos de alta resolução e propriedades físicas (tamanho do grão e porosidade) e químicas (conteúdo de matéria orgânica) foram analisados em cinco testemunhos sedimentares retirados em dois ambientes diferentes: uma baía estuarina (North Santee Bay/NSB) e um sistema de canal pantanoso (Alligator Creek/AC). Os dados sísmicos mostram que os depósitos de gás livre abundante estão esparsamente distribuídos no NSB, onde os dados indicam que a sucessão de fácies sedimentares restringe o acúmulo de gás, com os depósitos de gás livre em canais ao redor de um banco de areia devido à concentração de depósitos lamosos ricos em matéria orgânica. Especulamos que a permeabilidade do sedimento tenha um papel principal neste caso. Os estratos AC, em contraste, contêm bolhas de gás que se concentram em um determinado horizonte dentro da coluna sedimentar, mas sua distribuição não mostra uma dependência óbvia de parâmetros sedimentares que possam explicar sua aparência estratigráfica. Especulamos, neste último caso, que a reatividade da matéria orgânica e a taxa de sedimentação ao longo da unidade sísmica recente controlam as janelas estratigráficas no canal.

Palavras-chave: Delta Santee; Sísmica de alta resolução; Gás biogênico; Sedimentos carregados de gás.

1 Introduction

Methane gas has been in the focus of various studies due to its significance in planetary climate regulation (e.g., Judd, 2003; Reay, 2010; Schaefer, 2019). Discoveries of large methane deposits in sediments, both in shallow and deep waters, have marked the last decades of coastal and marine exploration (Borges et al., 2016; Judd and Hovland, 1992), indicating that there may be an even greater emission of methane gas from coastal and marine environments than the $33.2 \pm 37.6 \text{ Tg CH}_4 \text{ yr}^{-1}$ estimative (Rosentreter et al., 2021). Also, there is a high spatial and temporal variability in CH_4 emission misconducting statistical analyses (Rosentreter et al., 2021) which can explain recent emissions estimates that adds global marine CH_4 budget (Al-Haj & Fulweiler, 2020; Rosentreter et al., 2021) by more than 60% from previous studies (Weber et al., 2019). Recent studies have also shown that climate warming can accelerate both the release of this sediment-trapped gas into the water column and the significant generation of this gas from the buried organic matter in these coastal environments (Egger et al., 2018; Wallenius et al., 2021).

Seismo-acoustic reflection methods are the most efficient tool for mapping the accumulation of methane gas in the sedimentary sub-bottom (Judd and Hovland, 1992;

Pezza Andrade et al., 2021). When the amount of methane reaches a certain threshold within a deposition succession, depending on production rate as well as the ambient pressure and temperature, through Henry's Law (Serra et al., 2006; Wilhelm et al., 1977), the previously dissolved gas crosses the stage of over-saturation and forms free-gas bubbles. After reaching a certain abundance, these bubbles generate a sharp contrast of acoustic impedance, reflecting most of the seismo-acoustic signal, which results in both a high-amplitude horizon and an effective masking of the underlying strata.

Increasingly, seismo-acoustic surveys in estuaries and bays indicate that these environments are rich in shallow accumulations of methane gas (e.g., Borges and Abril, 2012; Garcia-Gil et al., 2002; Pezza Andrade et al., 2021; Weschenfelder et al., 2016). Due to the high production, rapid deposition, and efficient burial of large amounts of organic matter in these coastal environments, the estuarine deposits produce biogenic methane at high rates through microbial decay (Borges and Abril, 2012; Rice and Claypool, 1981). However, great spatial variability of gas accumulation, detected in seismo-acoustic surveys, is still a matter of debate: While some studies indicate a preference for gas accumulation inside paleo-topographic lows due to the preservation of transgressive muddy infilling packages (Flury et al., 2016; Weschenfelder et al., 2016), other relate the distribution pattern to specific sedimentary facies that constitute the source and seals of gas-charged deposits (Frazão and Vital, 2007; Garcia-Gil et al., 2002). In addition, seismo-acoustic data suggest that most bubble accumulations are defined by sharp lateral boundaries (Pezza Andrade et al., 2021; Toth et al., 2014), thus seem not to correlate with specific, laterally extensive sedimentary facies.

Methanogenesis is the last step of organic matter decomposition in the sedimentary column, occurring in the oxygen-free zone after nitrate reduction, Fe/Mn oxides, and sulfate (Loyd et al., 2012; Rice and Claypool, 1981). Microbially mediated methanogenesis requires a depositional environment with specific characteristics, such as an open interstitial pore space of at least $\pm 1 \mu\text{m}$ (Gang and Jiang, 1985; Rice and Claypool, 1981). Additionally, sedimentation rates need to be relatively high, and a large amount of available organic matter is required as a primary source for methanogenesis. For the entrapment of free methane, the sedimentary stratum permeability must be limited so that the amount of methane generated and rising can both exceed the saturation threshold and accumulate at a certain depth (Katsmans, 2019). However, these pre-

conditions do not help to explain the sharp lateral boundaries of gas accumulations shown in seismo-acoustic data within most estuarine and coastal zones.

In this sense, the present study combines high-resolution sub-bottom echosounder data with physical and chemical properties obtained from sedimentary cores to unravel to what extent changes in sedimentary facies, lithology, and parameters control the vertical and lateral distribution of gas-charged deposits. For this purpose, we mapped the spatial distribution of gas-charged deposits in two environments the Santee River Delta (North Santee Bay/NSB and Alligator Creek/AC; South Carolina), and evaluated physical (grain size, porosity) and chemical (organic matter content) sediment properties that may have control on gas bubble formation and concentration within the sedimentary column. The results presented here may help to unravel controlling factors of free-gas availability within the estuarine systems.

2 Settings

The Santee River Delta (Fig. 1) is a mixed-energy estuarine river delta, located in South Carolina, with an area of approximately 100 km² (Hughes et al., 1995; Long et al., 2020). This coastal system is fed by the Santee River, which is a Piedmont-draining fluvial system, the second largest river along the US east coast, with a drainage area of 37,000 km² and an average annual discharge of 311 m³/s (Hughes et al., 1995; Long, 2020; Torres, 2017). On the innermost part of the delta plain 23 km apart from the coast, the Santee River bifurcates into the North Santee River and the South Santee River (Fig. 1). Both rivers split further into an estuarine channel network and significantly widen in proximity to the mouth, where the tidal range is approximately 1.16 m (Torres, 2017).

The Santee River Delta is placed on a limestone basement, which was incised by the 8 km wide buried Santee valley, and it is partly exposed at the bottom of fluvial channels at approximate depths of 10 meters below modern sea level (Eckard, 1986; Long, 2020; Payne, 1970; Weems & Lewis, 1997). The incised valley is filled with Pleistocene fluvial deposits overlain by Holocene delta-plain deposits that are bound by Pleistocene beach ridges (Long, 2020). The mid-Holocene sea-level highstand was marked by a freshwater floodplain environment covered by estuarine tidally influenced deposits that formed over the past 3.6 cal ka BP (Eckard, 1986; Long, 2020; Weems & Lewis, 1997).

The Santee River Delta has undergone several anthropogenic modifications (Lewis, 1979; Long, 2020; Miglarese & Sandifer, 1982). Two major dams along the lower reach of the river, built in 1941, dramatically reduced the freshwater discharge and sediment flux of the Santee River (McCarney-Castle et al., 2010). Also, an artificial canal (Atlantic Intercoastal Waterway) was constructed in the 1930s that connects naturally not connected hydrographic systems of the Winyah Bay estuary to the north, the Santee system, and the Cape Romain barrier island region to the south (Fig. 1). Currently, the Atlantic Intercoastal Waterway is approximately 3 m deep and 120 m wide and affects tidal currents, salinity, and sediment transport (Hockensmith, 2004). In addition, rice cultures from the 18th to the early 20th century led to a region-wide conversion of river swamps and freshwater marshes into patties with dense canal networks, embankments, artificial levees, and flood gates. Long (2020) showed that this modification has strongly influenced the distribution of modern depositional facies due to a reduction of tidal flats, channels, and banks stabilization, isolation of channels and floodplain environments, and alteration of the tidal prim of the back barrier system.

Marsh that composes most of the Santee Delta (Fig.1) has about 10% of organic content (Settlemyre & Gardner, 1977), and are dominated by *Spartina alterniflora*, a perennial rhizomatous grass native to the North America Atlantic and Gulf coasts (Broome et al., 1973; Hughes et al., 1995; Wang et al., 2006). *Spartina* biomass production in the SD is between 280 to 1550 g/m²year (Broome et al., 1973; Settlemyre & Gardner, 1977). Also, the marsh platform channel creeks have a fast headward erosion of ~2m/year (Hughes, 2010; Hughes et al., 2009) enhanced by degradation of the *Spartina* roots and rhizomes biomass associated to crab bioturbation (Wilson et al., 2012).

Two locations in the Santee River Delta were chosen for this study (Fig. 1). North Santee Bay (NSB) is a 1 km wide, and 3 m shallow bay located near the mouth of the North Santee River (Fig. 1, 2a). The northwestern area of the bay is shallower than the margins due to the existence of a diagonal sand shoal that is bound by two channels between this shoal and the marsh edges which lies at approximately 10 cm water depth during spring low tides (Long, 2020). This bar extends over 2 km and has a vertical elevation of approximately 2.5 m with a maximum width of 500 m (Fig. 2a; Long, 2020). The second location, Alligator Creek (AC) is a 2 m deep and 25 m wide natural tidal channel of the South Santee River with a predominantly muddy seabed (Fig. 1, .3a).

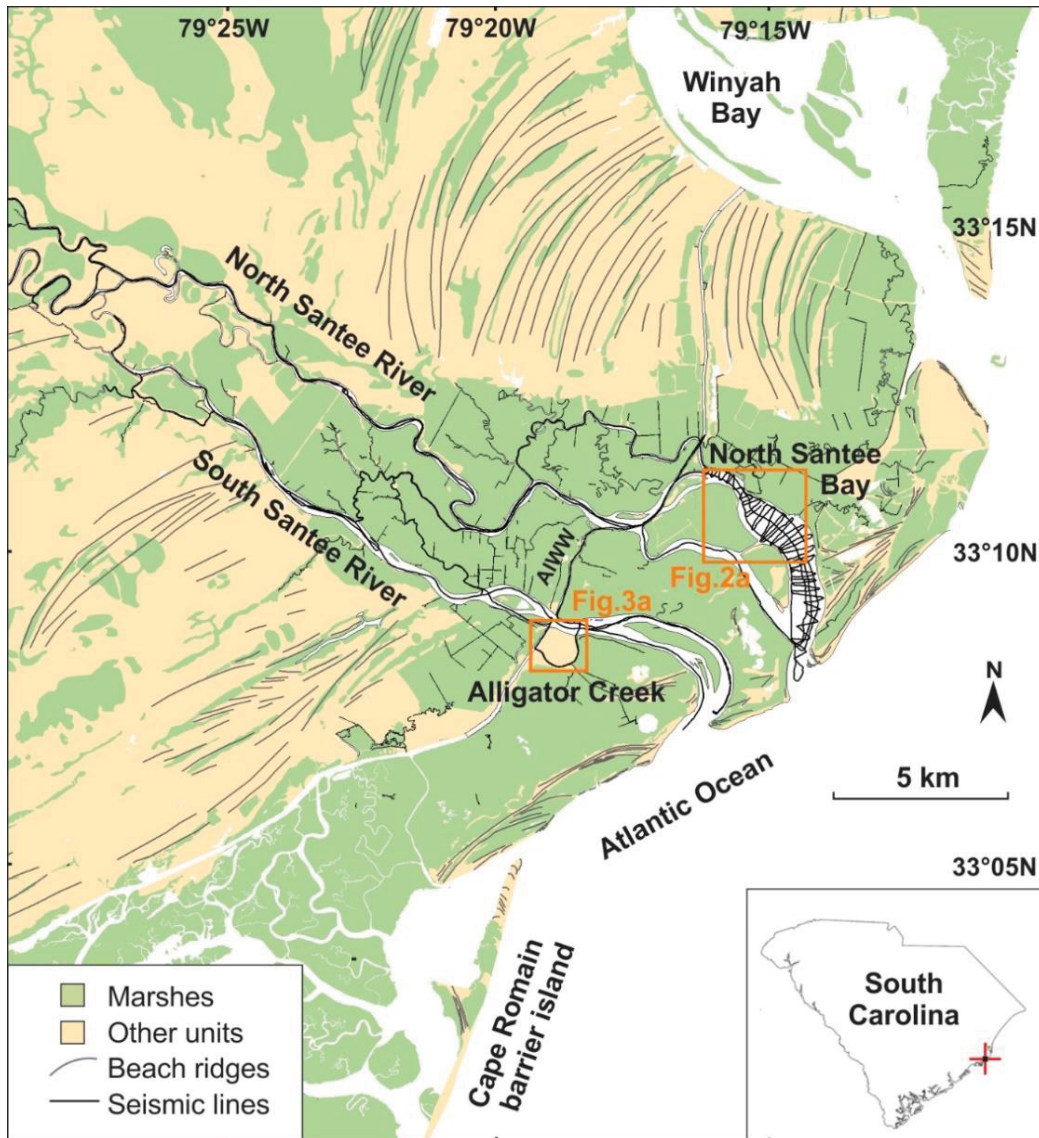


Fig. 1: The Santee River Delta with the two study areas: The North Santee Bay and the Alligator Creek. Black lines indicate the seismo-acoustic survey coverage.

3 Material and Methods

Approximately 800 km of high-resolution sub-bottom echosounder data was analyzed to trace down the appearance of shallow sub-bottom gas accumulations in the Santee River Delta (Fig. 1). The data were collected in 2016 and 2017 using a 3200 sub-bottom profiling system with a CHIRP source providing a frequency range of 2 – 4 kHz (Long, 2020). These data sets were processed and interpreted using the software IHS Kingdom Suite™. Seismo-acoustic gas signatures were identified where high-amplitude horizons that also led to a masking of the underlying and adjacent strata were present (Pezza Andrade et al., 2021; Weschenfelder et al., 2016). Based on this identification,

NSB and AC sites that showed a significant free gas concentration were selected for sedimentary core retrieval.

Five sediment cores were acquired using a hand-operated piston corer, of which three were taken in the NSB (Fig. 2) and two in the AC (Fig. 3). After core retrieval, the transparent PVC liners were cleaned immediately onboard, and all visible bubbles were outlined with a permanent marker pen. In the lab, the marked bubble positions were sketched and digitalized. The bubbles were classified into three specific size categories, which were most representative of the overall size variation spectrum observed in the cores: <5 mm, 5 – 20 mm, and > 20 mm. The sediment cores were opened in the laboratory, and their lithological characteristics were visually described. Lithological units were separated mainly by color variations.

Using 10 ml syringes with a cut tip, 4 ml of sediment was extracted at step intervals of 5 cm. Each sample was divided in half; 2 ml of sediment was used for determining porosity and total organic matter content (TOC) analysis, and 2 ml was used for granulometric analysis.

Dry bulk density and porosity were acquired using the drying technique. The samples were weighed before and after drying in an oven at 105°C for at least 48 hours for measurements of dry mass and water content. The dry mass was divided by the sample volume for calculating dry bulk density. The water volume was calculated through the water content (1ml/g) and then divided by the sample volume for the porosity (Boyce, 1973). For TOC measurement, the same samples were heated up to 550 °C for 5 hours and weighed again (Loss-On-Ignition Method; Schulte 1996). The granulometry samples were pretreated with 30% hydrogen peroxide to remove organic constituents and aid particle deflocculation and boiled off after 24 hours. Carbonate removal was done by adding 2-3 mL 10% hydrochloric acid to each sample overnight which was then removed by centrifugation. Lastly, 3 ml dispersant (Calgon) was added and boiled off for 2 minutes. The grain-size analysis was performed using a 1090 CILAS laser refractometer. The granulometric data was analyzed using the Sysgram software to determine mean grain size and to separately display clay, silt, and sand contents (Camargo, 2006).

Comparison of physico-chemical properties of the sediments between cores section with and without bubbles presence were performed with the non-parametric

Mann-Whitney test. Significance was set at $p < 0.05$. Statistics were performed in the PAST 4.03 software.

4 Results

4.1 North Santee Bay (NSB) sub-bottom profiles

NSB sub-bottom echosounder data shows three isolated patches of shallow-gas accumulation recognized via the presence of a high amplitude horizon (Fig. 2): one patch of about $1,180 \text{ m}^2$ is located where the river channel begins to widen into the bay; the second sits north of the sand shoal with an area of approximately $1,540 \text{ m}^2$; and the most extensive third gas zone of about $2,400 \text{ m}^2$ at the southern margin of the bay, half on the sand shoal and half in the tidal channel along the marsh edge (Fig. 2b). The main gas area shows its top reflection halfway down within the channel filling unit. The sub-bottom profiles indicate that the internal reflectors within the sand shoal dip towards the south (Fig. 2d) and is possible to differentiate seismo-acoustic signature characteristics of free gas in the form of an enhanced reflector and a local pinnacle (Fig. 2c). Noteworthy, the top of the gas horizon follows the bottom topography (Fig. 2d).

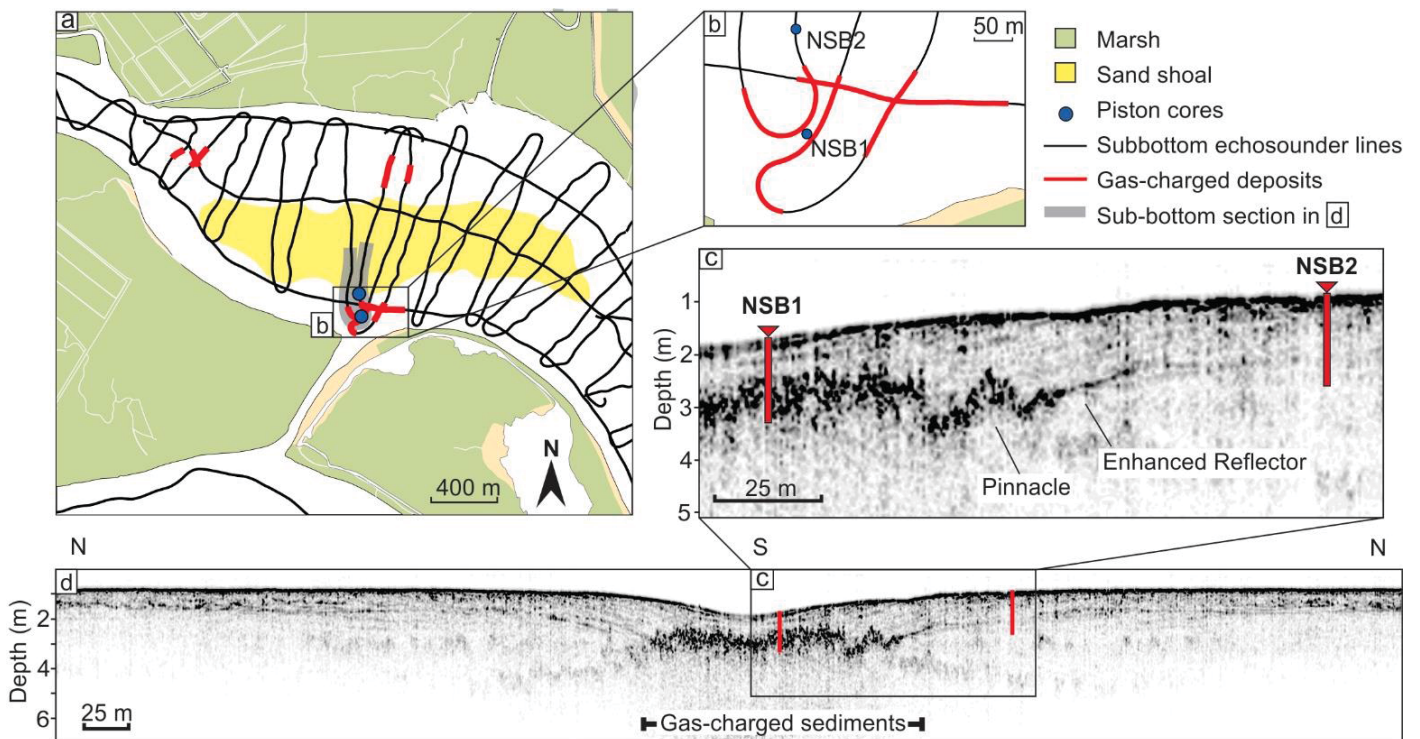


Fig. 2: The North Santee Bay study area. a) Location of the sub-bottom echosounder lines (black lines), core sites (blue dots), and gas-charged deposits (red lines); b) A closer view

on the most extensive gas zone at the southern margin of the bay chosen for the NSB1 and NSB2 core sites; c) Echosounder profile with gas signatures and cores; d) A closer view on the gas signature and cores position.

4.2 NSB Sediment cores

Core NSB1 was retrieved from the gas-charged deposits located close to the southern margin of the bay, while for comparison Core NSB2 was recovered from a gas-free zone 50 m north of the lateral gas limit (Fig. 2b).

Tab. 1: Studied sediment cores (ID; see Fig. 2 and 4 for core sites), geographic coordinates, water depth (m), sediment recovery (cm), indication of gas deposits presence, depth of gas signature top in the seismic data (cm), shallower and deeper depth of bubble occurrence (cm) and thickness (cm)

ID	Coordinates	Water depth	Sediment recovery	Gas zone	Seismic gas top depth	Core gas top depth	Core gas bottom depth	Gas horizon tickness
NSB1	79.25404° W 33.16768° S	1.70 m	162 cm	Yes	80 cm	80 cm	Not reached	–
NSB2	79.25359° W 33.16863° S	0.85 m	175 cm	No	–	–	–	–
AC1	79.31392° W 33.13636° S	1.15 m	185 cm	Yes	45 cm	40 cm	160 cm	120 cm
AC2	79.31356° W 33.13650° S	1.70m	120 cm	No	–	–	–	–
AC3	79.31436° W 33.13606° S	1.20 m	200 cm	Yes	50 cm	40 cm	140 cm	100 cm

4.2.1 Sediment core NSB1

Core NSB1 comprises two distinct lithological units separated by a sharp contact (Tab. 1; Fig. 3a). The older unit (162 – 132 cm) is composed of light gray mud (mean diameter 9.96 μm) with several grass fibers throughout. TOC varies between 12.2% to 16.3% (median 14.6%). Porosity ranges from 70.8 and 80.9% (median 74.6%). The younger unit (132 – 0 cm) is composed of dark gray sandy mud and mud (mean diameter 10.97 μm), with two bivalve shell fragments at 37 and 118 cm depth. TOC values are between 6.7 and 19.5%, with a median value of 15.7%. Porosity is slightly higher than in the older unit ranging between 69.9 to 87.9% with a median of 81.4%. Gas bubbles are mainly present in the older unit with a density of 4 to 5 bubbles per 10 cm where half of the bubbles are bigger than 20 mm in diameter. Upwards the bubbles decrease in

abundance and size with a mean density of 1 to 2 bubbles per 10 cm and $\frac{3}{4}$ of them are less than 5 mm in diameter, until completely disappearing above 80 cm sediment depth. Within the bubble depth interval, TOC is always above 12.5% around a median value of 15.8%. At 80 cm, the last few isolated gas bubbles occur in relatively coarser sediment (10% sand) of lower porosity (60.9%) and TOC (6.7%) (Fig.3). There are no significant differences between porosity, TOC, and clay and silt contents in sections with and without bubbles (Tab. 2). However, core section with bubbles showed significant less sand content (Tab. 2).

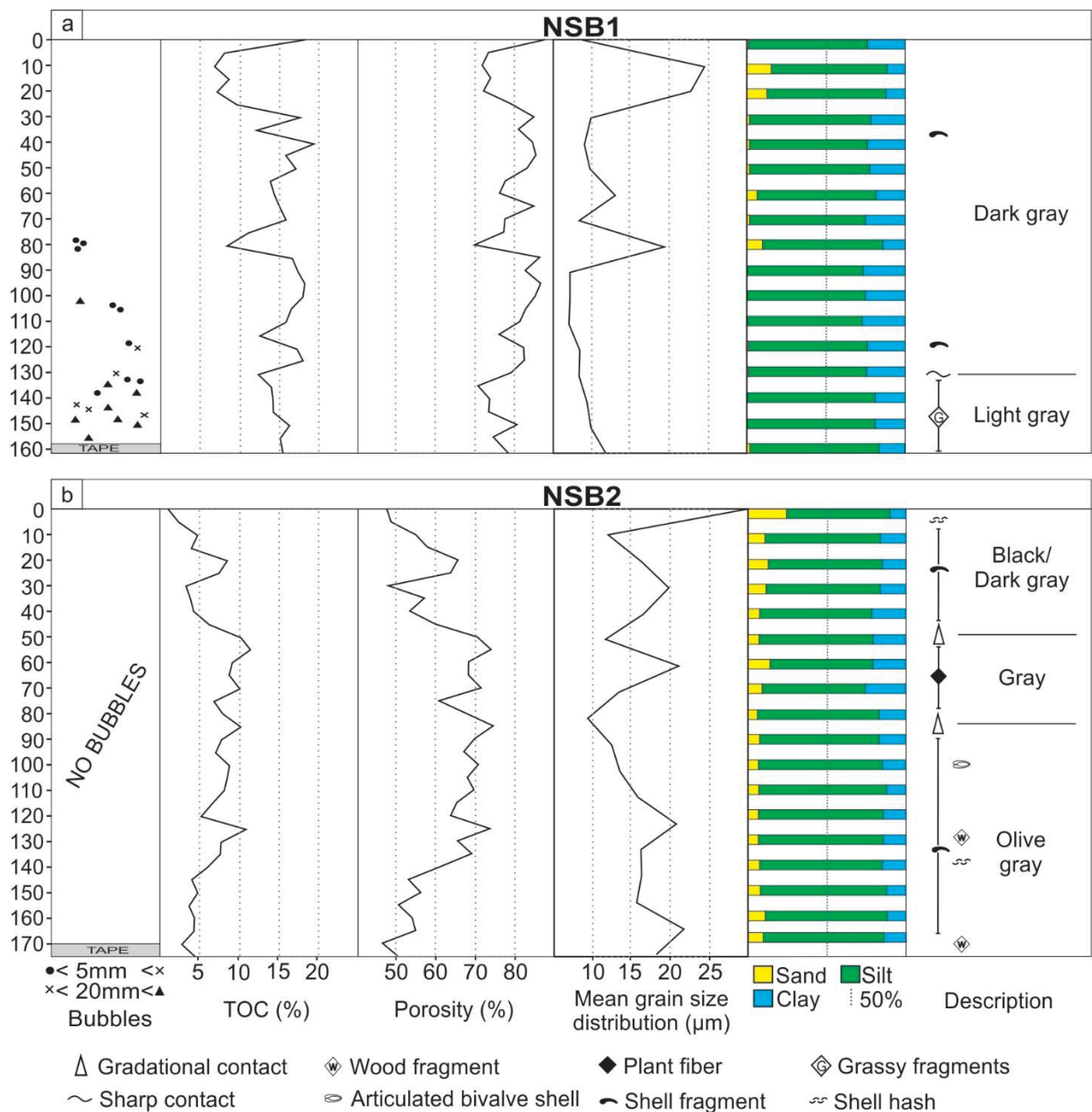


Fig. 3: North Santee Bay sediment cores (a) NSB1 and (b) NSB2 showing the free-gas bubbles detected through the transparent PVC pipes and separated in three sizes; organic

matter content (TOC) in percentage (%); porosity in percentage (%); mean grain size (μm); clay-silt-sand contents.

4.2.2 Sediment core NSB2

Core NSB2 comprises 175 cm of sediment separated into three distinct lithological units, mainly by color variations, with gradual contacts with each other (Tab. 1; Fig. 3b). The older unit (175 – 85 cm) is composed of olive gray silt (mean diameter 16.63 μm) with shell fragments. This older unit shows two big wood fragments at 128 and 170 cm, a bivalve shell at 100 cm, and a 2 cm thick shell hash layer at 137 to 135 cm. TOC varies between 2.6 and 10.8% (median 6.2%) and porosity ranges between 46.6 and 73.8% (median 64.5%). The middle unit (85 – 50 cm) is composed of gray silt with few plant fragments throughout and no shells/fragments present. This unit has the highest TOC and porosity values with median values of 8.9% (max. 11.3%, min. 6.7%) and 68.4% (max. 74.8% and min. 60.9%), respectively. The young unit (50 – 0 cm) consists of dark gray to black sandy silt with sparse shell fragments and a 2 cm shell hash close to the surface (4 – 6 cm). TOC ranges between 1 to 8.4% with a median value of 4.1% and porosity between 47.5 to 70.6% with a median of 57.3%.

4.3 Alligator Creek (AC) sub-bottom profiles

The AC sub-bottom profiles show a high amplitude and irregular horizon that masks the underlying stratigraphy (Fig. 4d). This seismo-acoustic signature is associated with the concentrated presence of free gas within the deposit. Although this horizon appears laterally irregular, it displays a rough correlation with the channel bottom topography (Fig. 4d). Between the gas-charged zones, the stratigraphic windows over a stretch of about 500 meters allow for an insight into at least two main seismo-acoustic units (AC-SU2 and AC-SU1 in Fig. 4d). The younger unit shows undulating parallel near-horizontal reflectors of low to moderate amplitude (Fig. 4d). The older unit is characterized by a high-amplitude top reflector and sets of southward-dipping internal reflectors (Fig. 4d). Along and around these stratigraphy windows, five laterally confined areas of gas are present within the younger unit, of which three are less than 20 m in extent. The main gas area is 1645 m wide (Fig. 4a and d). The top of the gas reflection of each of these five gas-containing areas is positioned below the upper third of sediment within the younger unit.

Tab. 2: P values of the Mann-Whitney comparison of porosity, TOC, clay, silt, and sand contents between core sections with and without bubbles presence. Significant differences occur when $p < 0.05$ (bold values).

	Porosity	TOC	Clay	Silt	Sand
NSB1	0.9425	0.1654	0.0806	0.6267	0.00006
AC1	0.6891	0.3401	0.8294	0.8055	0.2953
AC3	0.9272	0.5573	0.4263	0.4416	0.0609

4.4 AC Sediment cores

Two sediment cores, AC1 and AC3, were taken in the eastern portion of the gas-charged deposits, 18 and 80 m apart of the to the stratigraphy window respectively (Fig. 4). Core AC2 was taken in the western region of the stratigraphy window, between the main gas-charged area (26 m apart) and an isolated gas spot right north of it (20 m apart; Fig. 4). The cores are aligned with distances of 64 m between AC1 and AC3, and 46 m between AC3 and AC2 (Fig. 4b).

4.4.1 Sediment core AC1

Core AC1 comprises 185 cm of the sediment column (Tab. 1; Fig. 5). It is possible to distinguish four lithological units with gradational contacts. The lower unit (185 – 145 cm) is composed of light yellowish mud (mean diameter 4.39 μm) with a 2 cm thick wood-fragment layer at 180 cm. TOC ranges from 14.0 to 19.3% (median 15.8%) and porosity between 67.1 and 79.5% (median 73.4%). The second unit (145 – 72 cm) consists of olive brown mud (mean diameter 4.88 μm) showing faint dark gray lamination becoming more visible with increasing depth. This unit shows 14.5 to 18.0% in TOC (median 15.6%) and a porosity between 70.3 and 85.3% (median 79.6%). The third unit (70 – 20 cm) is a black to dark gray mud (mean diameter 4.49 μm) layer with a TOC between 14.9 and 20.2% (median 16.1%) and a porosity of 76.3 to 86.0% (median 79.8%). The youngest unit comprises gray mud (mean diameter 4.91 μm) with median TOC and porosity values of 17.3 and 82.3%, respectively. Core AC1 contains a gas bubble horizon at 160 to 40 cm sediment depth, stretching from the central part of the lower unit across the second unit and up into the central part of the third unit. The abundance of bubbles between 160 and 130 cm is about 4 bubbles per 10 cm with sizes

always bigger than 5mm and half of it is bigger than 20mm, it decreases in the section of 130 to 90 cm with densities of about 1 bubble per 10 cm with sizes between 5 to 20 mm, and it increases again between 90 and 40 cm with a mean density of 5 bubbles per 10 cm. There are no significant differences between porosity, TOC, and clay, silt and sand contents in sections with and without bubbles (Tab. 2).

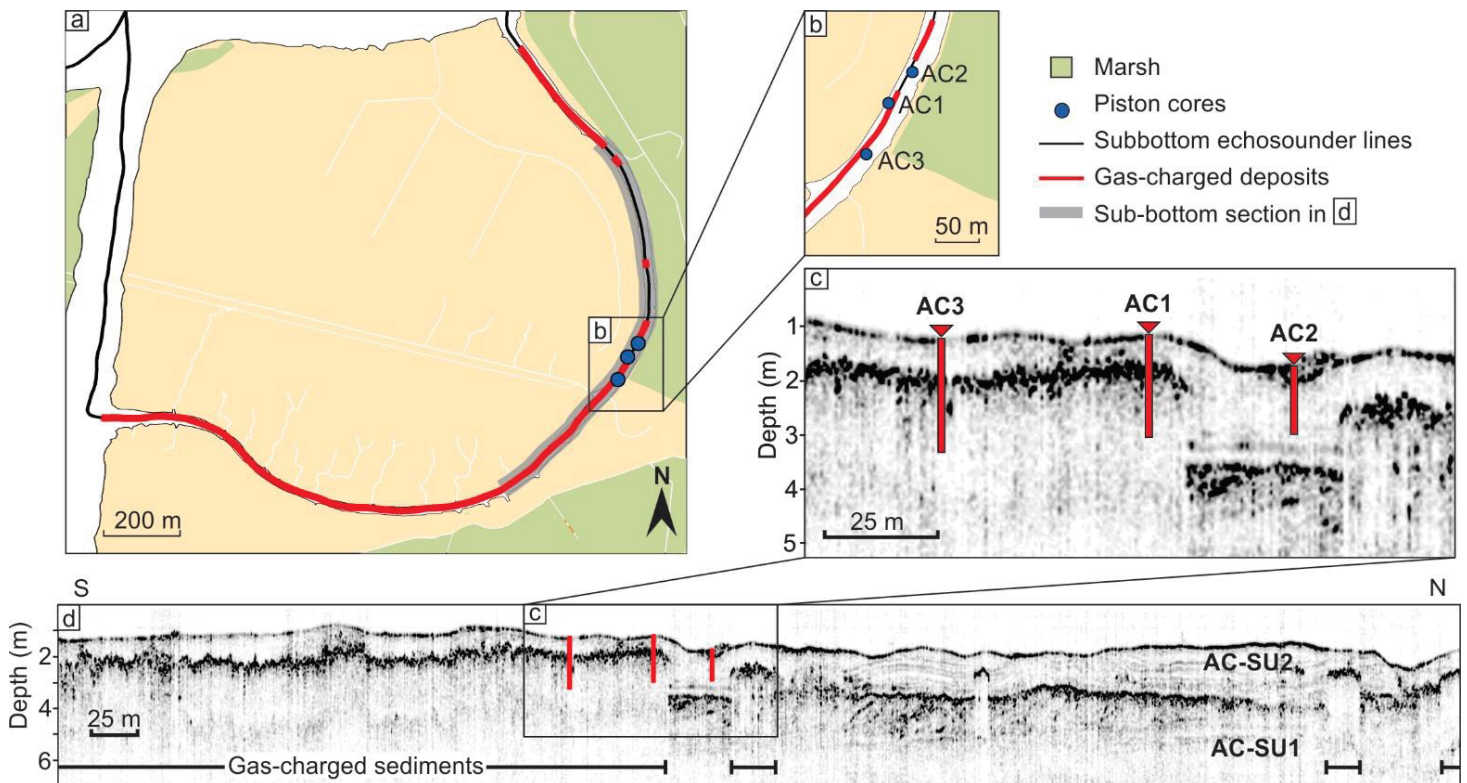


Fig. 4: The Alligator Creek study area. a) Location of the sub-bottom echosounder lines (black lines), sediment core sites (blue dots), and gas-charged deposits (red lines); b) A closer view on the stratigraphy window chosen for Core AC2 and nearby gas zone chosen for Cores AC1 and AC3; c) Sub-bottom profile with gas signatures and core sites; d) A closer view on the gas signature and cores locations.

4.4.2 Sediment core AC2

Core AC2 has a recovery of 120 cm, comprises four distinct lithological units, and does not contain any gas bubbles (Tab. 1; Fig. 5). The lower unit (120 – 108 cm) comprises a light yellowish-brown mud (mean diameter 4.55 μm), which is faintly laminated, with median TOC and porosity of 15.9% and 73.8%, respectively. The second

unit (108 – 90 cm) is separated by a sharp contact from the underlying unit and consists of olive brown mud (mean diameter 4.61 μm). This unit contains a 3-cm thick organic layer at 96 cm and displays median TOC and porosity values of 15.8% and 74.8%, respectively. The third unit (90 – 55 cm) is composed of olive brown mud (mean diameter 4.43 μm) with a wood fragment at 84 cm and is separated by a gradual contact from the above and underlying units. TOC ranges from 14.8 to 16.0% (median 15.4%) and porosity from 78.3 to 81.3% (median 79.6%). The youngest unit (55 – 0 cm) is composed of black to dark gray mud (mean diameter 4.55 μm) with a wood fragment at 33 cm. TOC unit varies between 14.1 and 18.2% (median 15.2%) and porosity between 69.1 and 90.4% (median 82.1%). Small plant fragments and fibers are abundant throughout the entire core.

4.4.3 Sediment core AC3

Core AC3 has a length of 200 cm and comprises four lithologic units with gradual contacts with each other (Tab. 1; Fig. 5). The lower unit (200 – 120 cm) is composed of light yellowish-brown mud with a great abundance of small wood fragments and a detrital organic layer at 177 cm. This unit shows the lowest porosity across the core ranging from 65.7 to 77.0% (median 72.7%) and a slightly lower TOC ranging from 12.9 to 17.2% (median 15.7%). The second unit (120 – 95 cm) displays a strikingly laminated olive-brown and gray mud. TOC varies between 14.6 and 17.3% (median 16.1%) and porosity between 67.9 and 82.5% (median 76.9%). The third unit (95 – 31 cm) consists of gray to dark gray mud with a layer of organic detrital fragments at 38 cm. TOC spans 15.3 to 20.4% (median 16.2%) and porosity 74.3 to 87.3% (median 79.8%). The youngest unit (31 – 0 cm) is composed of black to dark gray mud with faint lamination. TOC varies from 15.7 to 17.4% (median 15.9%), except for a maximum of 24.3% within the surface sample. The median porosity in this unit is 84.5%, ranging from 75.5 to 88.5%. The core shows a well-defined gas bubble layer between 140 cm and 40 cm with the higher abundance observed in this study of about 10 bubbles per 10 cm. Noteworthy, the 20 cm of the gas layer on top and the bottom shows bigger bubbles with about 2/3 of the bubbles being between 5 to 20 mm and 1/3 being bigger than 20 mm. There are no significant differences between porosity, TOC, and clay, silt and sand contents in sections with and without bubbles (Tab. 2).

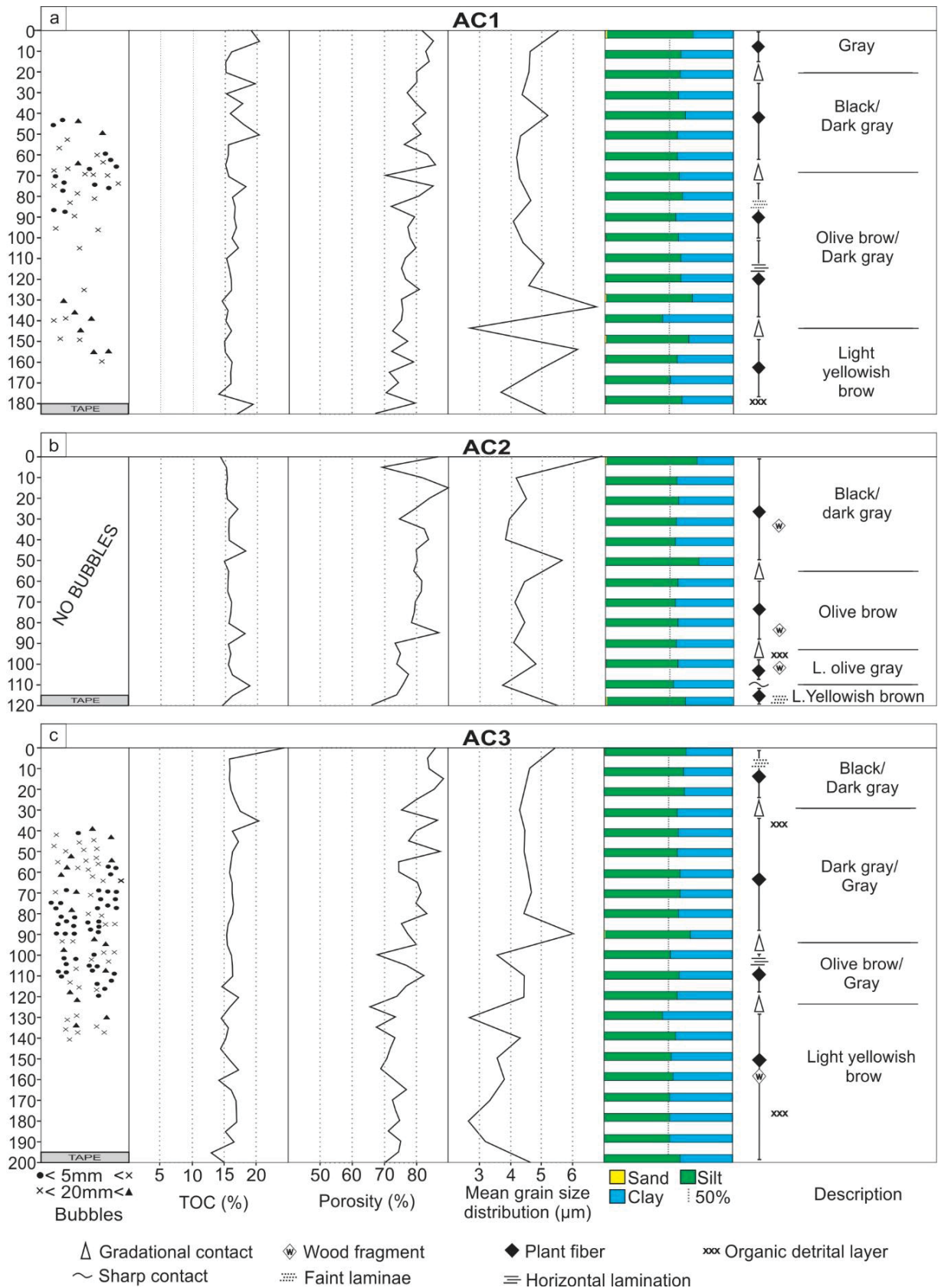


Fig. 5: Alligator Creek sediment cores (a) AC1, (b) AC2, and (c) AC3 showing the gas bubbles recognized in the cores through the transparent PVC pipes and separated in three sizes; Organic matter content (TOC) in percentage (%); Porosity in percentage (%); Mean grain size (μm) Clay-silt-sand content.

5 Discussion

5.1 Horizontal variability of free gas in the Santee Delta

Shallow gas formation and accumulation in submerged sedimentary deposits occur under a regime of significant organic matter input associated with fine-grained lithic material (Grasset et al., 2021; West et al., 2012; Bergamaschi et al., 1997). In coastal zones, free-gas presence is normally related to Holocene mud facies (Garcia-Gil et al., 2002; Lee et al., 2002; Pezza Andrade et al., 2021) that became preserved within paleo-topographic lows (Weschenfelder et al., 2016). As in these specific accumulation settings, the hosting mud deposit is thick enough for the local amount of methane to exceed saturation limit in the porewater (Jensen and Bennike, 2009; Thießen et al., 2006; Tóth et al., 2014), resulting in free gas deposits (Abbeg 1997). In this sense, both studied areas (AC and NSB) meet the prerequisites as bubbles deposits were recognized in the two locations. However, the NSB is a wide bay where the gas accumulation is restricted to few locations and the AC is a narrow creek dominated by gas with few stratigraphy windows (Fig. 1).

Our data indicate an apparent relationship between gas-charged sediment zones with the NSB morphology as the presence of the sand shoal restricts the deposition of fine sediments in the NSB margins. Mud deposits containing free gas are spatially restricted to paleo-reliefs associated with channel fill facies (Weschenfelder et al., 2016). Our core results together with previous mapping of the sand shoal (Long, 2020) indicate that the sedimentary facies distribution in NSB is an important factor in the spatial restriction of gas-charged sediments (Brothers et al., 2012; Frazão and Vital, 2007; Garcia-Gil et al., 2002) as it is associated with the muddy facies (Weschenfelder et al., 2016). However, the reason of the three preferred locations of gas deposits formation is beyond the results presented here as it would be necessary to evaluate a larger number of cores to investigate sedimentary differences along the side channels of the sand shoal.

On the other hand, the AC bottom morphology shows no singular characteristic, and its seismic units are apparently constant along the channel. our results indicate that the youngest seismic unit (AC-SU2) comprises the gas source and sealing, has a relatively flat bottom, and probably extends to most of the AC. The stratigraphy window of the AC-SU2, where the AC2 core was retrieved, is associated to a bathymetric low, thus it is in a thinner section of the AC-SU2 (Fig. 4). Variation in thickness of the sedimentary stratum

corresponding of the CH₄ source were associated to the presence of bubbles since it promotes higher rates of methanogenesis and a shallowing of sulfate-methane transition zone (SMTZ) (Flury et al., 2016), which may explain the lack of bubbles. However, this do not seem to be the case as northward of the AC2 the AC-SU2 get thicker again, and no gas is recognized in the acoustic profile (Fig. 4d).

Additionally, TOC, porosity, and grain-size sort are similar between the gas-charge sediments and the stratigraphy windows which results in a similar acoustic impedance and thus a single seismic unit (Hamilton, 1971; Wang et al., 2021). However, AC coring results showed different lithologic units composing the AC-SU2 that may reflect in distinct sedimentation rates, and thus oxygenation during the deposition (Canfield, 1993), and organic matter reactivity along the AC-US2, which is directly correlated to methane production (Sobek et al., 2012; West et al., 2012). Therefore, although the variation of thickness of the AC-SU2 do not appear to control the horizontal distribution of the gas, the undulated characteristic of its internal reflector and the different units retrieved in the cores indicated important sedimentary variations along the AC-SU2.

Results showed that in both locations (NSB and AC) the gas deposits spatial distribution is associated to muddy channel fill facies. However, although sedimentary facies can restrict the gas deposit spatial distribution, the same depositional environment can display location with and without free gas. We speculate that variation of sedimentation rates and organic matter reactivity within the AC-SU2 along the extension of the AC is responsible by the spatial distribution of the stratigraphy windows. In the NSB, same variations should occur along the sand shoal side channels infill in the deep source unit and, also, changes in sediment grain size sort along the channel younger unit which should change permeability.

5.2 Vertical variability of free gas

The seismic data showed high-amplitude horizons interpreted as gas accumulation in the sub-bottom sediments of the Santee Delta (Fig. 2 and 4). This interpretation was evidenced by the presence of bubbles in the sedimentary records at similar depths to the high-amplitude horizons in the seismic profiles (Tab. 1). The accumulation of bubbles in the sedimentary column can form by *in-situ* saturation of CH₄ (Li et al., 2016) and

upwards migration of CH₄ bubbles (Katsman, 2019; Pezza Andrade et al., 2021). The NSB1 core result showed an increase in bubbles density downward and seismic profiles displayed a pinnacle signature which indicate migration (Iglesias and García-Gil, 2007; Klein et al., 2005; Pezza Andrade et al., 2021; Weschenfelder et al., 2016). On the other hand, AC core results showed that in the AC the bubbles deposit has only about 1 m thick and thus should be formed by *in-situ* saturation.

The saturation of methane and formation of bubbles depends on the salinity, temperature, pressure, and amount of methane (Abegg & Andersonb, 1997; Yamamoto et al., 1976). Along the acoustics profiles the temperature and salinity should be similar due the small length of the profiles and pressure in the pores of shallow unconsolidated sediments is associated with the water column weight (normal pore pressure; Zhang, 2011). Therefore, methane saturation in the studied areas depends mainly on the amount of methane and the depth. However, seismic profiles indicate that gas top horizon seems to follow the bottom topography rather than to the water depth (Fig. 3 and 5).

Additionally, the amount of methane depends on production and consumption rates (Barnes & Goldberg, 1976; Crill & Martens, 1983). Methanogenesis in the sedimentary column occurs in the oxygen-free zone after the reduction of nitrate, Fe/Mn oxides, and sulfate (Loyd et al., 2012; Rice and Claypool, 1981). Thus, salinity and sulfate content are important factors regulating the dynamics of methanogenic communities in coastal environments (Torres-Alvarado et al., 2013), since it affects the depth of the SMTZ coupled with the anaerobic oxidation of methane (AOM; Borges and Abril, 2012; Sawicka and Brüchert, 2017; Treude et al., 2005). The gas top horizon in AC seismic data roughly follows the bottom topography being around half a meter under the bottom surface (Fig. 4d). This characteristic may indicate that this free gas zone top limit is associated with the SMTZ (Baltzer et al., 2005; Boetius et al., 2000; García-Gil et al., 2011). The NSB free gas also has a gas top horizon that follows the bottom topography getting deeper in the deepest section of the channel. However, different than the AC, internal reflectors in NSB acoustic profiles dip to the channel center (Fig. 3).

In the NSB the free-gas zone has similar TOC values (Tab. 2) of the above no-gas zone. However, bubbles starts with low density between 80 to 130 cm (Fig. 5), where the sand content significantly decreases (Tab. 2) which should decrease the permeability (Bryant et al., 1975; Dasgupta & Mukherjee, 2020). The high density of bubbles concentrates in the lower muddy unit (Fig. 5). There is no significant difference in TOC

(Mann-Whitney test, $p = 0.4530$) and grain size (Mann-Whitney test, $p = 0.0564$) between the free gas section of the upper and lower units that justify the increase of bubbles (Tab. 2; Fig. 3). However, data shows significant less porosity (Mann-Whitney test, $p = 0.0127$) and a considerable increase of the dry bulk density (measured for porosity calculations) that can be associated to a high compaction degree since TOC and grain size maintained similar values (Fig. 6). As compaction increases for the old unit it generates a decrease in the unit permeability (Bourg & Ajo-Franklin, 2017; Dasgupta & Mukherjee, 2020) elevating the free gas retention capacity. Also, methanogenesis and CH_4 concentration decreases close to the surface due the SMTZ ((Martens et al., 1998; Rice & Claypool, 1981). On the other hand, in the AC there is no threshold of inferred compaction degree associated to the bubbles accumulation (Fig. 6).

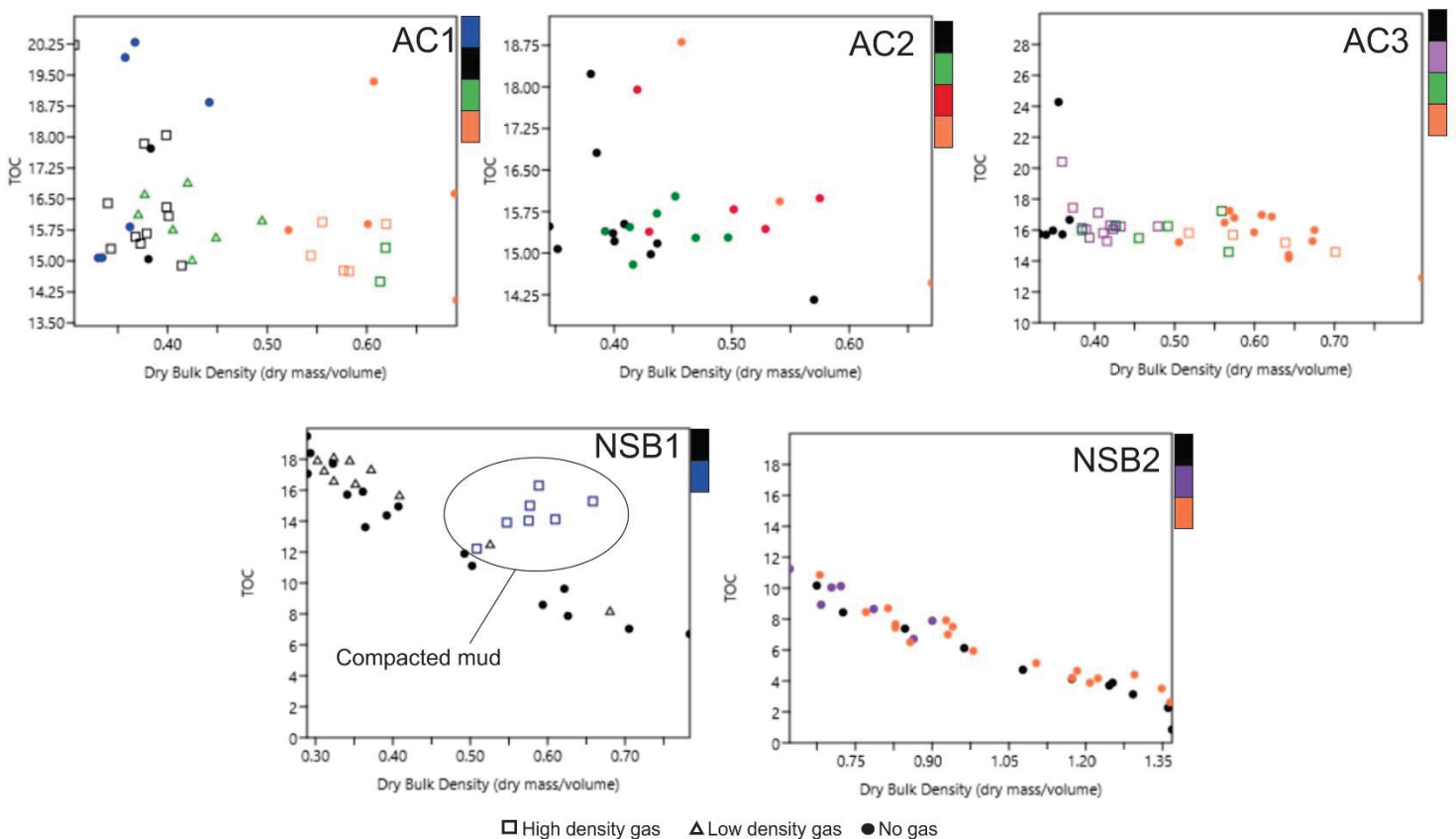


Fig. 6: Cross-plot of total organic carbon (TOC) and Dry Bulk Density of the lithologic units (color bar, top to bottom colors represent units sequence) retrieved in the sedimentary cores.

In addition, the bottom boundary of the free gas deposits in the AC is about 1 m thick. The vertical size of the bubble deposit is hard to compare to other locations since most studies don't recognize the thickness of the gas deposits due high resolution seismic data and most cores are restricted to the upper part of it (Flury et al., 2016; Gorgas et al., 2003; Jensen and Bennike, 2009; Thießen et al., 2006). The bubbles accumulation in the AC seems to be limited by the lower yellowish unit. At depth, organic matter is older and presents lower reactivity, being more difficult to be degraded (Meister et al., 2013). Also, variations in the source of organic matter and accumulation rates over time can result in different reactivities (García-García et al., 2007; Zander et al., 2020). In addition, the yellowish color at the bottom of the cores may indicate a lower sedimentation rate and thus enhanced oxygenation during the deposition (Giosan et al., 2002; Pantin, 1969).

Therefore, we speculate that the main factor that controls the top boundary of the free-gas deposits in the AC is the SMTZ. On the other hand, the retention capacity of the sediments has an important role in the location of the top boundary of the free-gas in the NSB where the upwards migration of bubbles occurs.

Conclusion

Acoustic data is the most powerful tool to map free-gas deposits as it showed similar results to the direct sampling of the cores. However, sedimentary facies with similar elastic properties, indicated in sub-bottom profiles as seismic units, for itself are insufficient to explain the presence of free gas formation in the sediments. The results of this work indicate that, although sedimentary facies distribution can restrict the locations of free gas deposits, slight changes in sediment properties should affect the bubbles presence in the same depositional environment.

The AC cores results showed different lithological mud units along the seismic unit with similar TOC, grain size sort and porosity. The color differences probably indicate variation in age and sedimentation rate that can be correlated with organic matter reactivity, and thus with methanogenesis rate. The difference of thickness of units between cores and the undulate characteristic of internal reflector in the AC-SU2 indicate important horizontal variations which should be responsible by the stratigraphy windows locations. These variations can also occur in the NSB deeper source unit. Also, in this locations, small variations in grain size along the shoal side channel can change

permeability and thus the gas retention capacity. We speculate that the top boundary of the bubbles accumulation in the NSB is associated to changes in sediment permeability. On the other hand, in the AC, the top boundary probably can be associated to the SMTZ.

Acknowledgment

The authors would like to thank Brazilian Coordination for Improvement of Higher Education (CAPES) for the research grants and to the Center for Marine Studies of the Federal University of Paraná for the infrastructure. Thanks are also due to the Coastal Carolina University for the technical support and infrastructure.

References

- In the end of this document –

CAPÍTULO III

Influence of sedimentary shallow gas on methane concentrations and emissions in a subtropical estuary

Authors: J. F. Pezza Andrade¹; L. C. Cotovicz Jr.²; M. A. Noernberg¹; R. H. Nagai¹

Potential co-authors: P. C. Alvalá³; W. J. Ferreira³

¹Federal University of Paraná, Campus Pontal do Paraná - Center for Marine Studies, Brazil;

²Leibniz Institute for Baltic Sea Research Warnemünde (IOW), Department of Marine Chemistry - Rostock, Germany

³National Institute for Space Research (INPE), São José dos Campos - SP, Brazil

To be submitted: *Estuaries and Coasts* (ISSN 1559-2731; IF 3.246; Qualis CAPES A2)

Abstract

Estuarine systems are an important source of methane (CH₄) to the atmosphere. Large shallow bubbles deposits in estuarine sediments are a common feature. However, the link between shallow gas-charged sediments and CH₄ concentration in the water column and water-atmosphere CH₄ fluxes is poorly understood. This work aims to investigate how the presence of gas-charged sediments affect dissolved CH₄ concentrations and emissions of CH₄ in the subtropical Paranaguá Estuarine Complex (PEC). Gas-charged sediments were mapped with high-resolution seismic and CH₄ dissolved concentrations were measured at the near-surface and near-bottom of the water column in sites with and without the presence of free-gas. CH₄ water-atmosphere fluxes were obtained with floating chambers and through calculation using the dissolved concentrations data and gas transfer velocity parameterizations. Dissolved CH₄ concentrations in PEC are low, ranging from 10.52 to 49.92 nmol L⁻¹. The dissolved CH₄ concentrations were always oversaturated with respect the atmosphere, indicating a permanent weak source of CH₄ to the atmosphere. The CH₄ water-air fluxes measured with the chambers were between 0.25 and 0.33 μmol m⁻²d⁻¹. In contrast, the computed fluxes were two orders of magnitude higher, between 11.65 ± 5.76 and 30.73 ± 16.60 μmol m⁻²d⁻¹ above CH₄ bubbles deposits and between 16.94 ± 13.23 and 23.98 ± 8.73 μmol m⁻²d⁻¹ above sites without gas. Our results suggest that the CH₄ concentrations and emissions are not significantly affected by the presence of bubble accumulations. However, high dissolved oxygen values in the water column with the smaller values above the bubble deposits, probably due its consumption, point to an important role in the aerobic oxidation of methane in PEC. Ebullitive fluxes were not recognized.

Keywords: Sediment gas bubbles; Estuarine CH₄ emissions; Aerobic oxidation of methane; Seismic Black Shadows.

Resumo

Os sistemas estuarinos são uma importante fonte de metano (CH_4) para a atmosfera. Grandes depósitos de bolhas rasas em sedimentos estuarinos são uma característica comum. No entanto, a ligação entre sedimentos rasos carregados de gás e concentração de CH_4 na coluna de água e fluxos de CH_4 da água para a atmosfera é pouco compreendida. Este trabalho tem como objetivo investigar como a presença de sedimentos carregados de gás afeta as concentrações de CH_4 dissolvido e as emissões de CH_4 no subtropical Complexo Estuarino de Paranaguá (CEP). Os sedimentos carregados de gás foram mapeados com sísmica de alta resolução e as concentrações de CH_4 dissolvido foram medidas perto da superfície e perto do fundo da coluna de água em locais com e sem a presença de gás. Fluxos de CH_4 da água para a atmosfera foram obtidos com câmaras flutuantes e através de cálculos usando os dados de concentrações dissolvidas e parametrizações de velocidade de transferência de gás. As concentrações de CH_4 dissolvido no PEC são baixas, variando de 10,52 a 49,92 nmol L^{-1} . As concentrações de CH_4 dissolvido sempre foram supersaturadas em relação à atmosfera, indicando uma fonte fraca permanente de CH_4 para a atmosfera. Os fluxos de CH_4 água-ar medidos com as câmaras estavam entre 0,25 e 0,33 $\mu\text{mol m}^{-2}\text{d}^{-1}$. Em contraste, os fluxos calculados foram duas ordens de grandeza maiores, entre $11,65 \pm 5,76$ e $30,73 \pm 16,60 \mu\text{mol m}^{-2}\text{d}^{-1}$ acima de depósitos de bolhas de CH_4 e entre $16,94 \pm 13,23$ e $23,98 \pm 8,73 \mu\text{mol m}^{-2}\text{d}^{-1}$ acima de locais sem gás. Nossos resultados sugerem que as concentrações e emissões de CH_4 não são significativamente afetadas pela presença de acúmulos de bolhas. No entanto, altos valores de oxigênio dissolvido na coluna d'água e com os menores valores acima dos depósitos de bolhas, provavelmente devido ao seu consumo, apontam para um importante papel na oxidação aeróbica do metano no CEP. Fluxos ebulitivos não foram reconhecidos.

Palavras-chave: Bolhas de gás em sedimentos; Emissões estuarinas de CH_4 ; Oxidação aeróbica do metano; Sombras Negras sísmicas.

1 Introduction

Methane (CH_4) is a key gas in planetary climate regulation (Canadell et al., 2021). It is the second most important anthropogenic greenhouse gas, contributing with about 18% of the global warming (Canadell et al., 2021; Cheng & Redfern, 2022). The global warming potential (GWP) of CH_4 is 28 for a 100 yr time horizon, meaning that a molecule of CH_4 is more efficient in trapping radiation than a molecule of carbon dioxide (Stocker et al., 2013). Oceanic CH_4 emissions range between 9–22 Tg CH_4 per year (Canadell et al., 2021), with coastal systems responsible for approximately 75% of this amount (Bange, 2006).

Previous investigations showed a wide range of dissolved CH_4 amount in estuarine systems (Cotovicz et al., 2016; Jacques et al., 2021; Song & Liu, 2016; Ye et al., 2019). There are different sources of CH_4 in estuaries, including the allochthonous sources such as riversfluvial, mangroves, tidal flats, sewage discharge, and the

autochthonous sources such as the internal production in sediments and water column (Cotovicz et al., 2016; Maher et al., 2015; Rosentreter et al., 2018; Sturm et al., 2016). The diffusive flux of methane from estuarine waters to the atmosphere can also vary significantly; a compilation of European (Upstill-Goddard & Barnes, 2016) and Indian (Rao & Sarma, 2016) estuaries estimate an atmospheric CH₄ release between 10 to 9100 and 0.06 to 17482 CH₄ mg m⁻²yr⁻¹, respectively.

In estuarine sediments, organic matter is consumed by different aerobic and anaerobic processes. The balance between CH₄ production (methanogenesis) and consumption (methanotroph) controls the CH₄ concentration in estuaries, and depend on several factors, including the amount of organic matter deposited in sediments, availability of electron acceptors, hydrodynamic, hydrostatic pressure, salinity, and temperature (Borges & Abril, 2012; Loyd et al., 2012; Martens et al., 1998; Rice & Claypool, 1981). When the amount of CH₄ reaches a certain value, it saturates, forming bubbles in the sedimentary column (Serra et al., 2006; Wilhelm et al., 1977). These bubble-charged sediments in estuaries floor can be investigated through acoustic methods. High-resolution seismic surveys in estuarine systems show massive deposits of CH₄ occurring in different sedimentary column depths and with diverse shapes (Garcia-Gil et al., 2002; Pezza Andrade et al., 2021; Weschenfelder et al., 2016). Also, some seismic signatures indicate migration patterns within the sediment column (Pezza Andrade et al., 2021; Taylor, 1992). There is evidence that the CH₄ accumulated in these deposits can escape the sediments which generate plumes in the water column, registered in seismic profiles as water plumes (Diez et al., 2007; Garcia-Gil et al., 2002; Lee et al., 2005), and pockmarks in the estuary's bottoms (Brothers et al., 2012; Rogers et al., 2006). Noteworthy, bubble accumulation can occur very close to the sediment-water interface in estuaries, within the firsts few centimeters of the sedimentary column, below the resolution limit of most high-frequency seismic equipment (Baltzer et al., 2005; Pezza Andrade et al., 2021).

Nevertheless, most of the studies of CH₄ in estuarine systems sediments apply two separate approaches, one focusing on biochemistry features and the other on sedimentological and geological features. The later focus on studying methane accumulation in sediments using acoustic methods concerning paleo morphology of the estuary bottom (Flury et al., 2016; Weschenfelder et al., 2016), sea-level variation (García-García et al., 2007), and sediment types (Diez et al., 2007; Pezza Andrade et al.,

2021). On the other hand, the biogeochemical approach aims to study methane concentration in the water, inferring methane sources and sinks, and its flux to the atmosphere (Cotovicz et al., 2016; Matoušů et al., 2017; Rosentreter et al., 2018). Most of studies focusing biochemistry ignore acoustic mapping of gas charge sediments, even when using incubation data (Sturm et al., 2016; Wells et al., 2020) and sampling sediments for methane analyses (Sawicka & Brüchert, 2017). Therefore, few studies have reported the effects of substrate heterogeneity in dissolved CH₄ concentrations and emissions of estuarine systems.

In this context, this study investigates the relationship between shallow methane gas accumulation heterogeneity in the estuarine sediments and CH₄ concentration in the water column and water-atmosphere flux in the Paranaguá Estuarine Complex (PEC), a subtropical estuary located at the Southern coast of Brazil. We hypothesize that the spatial distribution of extensive gas deposits in contact with the estuary bottom affect the methane dynamics in estuarine system enhancing CH₄ concentrations and emissions.

2 Settings

The PEC is a subtropical estuarine system in south Brazil that encompasses a water body area of approximately 552 km² and about 287 km² of mangroves and salt marshes (Noernberg et al., 2006). The average depth is about 5.4 m (reaching 33 m maximum), and it harbors around 1.4 km³ of water with a residence time of 3.49 days (Lana et al., 2001). The estuary is characterized as a coastal plain estuary with the presence of tidal deltas (Lessa et al., 1998) comprising two main segments (Fig. 1), one with an East-West axis and another on a North-South axis. The first comprises the sampling sites of this work and can be divided into three sectors: upper zone, central zone, and mouth zone (Fig. 1) (Lessa et al., 1998). Fluvial processes mainly dominate the upper zone with predominantly sandy sediments in river mouths, decreasing sediment diameter gradually to fine silt in distal regions (Cattani & Lamour, 2016; Lamour et al., 2004). The central zone, where fine sediments are deposited, encompasses the turbidity maximum zone. This zone plays a significant role in the PEC sedimentary dynamics due to the high concentration of suspended sediments, and the continuous mixture of river and marine waters (Cattani & Lamour, 2016; Noernberg, 2002). The mouth zone has a more

considerable marine influence with sandy sediments brought by alongshore currents (Martins et al., 2015).

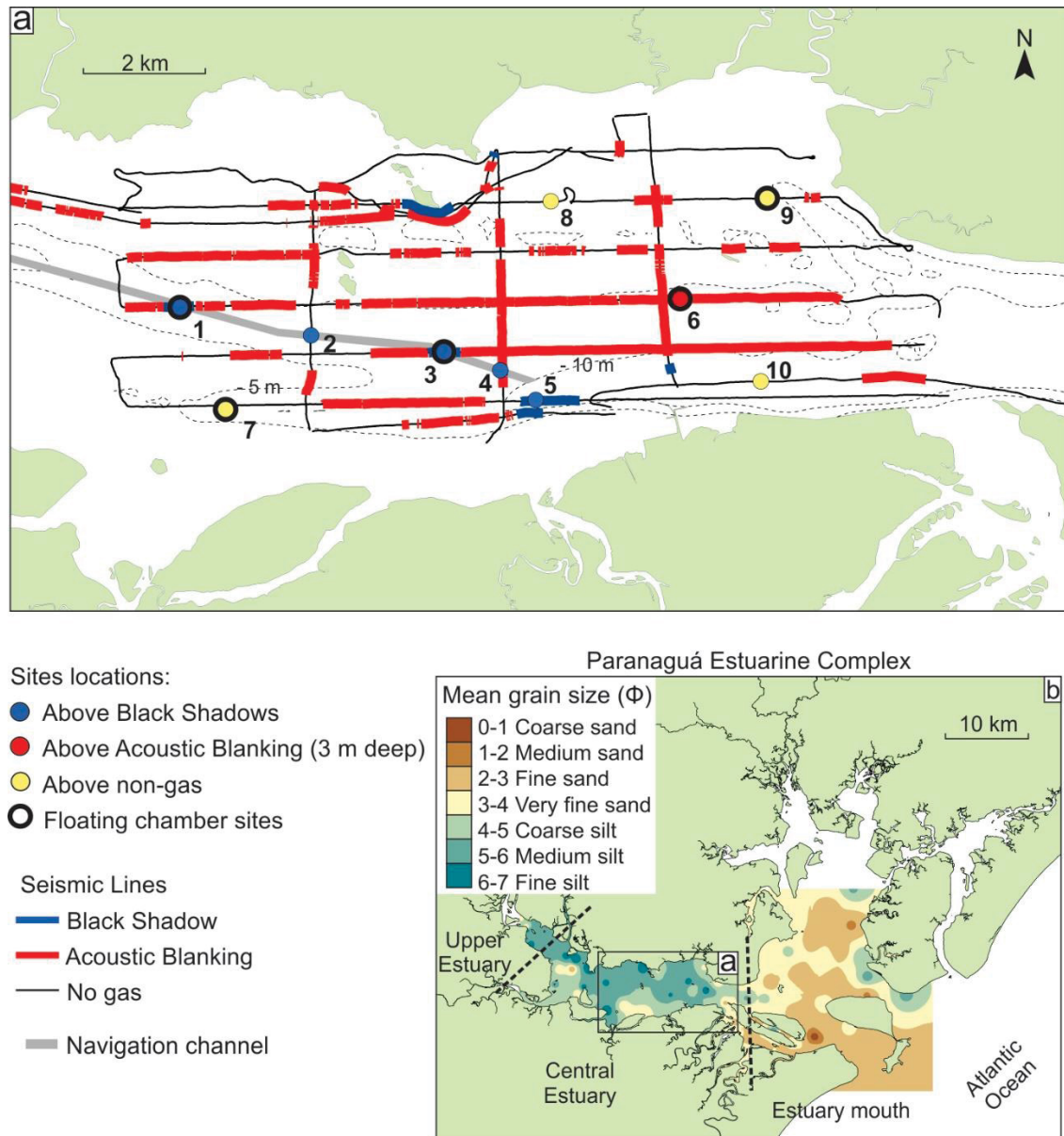


Fig. 1: Map of the Paranaguá Estuarine Complex (PEC) with the sampling sites for dissolved CH_4 concentrations and floating chambers measurements, the seismic lines interpreted for the presence of gas (based on Pezza Andrade et al., 2021), the navigation channel from the Paranaguá Port to Antonina Port, and mean grain size distribution (from Paladino et al., 2022).

According to Pezza Andrade et al. (2021), the PEC has, at least, 50 km of free gas deposits within its sedimentary column. Sismo-acoustic data showed different depth of

the gas top horizons ranging from 0 to 8 m. Free gas deposits in contact with the sediment-water interface are denominated Black Shadows (BS) due their unique seismic signature and signal characteristics (Baltzer et al., 2005; Klein et al., 2005; Weschenfelder et al., 2016). In PEC, BS were recognized in 8,2 km of seismic profiles and comprises 16% of PEC gas mapped charged sediments (Pezza Andrade et al., 2021).

3 Method

3.1 Sampling strategy

Sampling sites were chosen based on the presence/absence of gas seismic signatures interpreted by Pezza Andrade et al. (2021). The sampling campaign occurred in September 2021 during neap tide to avoid water disturbances from strong currents. A total of 10 sites were selected: five sites located near the surface bubble accumulation zone (Black Shadow seismic signatures; Pezza Andrade et al., 2021), four located where there is no free gas, and one located in a bubble accumulation zone 3 m below the water-sediment interface (Acoustic Blanking; Pezza Andrade et al., 2021) (Fig.1). At each site, one surface sediment (0-3 cm), one atmospheric air and six water samples were retrieved. Three water samples were retrieved at 0.5 m below the water surface, and three at 0.5 m above the estuary water-sediment interface. Five of the ten sites were chosen for floating chamber sampling to perform the water-atmosphere methane flux estimates (diffusive and ebullitive) (Fig.1).

3.2 Water and sediment physical parameters analysis

Temperature and salinity measurements were performed along the water column using a handheld CDT (SonTek CastAway) launched at each sampling station. Dissolved oxygen (DO) was measured using an AT 170 Alfakit oximeter with a Clark Cell at the surface and bottom water samples.

Sediment samples (0-3 cm) were carried out with a Van Veen sampler for grain size and organic matter content (OMC) analysis. An aliquot of 2g of sediment was submitted to 10% hydrochloric acid (HCl) and 30% hydrogen peroxide (H₂O₂) for calcium carbonate and organic matter removal, respectively. Grain size was obtained by laser diffraction with a Malvern Mastersizer 2000 and raw data were processed with the

Sysgran 3.2 Software (Camargo, 2006). OMC was obtained by weight difference before and after HCl attack.

3.3 Dissolved and atmospheric CH₄ concentration analyses

For dissolved CH₄ concentration estimates, six water samples were retrieved at each sampling site with the aid of a Niskin bottle, three replicates at 0.5 m below the water surface (near surface), and three replicates at 0.5 m above the estuary water-sediment interface (near bottom). A total of 30 ml of water sample was transferred to a syringe, another 30 ml of atmospheric air was added to the headspace, and samples were shaken vigorously for 2 minutes. Next, the sample from the syringe headspace was transferred to a 20 ml glass vial sealed with an aluminum cap and silicone septum with a vacuum. For each station, an atmospheric air sample was also collected to calculate dissolved CH₄ concentrations and for the validation procedure of the floating chamber samples (Marani & Alvalá, 2007). Dissolved CH₄ data was also used for estimating water-atmosphere fluxes for all sites as described in item 3.4.

For floating chamber-based CH₄ flux estimates, samples were retrieved in sites 1, 3, 6, 7, and 9 (Fig. 1) using the technique described by Khalil et al. (1998) and Marani & Alvalá (2007). At each site, six samplings were performed, using three floating chambers. The floating chamber is a cylindrical chamber made of PVC with a diameter of 30 cm and a height of 20 cm supported by foam floats with a Teflon® tube connected to a syringe (half-height) with a three-way faucet (Luer lock type) to retrieve air samples. In the field, with the boat anchored, chambers were carefully placed on the water's surface to avoid water perturbation. Sampling occurred in low wind conditions (< 7 km/h) for 18 min, one air sample was collected in the first minute, to verify possible disturbance and linearity, and three other air samples were collected every 6 minutes. Each air sample on the syringe was transferred to a 20 ml glass vial with a vacuum. Floating chambers fluxes were validated if the initial CH₄ concentration was close to the measured atmospheric air concentration and if the linear correlation between the change in mixing ratio and the elapsed time had R² greater than 0.90 (Marani & Alvalá, 2007; Sass et al., 1992). If only the second criterion is not met, the data was analyzed for peaks indicating ebullitive flux.

Dissolved and atmospheric CH₄ concentrations samples were analyzed using a gas chromatograph TRACE 1310 Series GC (Thermo Scientific) equipped with a flame

ionization detector (FID) at the Environmental Biogeochemistry Laboratory of the National Institute for Space Research (INPE) of Brazil. Dissolved CH₄ concentration estimates for each sample were obtained using Henry's law and Bunsen solubility from Wiesenburg & Guinasso (1979) as a function of water salinity and temperature.

3.4 Water-atmosphere CH₄ flux calculated based in CH₄ dissolved concentrations

Water-atmosphere CH₄ fluxes were also estimated through calculations based in CH₄ dissolved concentrations and gas transfer velocity according to the following equation (Cotovicz et al., 2016):

$$F(\text{CH}_4) = k_{g,T} * \Delta \text{CH}_4 \quad (1)$$

Where, $F(\text{CH}_4)$ is the diffusive flux, $k_{g,T}$ is the gas transfer velocity of a specific gas (g) at a given temperature (T), ΔCH_4 ($\text{CH}_4\text{w} - \text{CH}_4\text{eq}$) is the CH₄ concentration gradient between the water (CH_4w) and the water at equilibrium with the atmosphere (CH_4atm). We considered the CH₄ atmospheric partial pressure of 1.8 μatm corresponding to CH₄ concentrations (CH_4eq) in the range of 2.3–2.4 nmol L^{-1} due to variations in water and air temperature, and salinity (Cotovicz et al., 2016).

The gas transfer velocity $k_{g,T}$ was computed with the following equation 2 (Jahne et al. 1987):

$$k_{g,T} = k_{600} * (600/\text{Sc}_{g,T})^n \quad (2)$$

with k_{600} the gas transfer velocity normalized to a Schmidt number of 600 for CO₂ at 20°C, $\text{Sc}_{g,T}$ the Schmidt number in function of the gas type and temperature, and n equal to 2/3 for wind speed < 3.7 m s^{-1} or equal to 0.5 for higher wind speed (Jahne et al. 1987; Guérin et al. 2007, Cotovicz et al. 2016).

In this study, we used four empirical equations to derive the k_{600} values in order to provide ranges of estimations: the parameterization as a function of wind speed by Raymond and Cole, 2001 (RC01); McGillis et al., 2001 (M01); Jiang et al., 2008 (J08); and Wanninkhof, 2014 (W14). The computed wind speeds were a mean value of several measurements along the campaign day with a hand anemometer model LM-8000.

The parameterization of Raymond and Cole (2001) is computed by the follow equation:

$$k_{600}(\text{RC01}) = 1.91 \exp(0.35 U_{10}) \quad (3)$$

$$M01 = (3.3 + 0.026 * U3) \quad (4)$$

$$J08 = (0.314 * U2 - 0.436 * U + 3.99) \quad (5)$$

$$W14 = 0.251 * U2 \quad (6)$$

where k_{600} is the gas transfer velocity normalized to a Schmidt number of 600, and U_{10} is the wind speed at 10 m height.

3.5 Statistical analyzes.

To compared physico-chemical properties of the water and sediment, CH_4 concentrations, and the gas deposits presence or absence data was submitted to statistical analysis. First, normality was tested by Shapiro–Wilk test and homogeneity of variance with Levene's test. Comparisons of data between zones with BS and no gas were carried out using the parametric t test. Comparison between data that fail in the normality test were performed with non-parametric Mann-Whitney test. Comparisons between same parameters at near-bottom and near-surface measurements were carried out with the paired Wilcoxon test. Pearson test was applied for identify significant correlations between variables. Significance was set at $p < 0.05$. Statistics were performed in the PAST 4.03 software.

4 Results

4.1 Water and sediment physical parameters

Grain size analyzes show that the bottom sediments are composed of sandy silt with high mud content, between 62.4% and 85.4%. Site 8 is an exception comprising silty sand sediments with 54.6% sand content (Tab. 1). The clay content in the samples varies between 5 and 10%. The OMC varies between 2.7% at point 8 and 6.0% at point 2, with an average of 4.9% (Tab. 1). Statistical results showed that is a positive correlation between fine sediments and OMC (Tab.2)

DO concentration varied between 4.1 and 9.9 mg/L with a median of 7.1 mg/L, representing oxic waters in all sampling sites (Tab. 1). Near-bottom DO is lower than

near-surface, with significant difference (Mann-Whitney test, $p = 0.0019$), with values ranging from 4.1 to 8.7 mg/L and 7.0 to 9.9 mg/L, respectively. Additionally, near-bottom samples retrieved above BS, present OD ranging from 4.1 to 5.2 mg/L, lower than those from sites without free-gas in sediments, where it ranges from 5.5 to 8.7 mg/L.

Tab. 1: PEC's near-surface and near-bottom water dissolved oxygen concentration (DO, mg/L), and surface sediments (0-3 cm) grain size (sand, silt, and clay percentages), and organic matter content (OMC).

Site	Seismic Interp.	Grain size distribution			Dissolved oxygen (mg/L)		OMC (%)
		Sand (%)	Silt (%)	Clay (%)	Near-surface	Near-bottom	
1	BS	15.7	74.0	10.3	7.2	4.1	5.1
2	BS	23.8	67.6	8.4	7.4	5.2	6.0
3	BS	27.9	64.2	8.0	7.6	4.7	4.8
4	BS	37.5	55.5	7.0	8.1	4.8	4.6
5	BS	19.8	70.8	9.4	8.2	4.7	5.1
6	AB	19.9	69.8	10.4	8.9	6.3	5.1
7	No gas	14.6	75.4	10.0	7.0	5.5	5.2
8	No gas	54.6	40.1	5.3	9.3	8.7	2.7
9	No gas	-	-	-	9.7	5.9	-
10	No gas	22.6	67.3	10.2	9.9	5.5	5.6

Most temperature and salinity profiles indicate stratified water that becomes warmer and saltier with depth (Fig. 2). Salinity varied between 20.61 and 26.28 at the surface and between 25.68 and 29.67 at the bottom. Differences in salinity between near-surface water and at the bottom average 3.90 with a maximum difference of 7.23 (site 2). Statistical results showed no correlation between salinity and CH₄ concentration in both near-bottom and near-surface data (Tab. 2; Fig 3). The temperature varied between 23.15 and 24.26 °C at the surface and 21.13 and 22.80 °C near the bottom, with an average difference of 2 °C.

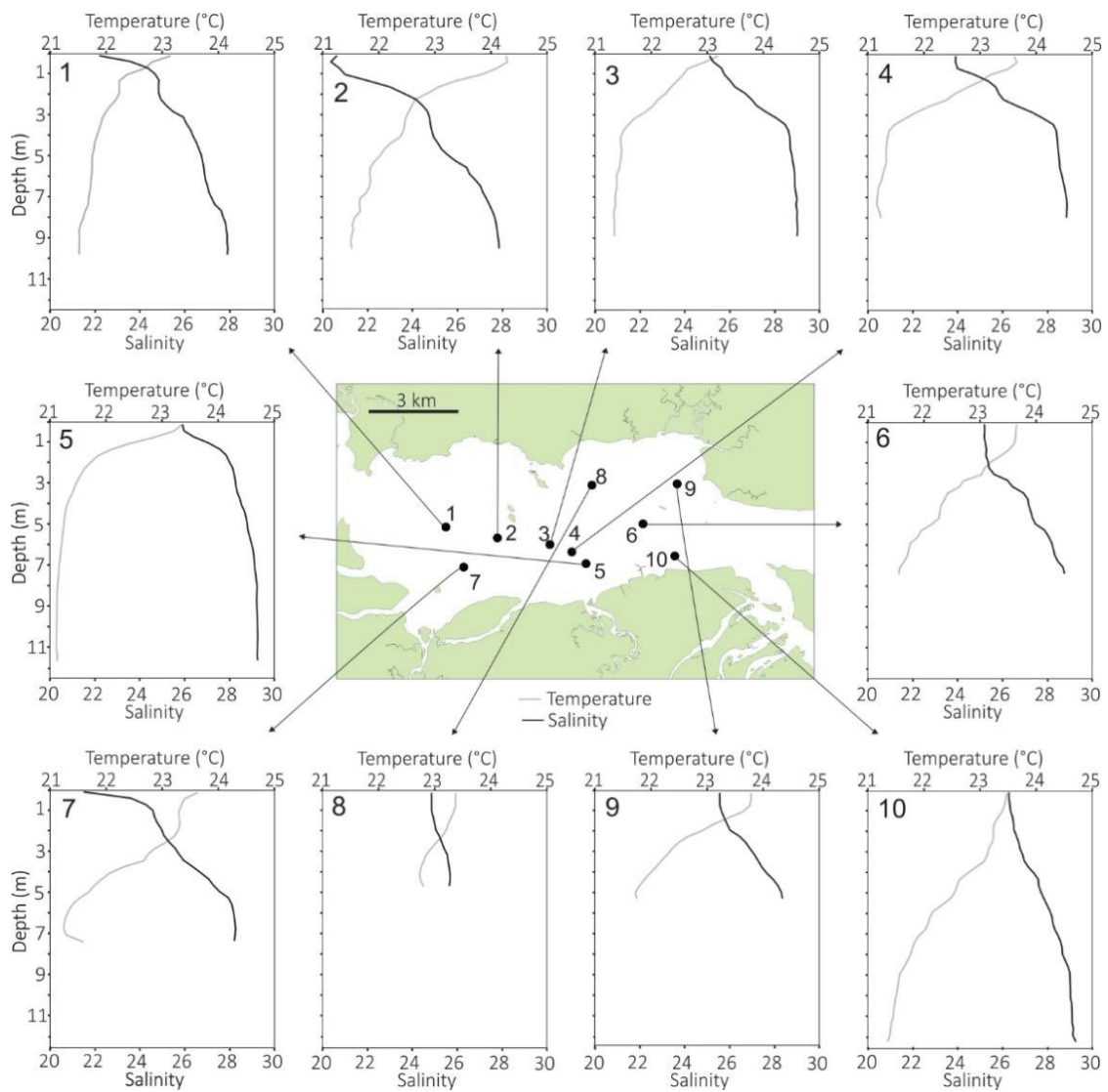


Fig. 2: Vertical profiles of water temperature (gray lines) and salinity (black lines) in the sampling sites during the sampling campaign (September 27 and 28, 2021 from 9 am to 3 pm).

4.2 Dissolved CH₄ concentrations

Dissolved CH₄ concentrations range from 10.52 to 49.92 nmol L⁻¹ (Tab. 3; Fig. 3). Near-surface dissolved CH₄ ranged between 12.90 to 30.51 nmol L⁻¹, generally smaller than near-bottom concentrations in most sampling sites, except for sites 1 and 6 (Tab. 3, Fig. 3). The CH₄ concentrations in PEC near-bottom waters ranged from 10.52 to 49.92 nmol L⁻¹, with the higher concentration is in site 4 (49.92 nmol L⁻¹) followed by site 5 (34.90 nmol L⁻¹), both above BS (Tab. 3, Fig. 3). The lowest value of near-bottom CH₄ is in site 6 (10.52 nmol L⁻¹; Tab. 3; Fig. 3), in an AB zone (Fig. 1). The difference between near-bottom and near-surface in the sites ranges from -13.05 nmol L⁻¹ at site 6 to 20.3 nmol L⁻¹ at site 4, with mean differences of 3.78 nmol L⁻¹ (Tab. 3). However, there is no significant difference between dissolved CH₄ near-surface and near-bottom values (t test, p = 0.1602). Also, statistical results indicate that there is no significant difference between CH₄ dissolved in zones with and without BS, both in near-bottom and in near-surface water (Tab. 4).

Tab. 3: Seismic gas signatures interpretations, average concentrations (\pm SD) of dissolved CH₄, average water-atmosphere fluxes calculated and with floating chambers (\pm SD) with minimum and maximum values. Sites with no floating chamber samples (NS) or with no validated results (NR) are indicated.

Site	Seismic interp.	Depth (m)	Dissolved CH ₄ (nmol L ⁻¹)		Water-atmosphere CH ₄ Flux (μ mol/m ² d)					
			Near-surface	Near-bottom	Calculated			Floating chambers		
					Mean	Min.	Max.	Mean	Min.	Max.
1	BS	9.69	27.85 \pm 11.93	26.38 \pm 13.03	27.68 \pm 14.51	10.51	54.40	0.25 \pm 0.006	0.24	0.25
2	BS	9.37	14.15 \pm 5.85	23.56 \pm 12.16	13.46 \pm 7.24	4.42	26.62	NS	NS	NS
3	BS	8.93	12.90 \pm 4.55	20.07 \pm 12.34	11.65 \pm 5.76	4.18	22.03	NR	NR	NR
4	BS	7.99	29.62 \pm 2.42	49.92 \pm 13.46	30.03 \pm 9.97	14.52	42.13	NS	NS	NS
5	BS	11.43	30.51 \pm 13.93	34.9 \pm 8.11	30.73 \pm 16.69	9.26	60.43	NS	NS	NS
6	AB	7.29	23.57 \pm 11.77	10.52 \pm 4.52	23.44 \pm 13.72	8.35	48.99	NR	NR	NR
7	No gas	7.33	17.60 \pm 12.40	26.82 \pm 11.82	16.94 \pm 13.23	4.44	41.65	0.33 \pm 0.093	0.26	0.46
8	No gas	4.70	24.25 \pm 4.20	25.49 \pm 2.98	23.98 \pm 8.73	9.94	35.60	NS	NS	NS
9	No gas	5.37	18.27 \pm 6.23	18.37 \pm 0.90	17.76 \pm 8.36	6.72	32.71	NR	NR	NR
10	No gas	12.18	19.81 \pm 13.49	20.3 \pm 9.47	19.26 \pm 14.46	3.02	44.58	NS	NS	NS

4.3 CH₄ water-atmosphere flux

In the PEC, the CH₄ water-atmosphere flux based on near-surface dissolved CH₄ concentrations presented a mean value of $21.49 \pm 13.03 \mu\text{mol m}^{-2}\text{d}^{-1}$ (Tab. 3). Site 5 has the highest flux ($30.73 \pm 16.6 \mu\text{mol m}^{-2}\text{d}^{-1}$), followed by sites 4 and 1, $30.03 \pm 9.97 \mu\text{mol m}^{-2}\text{d}^{-1}$, and $27.68 \pm 14.51 \mu\text{mol m}^{-2}\text{d}^{-1}$, respectively (Tab. 3). The lowest calculated flux was obtained for site 3 ($16.94 \pm 13.23 \mu\text{mol m}^{-2}\text{d}^{-1}$), followed by sites 2 and 7, $13.46 \pm 7.24 \mu\text{mol m}^{-2}\text{d}^{-1}$, and $11.65 \pm 5.76 \mu\text{mol m}^{-2}\text{d}^{-1}$, respectively (Tab. 3).

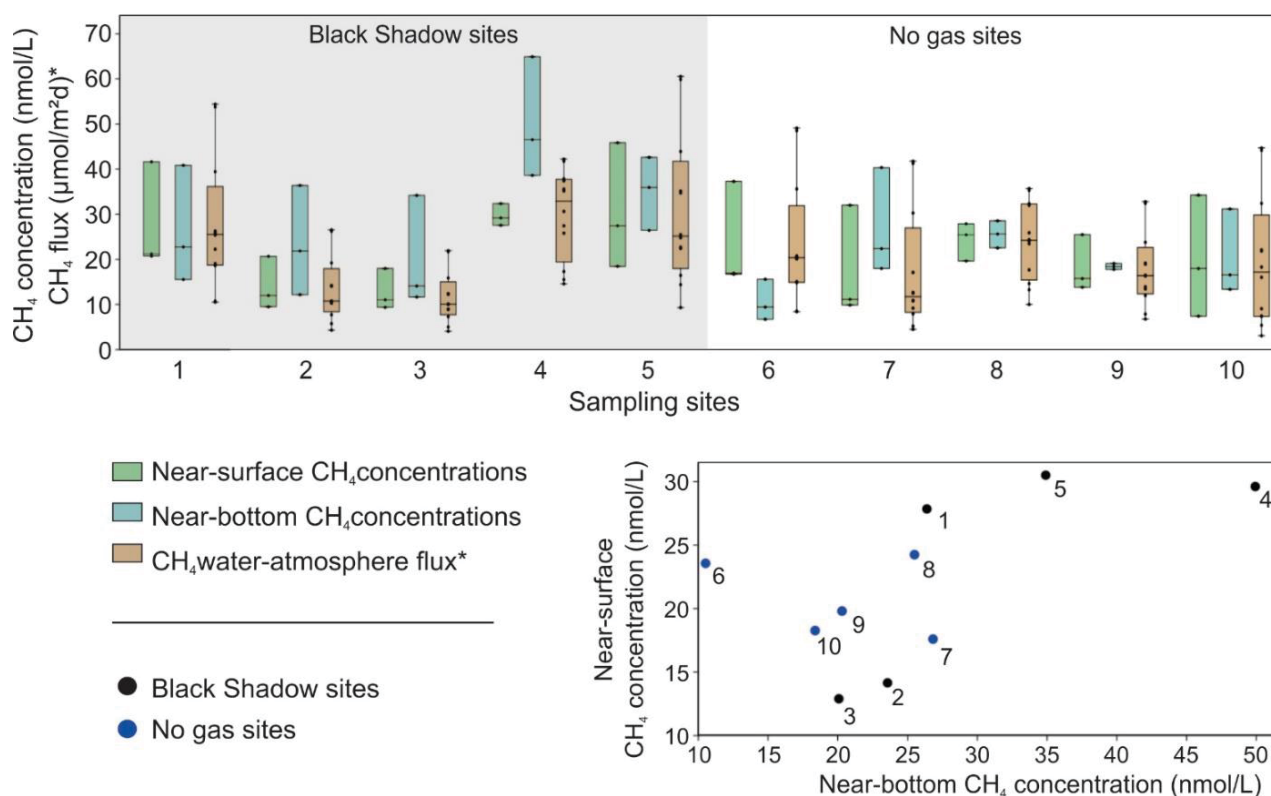


Fig. 3: Boxplot of sites dissolved CH₄ near-surface and near-bottom, and fluxes. Cross-plot of near-surface and near-bottom dissolved CH₄ concentrations.

The floating chambers results did not recognize an ebullitive flux, which was not considered in this study. Validated floating chambers methane flux analysis (1 and 7) shown in Table 3, reveal a CH₄ water-atmosphere flux two orders of magnitude smaller than those based on near-surface dissolved CH₄ concentrations. Floating chamber CH₄ water-atmosphere fluxes for sites 1 and 7 are 0.25 ± 0.006 and $0.33 \pm 0.09 \mu\text{mol m}^{-2}\text{d}^{-1}$, respectively.

Tab. 4: P values from comparison between CH₄ concentrations, physical and chemical variables of the water and sediments measured near-surface (ns) and near-bottom (nb) in the sites above BS (sites 1, 2, 3, 4, and 5) and without gas (sites 6, 7, 8, 9, and 10). T test was used for comparison of normal distribution data and Mann-Whitney test for comparison between data that fail in normality test. P value <0.05 (bold values) indicate a significant difference between the parameter measured in sites above BS and sites without gas presence.

	CH ₄ (ns)	CH ₄ (nb)	CH ₄ Flux	DO (ns)	DO (nb)	OMC	Clay	Silt	Sand
T test	0.592	0.117	0.589	0.051			0.785		
Mann-Whitney					0.008	0.904		1	0.904

5 Discussion

5.1 Sediment and water physicochemical parameters associated to the Black Shadows

The PEC bottom sediments have a typical grain size distribution in which fine sediments comprise the central estuary and get coarse oceanward (Paladino et al., 2022). Our sampling sites are located in the turbidity maximum zone (TMZ), where sediments have a mean grain size between fine silt to very fine sand (Fig.1; Paladino et al., 2022). However, estuarine sediments are normally mosaics with characteristics varying on smaller spatial scales (Meade, 1969). Our selected sites' bottom sediments are predominantly sandy silts with a high concentration of mud (Tab. 1). It is expected that within the sedimentary column, CH₄ bubbles accumulation is associated with muddy layers (Weschenfelder et al., 2016), due to the positive relationship between fine sediments and organic matter (Bergamaschi et al., 1997), resulting in a higher capacity of bubble retention (Liu et al., 2016) and methane production (Borges & Abril, 2011). Nevertheless, our results show that there is no significant difference between grain size or OMC in samples from BS and no gas zones (Tab. 4). Therefore, the spatial distribution of the BS in PEC does not appear to be delimited by fine sediments and high OMC surface sediments.

During the survey, it was noticed that sampling sites in the BS zone are located within the Antonina and Paranaguá ports navigation channel. The channel is about 120 m wide (Fig. 1) and can reach 20 m depth (Mayerle et al., 2015) with rapid sedimentation ($0.81 \pm 0.06 \text{ cm y}^{-1}$; Combi et al., 2013) and is under constant dredging activity (Mayerle et al., 2015), where about 4,000,000 m³ of sediment are removed every year (Rutyna et al.,

2021). The sedimentation rate has a major role in the CH₄ production as a rapid sedimentation favors metagenesis due to a better preservation of reactive organic matter (Borges & Abril, 2012). Therefore, the high sedimentation rate associated to the navigation channel may be responsible for the formation of BS in PEC.

Also, with exception of DO, results showed that sites water parameters do not have significant difference between sites with and without CH₄ bubbles. DO data showed high values and has a negative correlation with the presence of BS (Tab. 3). Aerobic methane oxidation (AOM) in the water column plays a strong role in controlling CH₄ dynamics and emissions in the coastal environments significantly reducing CH₄ concentrations (Fenchel et al., 1995; Matoušů et al., 2017). Indeed, around 60%–90% of CH₄ can be oxidized by methanotrophs in oxic layers (Le Mer & Roger, 2001). In addition, our study area is located within the PEC TMZ, where high suspended particulate matter concentration occurs, reaching almost 445 mg L⁻¹ in the rainy season (Zem et al., 2007), which can favor AOM (Abril et al., 2007). Previous study documented that high concentration of suspended particulate matter can favor the methane oxidation due to the methanotrophs present in the TMZ that were able to create even undersaturated conditions (Abril et al., 2007). Thus, the consumption of oxygen by the methanotrophs in the water column close to the free gas deposits is a plausible explanation for the lower concentration of oxygen close to the BS.

5.2 Sediment and water physicochemical parameters associated to CH₄ concentrations.

Our results show that dissolved CH₄ concentration in the PEC is low and there is no significant difference between near-surface and near-bottom values (t test, p = 0.1602). The similarity of near-bottom and near-surface dissolved CH₄ concentrations might be associated to intense water column mixing in the TMZ.

Also, no measured water parameters correlated to CH₄ concentrations in PEC (Tab. 2). Typically, dissolved CH₄ concentrations in estuarine systems have a salinity gradient related to the fluvial inlet, where the CH₄ concentrations decreases downstream with lowest values close to the estuarine mouth (Li et al., 2021; Rosentreter et al., 2018). Our results didn't recognize a salinity gradient along the studied area and, therefore, there is no correlation of salinity and dissolved CH₄ (Tab. 2).

Sediments grain size distribution and OMC also did not correlate to CH₄ concentrations, but there is a positive correlation between OMC and silt content (tab. 4). Also, mud content, mainly clay, can be correlated positively with sediment permeability, and thus affect CH₄ diffusion rate (Stranne et al., 2019). The site 4 has the lowest values of clay and silt content behind site 8, and thus should have a higher permeability. However, site 4 has a similar OMC of others BS sites and has sufficient permeability for the formation of the BS. We speculate that this relative higher permeability facilitates the diffusion of methane into the water column, explaining the high concentration of dissolved methane at this site, more than twice the average of the other sites.

5.3 Black Shadows influence in CH₄ water concentration and emission.

Methane concentration in porewater of surface sediments varies significantly, within 3 orders of magnitude (Sturm et al., 2016). Also, sediment-water methane fluxes in estuaries are variable, with common reported range of 2 and 250 $\mu\text{mol m}^{-2}\text{d}^{-1}$ (Abril & Iversen, 2002; Borges & Abril, 2012; Martens et al., 1998; Sansone et al., 1998; Sturm et al., 2016; Zhang et al., 2008), and reaching more than 1000 $\mu\text{mol m}^{-2}\text{d}^{-1}$ in some recent studies (Myllykangas et al., 2020; Sawicka & Brüchert, 2017). Within the sediment column in coastal and oceanic environments, the reduction of sulfate plays a strong role in reducing methane concentrations close to the sediment-water interface, above the methane-sulphate transition zone (Martens et al., 1998; Rice & Claypool, 1981). However, CH₄ in surface sediments can reach more than 100,000 nmols L⁻¹ (Sturm et al., 2016) and be the main source of CH₄ into the water body of estuaries (Myllykangas et al., 2020). Indeed, several studies showed that high dissolved CH₄ and sulfate concentrations in pore waters can overlap in surface sediments without a significant reduction in CH₄ concentration (Brüchert et al., 2009; Thang et al., 2013). We did not analyze the pore water for CH₄ and sulfate concentrations, however, the BS presence implies in high concentration of methane in surface sediments since CH₄ bubbles are located few centimeters apart of the sediment surface and the observation of the overlap of the diagenetic zones in the sediments were where no CH₄ saturation was reached (Myllykangas et al., 2020; Sturm et al., 2016). In addition, the methane concentration gradient can be altered by rising bubbles within the sediment (Haeckel et al., 2007).

Despite the presence of gas deposits indicating a high sedimentary methane accumulation, our results indicated that the BS are not associated to a higher concentration of methane dissolved in the water, and therefore, a higher diffusive emission, as the results showed no significant differences between sites with and without shallow bubbles deposits (Tab. 4). This result was not expected since it has been shown that diffusive sedimentary fluxes should be enhanced by bubbles as it makes sediment more porous (Flury et al., 2015). This result probably occurs because methanogenesis, although probably more intense, is not restricted to the points of bubble presence, being much broader and generalized in the study area. High sediment-water flux values, between 10 and 2400 $\mu\text{mol m}^{-2}\text{d}^{-1}$, were observed without saturation of methane (Sawicka & Brüchert, 2017) Also, AOM together with water circulation tends to balance the local methane concentration.

Also, ebullitive flux was not recognized in this study. The floating chambers data showed that, during the sampling campaign, no ebullitive flux of methane into the atmosphere related to the escape of bubbles from the BS was recorded. Pezza Andrade et al. (2021) showed high-resolution seismic profiles that display noises in the water column over the BS in the PEC. Other studies also recognized noises above bubbles deposits in coastal waters which were interpreted as a possible escape of gas bubbles (Garcia-Gil et al., 2002; Missiaen et al., 2002).

The bubbles escape of gas-charged sediment is mainly due to a drop in hydrostatic pressure (Liu et al., 2016) associated with tidal variations in coastal environments (Boles et al., 2001). The results presented here do not exclude this possibility, we hypothesize that an ebullitive flow was not recognized for two reasons: (1) the sampling area is restricted compared to the BS area, a few centimeters in diameter of the chambers for several meters in length linear of the BS; (2) data collection was carried out at neap tide and low wind conditions to avoid current and thus analyses errors in diffusive flow and dissolved CH_4 concentrations. In this sense, substantial CH_4 bubbling release (that is, ebullition) would occur only under water-level drawdown. As the depths in the black shadow area are relatively high ($>7\text{m}$), the hydrostatic pressure is supposed to block significant ebullition in the area. Storm and tidal-associated fluctuations of hydrostatic pressure can induce bulk gas-driven ebullitions (Chanton et al., 1989; Lohrberg et al., 2020). We did not sample during low tidal under spring tide conditions, when the water

level is at the lowest level and the variation in hydrostatic pressure can triggers CH₄ ebullition, and this should be better investigated.

Results showed that the floating chambers method was not efficient for measurements of the water-atmosphere diffusive flux since only about 16.5% of the chambers sampling displayed reliable flux values in this study. The floating chambers with valid flux ($R^2 > 0.90$) seems to be related to the wind speed during the samplings. The samplings from sites 1 and 7 occurred with low wind speed, an almost imperceptible breeze about 0.2 m/s wind speed. On the other hand, the other sites samplings with the floating chambers were carried out with winds between 0.8 and 1.9 m/s. Also, the few validated fluxes were two orders of magnitude smaller than the calculated fluxes (Tab.3; Fig. 4). Therefore, due to the several limitations pointed out for the floating chamber method, we considered that the most representative fluxes are the diffusive fluxes calculated with the distinct models of gas parameterizations (Tab. 3).

The calculated water-atmosphere CH₄ flux indicated that the first and second maximum fluxes observed were above BS (sites 3 and 2). However, statistical analysis showed no significance difference between CH₄ dissolved concentrations, and therefore water-atmosphere fluxes, in sites with and without bubbles deposits (Tab. 4). A significant relationship between diffusive water-air flux and bubbles deposits (BS) in PEC wasn't expected due the water circulation that can be complex in the TMZ of the PEC (Mayerle et al., 2015) and the methane oxidation in the water column (Fenchel et al., 1995; Abril et al., 2007; Matoušů et al., 2017) that are enhanced by high concentrations of suspended particulate material (Abril et al., 2007). Also, the flux was computed with dissolved CH₄ results which did had no significant difference between sites with and without gas (Tab. 4).

5.4 PEC in the context of estuarine emissions around the world

Our results indicate that the PEC has a low rate of CH₄ diffusive emission compared to other estuaries around the world (Fig. 4) (Matoušů et al., 2017; Rosentreter et al., 2018; Upstill-Goddard & Barnes, 2016). The diffusive CH₄ water-atmosphere flux calculated in PEC have lower values than most estuarine systems in Europe (3 – 1554 $\mu\text{mol}/\text{m}^2\text{d}$), considered strong CH₄ emitters (Upstill-Goddard & Barnes, 2016). In addition, PEC diffusive CH₄ water-atmosphere calculated flux values are similar to the low range of

CH₄ emissions observed for Australian estuaries (7 – 2603 $\mu\text{mol}/\text{m}^2\text{d}$) (Rosentreter et al., 2018). Compared with Indian estuaries (0.01 – 156 $\mu\text{mol}/\text{m}^2\text{d}$), PEC calculated diffusive fluxes are relatively higher (Rao & Sarma, 2016). The floating chamber flux measurements displayed values much lower than most of the studied estuarine systems, comparable only to a few Indian estuaries (Rao & Sarma, 2016). Our floating chamber results probably are associated with the lack of significant wind, which is an important factor in CH₄ emissions (Abril et al., 2009; Raymond & Cole, 2001).

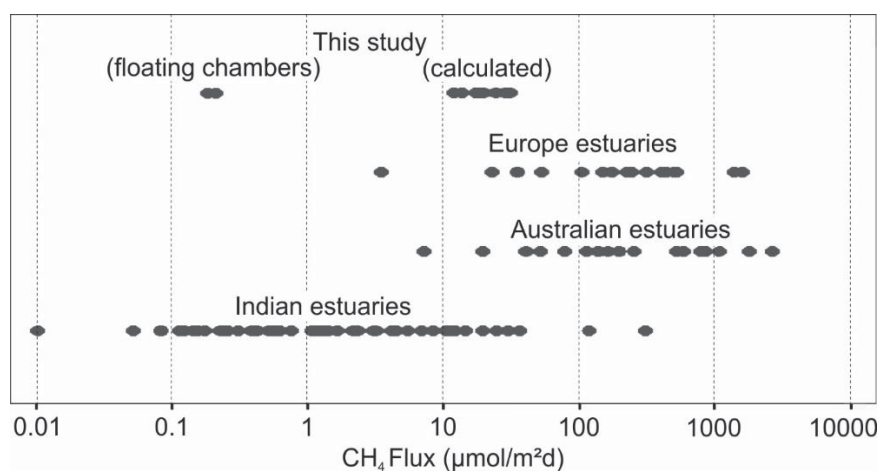


Fig. 4: Comparison between CH₄ water-atmosphere flux of this study and diverse estuaries in Europe (Upstill-Goddard and Barnes, 2016), Australia (Rosentreter et al., 2018), and India (Rao and Sarma, 2016).

Estuaries with a high rate of human alteration present higher values of CH₄ emission to the atmosphere than estuaries with low urbanization (Wells et al., 2020). In some polluted Brazilian coastal bays and lagoons, a few hundred kilometers north of the PEC, the calculated flux are a hundred times greater than in the PEC (Cotovicz et al., 2016, 2021).. A similar difference occurs in other estuaries located close to large urban centers (Li et al., 2021; Matoušů et al., 2017). Also, low emission values of Indian estuaries are associated to low density human settlement along the riverine banks (Rao and Sarma, 2016). In this sense, the PEC low CH₄ concentration and water-atmosphere flux are most likely related to its relatively high preservation conditions (Angeli et al., 2020; Gurgatz et al., 2023; Ribeiro et al., 2013), as this estuary is largely bordered by preservation areas protected by Brazilian federal law.

Additionally, TMZ are characteristically estuarine region with the highest accumulation of organic matter, suspended particulate material, and sedimentation rates (Geyer, 1993). The methanotrophs can be associated to the suspended particulate material (Abril et al., 2007). Tidal estuaries in France showed a sharp decrease of methane concentrations, from ~600 to only ~30 nmol L⁻¹ in a month, and the authors attributed this decline to the high concentration of suspended particulate matter (exceeding 100 mg L⁻¹) associated to methane oxidation in the TMZ (Abril et al., 2007). PEC showed concentrations of suspended particulate material exceeding 400 mg L⁻¹ (Zem et al., 2007), therefore, the enhancement of methane oxidation in the TMZ associated with low CH₄ emissions is likely to occur. Therefore, the values of CH₄ concentrations and flux presented in this study (Fig. 4), focused on the central estuary in the TMZ location, cannot be generalized to the estuary.

This study discussed an important feature of CH₄ accumulations within estuarine systems and its impact in its dissolved concentrations thought an interdisciplinary approach including geophysical and physicochemical data. However, we include only data from one survey campaign, and therefore did not include temporal variations. Estuarine temporal hydrodynamics variations corresponding to the seasons and tides affect the CH₄ dynamics (Abril et al., 2007; Li et al., 2021). During a spring tide cycle, the interaction of salty and fresh waters can affect CH₄ concentration and flux. Water horizontal advection during low tides introduces low salinity and high CH₄ waters to the estuarine systems (Li et al., 2021). Also, the PEC has an area of about 280 km² of mangrove (Noernberg et al., 2006). Mangrove-derived surface waters, normally, have CH₄ concentration because these waters are enriched in by-products of organic matter degradation that takes place in mangrove soils where significant rates of methanogenesis can occur (Al-Haj & Fulweiler, 2020; Rosentreter et al., 2018). Also, CH₄ concentration in estuaries are affected by seasonality, where in rainy periods, and consequently greater influx of fresh water, methane concentration tends to rise (Rao & Sarma, 2016). In this sense, we suggest more studies of CH₄ dynamics along different seasons and tides in the PEC for better comprehension of the temporal variations since this study focus on the relationship between the gas deposits and the CH₄ dynamics and thus it was performed in neap tides in sequential days.

6 Conclusion

The presence of large deposits of methane gas bubbles in the sediment in contact with the water column (Black Shadows) mapped by acoustic methods apparently does not indicate an influence on the dissolved concentrations and emissions of CH₄ to atmosphere. High DO values in the water column in the study area and slight smaller values above BS due its consumption suggest that aerobic methane oxidation is a key factor in the CH₄ dynamics in the PEC. Indeed, the Black Shadow is in the ZMT, where the high concentration of suspended particulate material can enhance the methane oxidation. Ebullitive fluxes were not recognized in this study. However, the data presented here do not rule out this possibility due to and a restricted area of the floating chambers and a period of hydrostatic pressure stability during the survey as the bubbles release normally is triggered by tides oscillations and storms events. Despite the presence of these methane gas deposits in the sediments, the PEC has a relative low level of methane dissolved in the water and atmosphere-water flux compared to other estuaries around the world due to relatively low urbanization and large pristine areas.

References

- In the end of this document –

CONSIDERAÇÕES FINAIS

Com auxílio de dados sedimentares e de sísmica de alta resolução, foi possível mapear e caracterizar uma grande quantidade de gás raso no CEP e no SD. A Baía de Paranaguá e Antonina apresenta acúmulos de gás que somam mais de 50 km lineares observados em perfis sísmicos. Provavelmente, o CEP como um todo deve apresentar uma quantidade ainda maior de gás em seu assoalho devido a restrição espacial dos levantamentos sísmicos aqui apresentados. Como visto no Cap. I o gás preso nos sedimentos do CEP apresenta diferentes assinaturas sísmicas sendo possível observar estruturas de migração do gás tanto lateralmente como verticalmente.

Em contrapartida, o DS apresenta uma quantidade muito inferior de gás acumulado em seu assoalho. Os dados indicam que o gás no DS é mais raso e praticamente não é possível observar características de migração. Essas distinções se dão provavelmente pela diferença ambiental dos dois sistemas estuarinos, sendo que o SD é muito menor e estreito, com morfologia e hidrodinâmica diferenciadas associado a um clima caracterizado por eventuais tornados. Dessa forma, a NSB no SD apresenta somente alguns pontos separados de acúmulo de gás devido a uma morfologia diferenciada com a presença de um baixio e um fundo mais arenoso do que no CEP. Já o canal AC, mais restrito e lamoso, possui gás em quase toda sua extensão. Como visto no Cap. II, as paleo-superfícies e as facies seismo-estratigráficas observadas pelos dados acústicos não são suficientes para caracterizar o controle e a variação espacial do acúmulo de gás em ambientes estuarinos.

A presença desses depósitos de gás natural não parece ter um impacto significativo na concentração de metano dissolvido e seu fluxo difusivo para atmosfera. Como visto no Cap. III, amostras de água e ar no CEP indicaram que os valores medidos não apresentam diferença significativa entre os pontos com e sem a presença dos depósitos de bolhas de metano. Fluxo ebulitivo (escape de bolhas) não foi reconhecido no CEP, porém essa hipótese não foi descartada devido a área restrita dos coletores e a condição de maré de quadratura durante a amostragem. Apesar do presente estudo ter mapeado uma grande quantidade de depósitos de gás no CEP (Cap. I), os resultados do Cap. III indicaram que o CEP é um estuário bem preservado com baixa emissão e concentração de metano.

Tendo em vista que esses acúmulos de gás podem influenciar tanto obras de engenharia como a ecologia local e o clima do nosso planeta. Sugerimos que trabalhos

futuros incluam mais dados relativos a parâmetros químicos, físicos e biológicos (i.e., tipo e reatividade de matéria orgânica; taxa de sedimentação; oxigenação no momento de deposição; entre outros) para maior compreensão e caracterização dos acúmulos de gás raso em ambientes estuarinos. Sugerimos também que futuros estudos incluam as variações temporais em diferentes escalas para compreender a dinâmica do metano em relação aos ciclos de maré e estações do ano.

REFERÊNCIAS

- Abegg, F., Anderson, A.L., 1997. The acoustic turbid layer in muddy sediments of Eckernförde Bay, Western Baltic: Methane concentration, saturation and bubble characteristics. *Marine Geology* 137, 137–147. [https://doi.org/10.1016/S0025-3227\(96\)00084-9](https://doi.org/10.1016/S0025-3227(96)00084-9)
- Abegg, F., Anderson, A.L., 1997. The acoustic turbid layer in muddy sediments of Eckernförde Bay, Western Baltic: methane concentration, saturation and bubble characteristics. *Journal of Marine Geology, Geochemistry and Geophysics* 137, 137–147.
- Abril, G., Commarieu, M.-V., Guérin, F., 2007. Enhanced methane oxidation in an estuarine turbidity maximum. *Limnol Oceanogr* 52, 470–475. <https://doi.org/10.4319/lo.2007.52.1.0470>
- Abril, G., Commarieu, M.V., Sottolichio, A., Bretel, P., Guérin, F., 2009. Turbidity limits gas exchange in a large macrotidal estuary. *Estuar Coast Shelf Sci* 83, 342–348. <https://doi.org/10.1016/j.ecss.2009.03.006>
- Abril, G., Iversen, N., 2002. Methane dynamics in a shallow non-tidal estuary (Randers Fjord, Denmark). *Mar Ecol Prog Ser* 230, 171–181. <https://doi.org/10.3354/meps230171>
- Al-Haj, A.N., Fulweiler, R.W., 2020a. A synthesis of methane emissions from shallow vegetated coastal ecosystems. *Glob Chang Biol*. <https://doi.org/10.1111/gcb.15046>
- Al-Haj, A.N., Fulweiler, R.W., 2020b. A synthesis of methane emissions from shallow vegetated coastal ecosystems. *Glob Chang Biol*. <https://doi.org/10.1111/gcb.15046>
- Angeli, J.L.F., Kim, B.S.M., Paladino, Í.M., Nagai, R.H., Martins, C.C., de Mahiques, M.M., Figueira, R.C.L., 2020. Statistical assessment of background levels for metal contamination from a subtropical estuarine system in the SW Atlantic (Paraná Estuarine System, Brazil). *Journal of Sedimentary Environments* 5, 137–150. <https://doi.org/10.1007/s43217-020-00008-5>
- Angulo, R.J., 2004. Mapa do Cenozóico do Litoral do Paraná. *Boletim Paranaense de Geociências* 55, 25–42.
- Angulo, R.J., 1995. Caracterização e reavaliação da Formação Alexandra (Terciário) e de sedimentos continentais associados a vertentes no litoral do Estado do Paraná, Brasil. *Anais, Acad. Bras. Ciên.* 67, 445–463.
- Angulo, R.J., Lessa, G.C., 1997. The brazilian sea-level curves: A critical review with emphasis on the curves from the Paranagua and Cananeia regions. *Marine Geology* 140, 141–166. [https://doi.org/10.1016/S0025-3227\(97\)00015-7](https://doi.org/10.1016/S0025-3227(97)00015-7)
- Angulo, R.J., Lessa, G.C., Souza, M.C. De, 2006. A critical review of mid- to late-Holocene sea-level fluctuations on the eastern Brazilian coastline. *Quaternary Science Reviews* 25, 486–506. <https://doi.org/10.1016/j.quascirev.2005.03.008>
- Angulo, R.J., Suguio, K., 1995. Re-evaluation of the Holocene sea-level maxima for the State of Paraná, Brazil. “*Palaeogeography, Palaeoclimatology, Palaeoecology*” 113, 385–393. [https://doi.org/10.1016/0031-0182\(95\)00055-Q](https://doi.org/10.1016/0031-0182(95)00055-Q)

- Baltzer, A., Tessier, B., Nouzé, H., Bates, R., Moore, C., Menier, D., 2005. Seistec seismic profiles: A tool to differentiate gas signatures. *Marine Geophysical Research* 26, 235–245. <https://doi.org/10.1007/s11001-005-3721-x>
- Bange, H.W., 2006. Nitrous oxide and methane in European coastal waters. *Estuar Coast Shelf Sci* 70, 361–374. <https://doi.org/10.1016/j.ecss.2006.05.042>
- Barnes, R. O., Goldberg, E.D., 1976. Methane production and consumption in anoxic marine sediments. *Geology* 297–300.
- Bergamaschi, B.A., Tsamakis, E., Ceil, R.G., Eglinton, T.I., Montlucon, D.B., Hedges, J.I., 1997. The effect of grain size and surface area on organic matter, lignin and carbohydrate concentration, and molecular compositions in Peru Margin sediments, *Geochimica et Cosmochimica Acta*.
- Bigarella, J.J., Becker, R.D., Matos, D.J., Werner, A., 1978. A Serra do Mar e a porção oriental do Estado do Paraná...um problema de segurança ambiental e nacional, Secretaria de Estado de Planejamento/ ADEA. Curitiba.
- Boetius, A., Ravensschlag, K., Schubert, C.J., Rickert², D., Widdel, F., Gieseke, A., Amann, R., Jürgensen, B.B., Witte, U., Pfannkuche², O., 2000. A marine microbial consortium apparently mediating anaerobic oxidation of methane, *NATURE*.
- Boles, J.R., Clark, J.F., Leifer, I., Washburn, L., 2001. Temporal variation in natural methane seep rate due to tides, Coal Oil Point area, California. *J Geophys Res Oceans* 106, 27077–27086. <https://doi.org/10.1029/2000jc000774>
- Borges, A. V., Abril, G., 2012. Carbon Dioxide and Methane Dynamics in Estuaries, in: *Treatise on Estuarine and Coastal Science*. Elsevier Inc., pp. 119–161. <https://doi.org/10.1016/B978-0-12-374711-2.00504-0>
- Borges, A. V., Champenois, W., Gypens, N., Delille, B., Harlay, J., 2016. Massive marine methane emissions from near-shore shallow coastal areas. *Scientific Reports* 6, 2–9. <https://doi.org/10.1038/srep27908>
- Bourg, I.C., Ajo-Franklin, J.B., 2017. Clay, Water, and Salt: Controls on the Permeability of Fine-Grained Sedimentary Rocks. *Acc Chem Res* 50, 2067–2074. <https://doi.org/10.1021/acs.accounts.7b00261>
- Bravo, M.E., Aliotta, S., Fiori, S., Ginsberg, S., 2018. Distribution, vertical position and ecological implications of shallow gas in Bahía Blanca estuary (Argentina). *Estuar Coast Shelf Sci* 202, 222–231. <https://doi.org/10.1016/j.ecss.2018.01.007>
- Broome, S.W., Woodhouse, W.W., Seneca, E.D., 1973. An investigation of propagation and the mineral nutrition of *Spartina alterniflora*, ea Grant Publication UNC-SG-73-14, Sea Grant Publication UNC-SG-73-14. Raleigh, N.C.
- Brothers, L.L., Kelley, J.T., Belknap, D.F., Barnhardt, W.A., Andrews, B.D., Legere, C., Hughes Clarke, J.E., 2012. Shallow stratigraphic control on pockmark distribution in north temperate estuaries. *Mar Geol* 329–331, 34–45. <https://doi.org/10.1016/j.margeo.2012.09.006>

- Brüchert, V., Currie, B., Peard, K.R., 2009. Hydrogen sulphide and methane emissions on the central Namibian shelf. *Prog Oceanogr* 83, 169–179. <https://doi.org/10.1016/j.pocean.2009.07.017>
- Bryant, W.R., Hottman, W., Trabant, P., 1975. Permeability of unconsolidated and consolidated marine sediments, gulf of Mexico. *Marine Geotechnology* 1, 1–14. <https://doi.org/10.1080/10641197509388149>
- Camargo, M.G. De, 2006. Sysgran: um sistema de código aberto para análises granulométricas do sedimento. *Revista Brasileira de Geociências* 36, 371–378.
- Camargo, M.G., 2006. SYSGRAN: Um Sistema De Código Aberto Para Análises Granulométricas do Sedimento. *Revista Brasileira de Geociências* 36, 371–378.
- Canadell, J.G., Monteiro, P.M., Costa, M.H., Syampungani, S., Zaehle, S., Zickfeld Canada, K., Alexandrov, G.A., 2021. Global Carbon and Other Biogeochemical Cycles and Feedbacks, in: Masson-Delmotte, V., Zhai, P., Pirani, A.C.S.L., Péan, C., Berger, S., Caud, N., Chen, Y., Goldfarb, L.G.M.I.H.M.L.K., Lonnoy, E., Matthews, J.B.R., Maycock, T.K., Waterfield, T., Yelekçi, O., Yu, R., Zho, B. (Eds.), *Climate Change 2021: The Physical Science Basis. Contribution of Working Group I to the Sixth Assessment Report of the Intergovernmental Panel on Climate Change*. Cambridge University Press, Cambridge, UK and New York, US, pp. 673–816. <https://doi.org/10.1017/9781009157896.007>
- Canfield, D.E., 1993. Organic matter oxidation in marine sediments, in: Wollast, R., Mackenzie, F.T., Chou, L. (Eds.), *Interactions of C, N, P and S Biogeochemical Cycles and Global Change*. Springer, Verlag Berlin Heidelberg, pp. 333–363.
- Castro, L.G., Ferreira, F.J.F., Angulo, R.J., 2008. Modelo gravimétrico-magnético do gráben de paranaguá-PR, Brasil 26, 273–292.
- Cattani, P.E., Lamour, M.R., 2016. Considerations Regarding Sedimentation Rates along the E-W Axis of the Paranaguá Estuarine Complex, Brazil: A Bathymetric Approach Considerations Regarding Sedimentation Rates along the ' Estuarine Complex, Brazil: A E-W Axis of the Paranaqua Bathymet. *J Coast Res* 32, 619–628. <https://doi.org/10.2112/JCOASTRES-D-14-00099.1>
- Catuneanu, O., 2006. Principles of sequence stratigraphy, First edit. ed, Elsevier. <https://doi.org/10.5860/CHOICE.44-4462>
- Cauchon-Voyer, G., Locat, J., St-Onge, G., 2008. Late-Quaternary morpho-sedimentology and submarine mass movements of the Betsiamites area, Lower St. Lawrence Estuary, Quebec, Canada. *Mar Geol* 251, 233–252. <https://doi.org/10.1016/j.margeo.2008.03.003>
- Chanton, J.P., Martens, C.S., Kelley, C.A., 1989. Gas transport from methane-saturated, tidal freshwater and wetland sediments. *Limnol Oceanogr* 34, 807–819. <https://doi.org/10.4319/lo.1989.34.5.0807>
- Ciais, P., Sabine, C., Bala, G., Bopp, L., Brovkin, V., Canadell, J., Chhabra, A., DeFries, R., Galloway, J., Heimann, M., Jones, C., Quéré, C. le, Myneni, R.B., Piao, S., Thornton, P., 2013. Carbon and Other Biogeochemical Cycles, in: Stocker, et. al. T.F. (Ed.), *Climate Change 2013: The Physical Science Basis. Contribution of Working Group I to the Fifth*

Assessment Report of the Intergovernmental Panel on Climate Change. Cambridge University Press, Cambridge, UK and New York, USA, p. 104. <https://doi.org/10.1017/CBO9781107415324.Summary>

- Claypool, G.E., Kaplan, I.R., 1974. The origin and distribution of methane in marine sediments, in: Kaplan, I.R. (Ed.), *Natural Gases in Marine Sediments*. Plenum Press, New York, pp. 99–139.
- Combi, T., Taniguchi, S., Alves, P., Ferreira, D.L., Michaelovitch, M., Rosalinda, D.M., Montone, C., Martins, C., 2013. Sources and Temporal Patterns of Polychlorinated Biphenyls Around a Large South American Grain-Shipping Port (Paranaguá Estuarine System, Brazil). *Arch Environ Contam Toxicol* 64, 573–582. <https://doi.org/10.1007/s00244-012-9872-2>
- Cotovicz, L.C., Knoppers, B.A., Brandini, N., Poirier, D., Costa Santos, S.J., Abril, G., 2016. Spatio-temporal variability of methane (CH₄) concentrations and diffusive fluxes from a tropical coastal embayment surrounded by a large urban area (Guanabara Bay, Rio de Janeiro, Brazil). *Limnol Oceanogr* 61, S238–S252. <https://doi.org/10.1002/lno.10298>
- Cotovicz, L.C., Ribeiro, R.P., Régis, C.R., Bernardes, M., Sobrinho, R., Vidal, L.O., Tremmel, D., Knoppers, B.A., Abril, G., 2021. Greenhouse gas emissions (CO₂ and CH₄) and inorganic carbon behavior in an urban highly polluted tropical coastal lagoon (SE, Brazil). *Environmental Science and Pollution Research* 28, 38173–38192. <https://doi.org/10.1007/s11356-021-13362-2>
- Crill, P.M., Martens, C.S., 1983. Spatial and temporal fluctuations of methane production in anoxic coastal marine sediments. *Limnol Oceanogr* 28, 1117–1130. <https://doi.org/10.4319/lo.1983.28.6.1117>
- Dasgupta, T., Mukherjee, S., 2020. Sediment Compaction and Applications in Petroleum Geoscience. *Sediment Compaction and Application in Petroleum Geoscience*. <https://doi.org/10.1007/978-3-030-13442-6>
- Delavy, F. P., Figueiredo, A.G., Abuchacra, R.C., Galvao, A., MacArio, K.C.D., 2016. Mapping of gas charged sediments in Guanabara Bay: Seismic characteristics and sediment properties. 2015 IEEE/OES Acoustics in Underwater Geosciences Symposium, RIO Acoustics 2015. <https://doi.org/10.1109/RIOAcoustics.2015.7473640>
- Delavy, Francielli Paula, Figueiredo Jr, A.G. de, Martins, M.V.A., Rodrigues, R., Pereira, E., Brito, M.A.R. de C. e, Fonseca, M.C.M. da, Laut, L.L.M., Bergamaschi, S., Miranda, P., Rodrigues, M.A.D.C., 2016. High-Resolution Acoustic Mapping of Gas Charged Sediments and Living Benthic Foraminifera Assemblages From the Ne Region of the Guanabara Bay (Rj, Brazil). *Journal of Sedimentary Environments* 1, 360–384. <https://doi.org/10.12957/jse.2016.26281>
- Diez, R., García-Gil, S., Durán, R., Vilas, F., 2007. Gas accumulations and their association with particle size distribution patterns in the Ría de Arousa seabed (Galicia, NW Spain): An application of discriminant analysis. *Geo-Marine Letters* 27, 89–102. <https://doi.org/10.1007/s00367-007-0064-4>

- Dimitrov, L., 2002. Contribution to atmospheric methane by natural seepages on the Bulgarian continental shelf. *Continental Shelf Research* 22, 2429–2442. [https://doi.org/10.1016/S0278-4343\(02\)00055-9](https://doi.org/10.1016/S0278-4343(02)00055-9)
- Eckard, T.L., 1986. *Stratigraphy and Depositional History of the Santee River Delta, SC*. University of South Carolina, Columbia.
- Egger, M., Riedinger, N., Mogollón, J.M., Jørgensen, B.B., 2018. Global diffusive fluxes of methane in marine sediments. *Nat Geosci* 11, 421–425. <https://doi.org/10.1038/s41561-018-0122-8>
- Emery, K.O., Hoggan, D., 1958. Gases in marine sediments. *AAPG Bulletin* 42, 2174–2188.
- Etiopé, G., Schoell, M., 2014. Abiotic gas: Atypical, but not rare. *Elements* 10, 291–296. <https://doi.org/10.2113/gselements.10.4.291>
- Felix, C.A., Mahiques, M.M., 2013. Late quaternary evolution and shallow gas formation in a tropical estuarine environment: The case of the Bertioga channel, Brazil. 2013 IEEE/OES Acoustics in Underwater Geosciences Symposium, RIO Acoustics 2013. <https://doi.org/10.1109/RIOAcoustics.2013.6684003>
- Fenchel, T., Bernard, C., Esteban, G., Finlay, B.J., Hansen, P.J., Iversen, N., 1995. Microbial diversity and activity in a danish fjord with anoxic deep water. *Ophelia* 43, 45–100. <https://doi.org/10.1080/00785326.1995.10430576>
- Floodgate, G.D., Judd, A.G., 1992. The origins of shallow gas. *Continental Shelf Research* 12, 1145–1156. [https://doi.org/10.1016/0278-4343\(92\)90075-U](https://doi.org/10.1016/0278-4343(92)90075-U)
- Flury, S., Glud, R.N., Premke, K., McGinnis, D.F., 2015. Effect of Sediment Gas Voids and Ebullition on Benthic Solute Exchange. *Environ Sci Technol* 49, 10413–10420. <https://doi.org/10.1021/acs.est.5b01967>
- Flury, S., Røy, H., Dale, A.W., Fossing, H., Tóth, Z., Spiess, V., Jensen, J.B., Jørgensen, B.B., 2016. Controls on subsurface methane fluxes and shallow gas formation in Baltic Sea sediment (Aarhus Bay, Denmark). *Geochim Cosmochim Acta* 188, 297–309. <https://doi.org/10.1016/j.gca.2016.05.037>
- Frazão, E., Vital, H., 2007. Estruturas rasas de gás em sedimentos no estuário Potengi (nordeste do Brasil). *Revista Brasileira de Geofísica* 25, 17–26.
- Gang, Z.Y., Jiang, C.H., 1985. Concepts on the generation and accumulation of biogenic gas. *Journal of Petroleum Geology* 8, 405–422. <https://doi.org/10.1111/j.1747-5457.1985.tb00281.x>
- García-García, A., Orange, D.L., Miserocchi, S., Correggiari, A., Langone, L., Lorenson, T.D., Trincardi, F., Nittrouer, C.A., 2007. What controls the distribution of shallow gas in the Western Adriatic Sea? *Cont Shelf Res* 27, 359–374. <https://doi.org/10.1016/j.csr.2006.11.003>
- García-Gil, S., de Blas, E., Martínez-Carreño, N., Iglesias, J., Rial-Otero, R., Simal-Gándara, J., Judd, A.G., 2011. Characterisation and preliminary quantification of the methane reservoir in a coastal sedimentary source: San Simón Bay, Ría de Vigo, NW Spain. *Estuar Coast Shelf Sci* 91, 232–242. <https://doi.org/10.1016/j.ecss.2010.10.038>

- Garcia-Gil, S., Vilas, F., Garcia-Garcia, A., 2002. Shallow gas features in incised-valley fills (Ría de Vigo, NW Spain): A case study. *Cont Shelf Res* 22, 2303–2315. [https://doi.org/10.1016/S0278-4343\(02\)00057-2](https://doi.org/10.1016/S0278-4343(02)00057-2)
- Geyer, W.R., 1993. The Importance of Suppression of Turbulence by Stratification on the Estuarine Turbidity Maximum.
- Giosan, L., Flood, R.D., Aller, R.C., 2002. Paleooceanographic significance of sediment color on western North Atlantic drifts: I. Origin of color. *Mar Geol* 189, 25–41.
- Gorgas, T.J., Kim, G.Y., Park, S.C., Wilkens, R.H., Kim, D.C., Lee, G.H., Seo, Y.K., 2003. Evidence for gassy sediments on the inner shelf of SE Korea from geoacoustic properties. *Cont Shelf Res* 23, 821–834. [https://doi.org/10.1016/S0278-4343\(03\)00026-8](https://doi.org/10.1016/S0278-4343(03)00026-8)
- Grasset, C., Moras, S., Isidorova, A., Couture, R.M., Linkhorst, A., Sobek, S., 2021. An empirical model to predict methane production in inland water sediment from particular organic matter supply and reactivity. *Limnol Oceanogr* 66, 3643–3655. <https://doi.org/10.1002/lno.11905>
- Gurgatz, B.M., Garcia, M.R., Cabral, A.C., de Souza, A.C., Nagai, R.H., Figueira, R.C.L., de Mahiques, M.M., Martins, C.C., 2023. Polycyclic aromatic hydrocarbons in a Natural Heritage Estuary influenced by anthropogenic activities in the South Atlantic: Integrating multiple source apportionment approaches. *Mar Pollut Bull* 188, 114678. <https://doi.org/10.1016/j.marpolbul.2023.114678>
- Haeckel, M., Boudreau, B.P., Wallmann, K., 2007. Bubble-induced porewater mixing: A 3-D model for deep porewater irrigation. *Geochim Cosmochim Acta* 71, 5135–5154. <https://doi.org/10.1016/j.gca.2007.08.011>
- Hamilton, E., 1971. Prediction of in-situ acoustic and elastic properties of marine sediments. *Geophysics* 36, 266–285.
- Hockensmith, B.L., 2004. Flow and salinity characteristics of the Santee River Estuary, South Carolina - Water resources report 35, South Carolina Department of Natural Resources. Land, Water and Conservation Division, South Carolina Department of Natural Resources.
- Horsfield, B., Rullkotter, J., 1994. Diagenesis, catagenesis, and metagenesis of organic matter. The petroleum system - from source to trap 189–199. https://doi.org/10.1007/978-3-642-96446-6_6
- Hughes, W.B., Abrahamsen, T.A., Maluk, T.L., Reuber, E.J., Wilhelm, L.J., 1995. Water Quality in the Santee River Basin and Coastal Drainages. U.S. Department of the Interior, U.S. Geological Survey Circular 1206, 1–40.
- Hughes, Z.J., 2010. Tidal channels on tidal flats and marshes, in: *Principles of Tidal Sedimentology*. Springer Netherlands, pp. 269–300. https://doi.org/10.1007/978-94-007-0123-6_11
- Hughes, Z.J., FitzGerald, D.M., Wilson, C.A., Pennings, S.C., Wiçski, K., Mahadevan, A., 2009. Rapid headward erosion of marsh creeks in response to relative sea level rise. *Geophys Res Lett* 36. <https://doi.org/10.1029/2008GL036000>

- Iglesias, J., García-gil, S., 2007. High-resolution mapping of shallow gas accumulations and gas seeps in San Simón Bay (Ría de Vigo , NW Spain). Some quantitative data 103–114. <https://doi.org/10.1007/s00367-007-0065-3>
- Jacques, C., Gkritzalis, T., Tison, J.L., Hartley, T., van der Veen, C., Röckmann, T., Middelburg, J.J., Cattrijsse, A., Egger, M., Dehairs, F., Sapart, C.J., 2021. Carbon and Hydrogen Isotope Signatures of Dissolved Methane in the Scheldt Estuary. *Estuaries and Coasts* 44, 137–146. <https://doi.org/10.1007/s12237-020-00768-3>
- Jaśniewicz, D., Klusek, Z., Brodecka-Goluch, A., Bolałek, J., 2019. Acoustic investigations of shallow gas in the southern Baltic Sea (Polish Exclusive Economic Zone): a review. *Geo-Marine Letters* 39, 1–17. <https://doi.org/10.1007/s00367-018-0555-5>
- Jensen, J.B., Bennike, O., 2009. Geological setting as background for methane distribution in Holocene mud deposits, Århus Bay, Denmark. *Cont Shelf Res* 29, 775–784. <https://doi.org/10.1016/j.csr.2008.08.007>
- Judd, A., Davies, G., Wilson, J., Holmes, R., Baron, G., Bryden, I., 1997. Erratum: Contributions to atmospheric methane by natural seepages on the U.K. continental shelf (Marine Geology (1997) 137 165-189) PII: S0025322796000874). *Marine Geology* 140, 427–455. [https://doi.org/10.1016/S0025-3227\(97\)00067-4](https://doi.org/10.1016/S0025-3227(97)00067-4)
- Judd, A.G., Hovland, M., 1992. The evidence of shallow gas in marine sediments. *Cont Shelf Res* 12, 1081–1095. [https://doi.org/10.1016/0278-4343\(92\)90070-Z](https://doi.org/10.1016/0278-4343(92)90070-Z)
- Karisiddaiah, S.M., Veerayya, M., Vora, K.H., Wagle, B.G., 1993. Gas-charged sediments on the inner continental shelf off western India. *Marine Geology* 110, 143–152. [https://doi.org/10.1016/0025-3227\(93\)90110-H](https://doi.org/10.1016/0025-3227(93)90110-H)
- Khalil, M.A.K., Rasmussen, R.A., Shearer, M.J., Chen, Z.L., Yao, H., Yang, J., 1998. Emissions of methane, nitrous oxide, and other trace gases from rice fields in China. *Journal of Geophysical Research Atmospheres* 103, 25241–25250. <https://doi.org/10.1029/98JD01114>
- Kirschke, S., Bousquet, P., Ciais, P., Saunoy, M., Canadell, J.G., Dlugokencky, E.J., Bergamaschi, P., Bergmann, D., Blake, D.R., Bruhwiler, L., Cameron-Smith, P., Castaldi, S., Chevallier, F., Feng, L., Fraser, A., Heimann, M., Hodson, E.L., Houweling, S., Josse, B., Fraser, P.J., Krummel, P.B., Lamarque, J.F., Langenfelds, R.L., le Quéré, C., Naik, V., O’doherly, S., Palmer, P.I., Pison, I., Plummer, D., Poulter, B., Prinn, R.G., Rigby, M., Ringeval, B., Santini, M., Schmidt, M., Shindell, D.T., Simpson, I.J., Spahni, R., Steele, L.P., Strode, S.A., Sudo, K., Szopa, S., van der Werf, G.R., Voulgarakis, A., van Weele, M., Weiss, R.F., Williams, J.E., Zeng, G., 2013. Three decades of global methane sources and sinks. *Nat Geosci.* <https://doi.org/10.1038/ngeo1955>
- Klein, A.H. da F., Demarco, L.F.W., Guesser, V., Flemming, G.R., Bonetti, J., Porpilhó, D., Neto, A.A., Antonio, J., Souza, G. de, Félix, C.A., 2005. Shallow gas seismic structures: forms and distribution on Santa Catarina Island, Southern Brazil 64, 157–160.
- Knoppers, B.A., Brandini, F.P., Thamm, C.A., 1987. Ecological studies in the bay of Paranaguá. II. Some physical and chemical characteristics. *Nerítica* 2, 1987.

- Lamour, M., Soares, C.R., Carrilho, J., 2004. Mapas De Parâmetros Texturais De Sedimentos De Fundo Do Complexo Estuarino De Paranaguá – Pr Textural Parameters Maps of Bottom Sediments on Paranaguá Bay Complex – Pr 77–82.
- Lamour, M.R., Angulo, R.J., Soares, C.R., 2007. Bathymetrical Evolution of Critical Shoaling Sectors on Galheta Channel, Navigable Access to Paranaguá Bay, Brazil. *Journal of Coastal Research* 231, 49–58. <https://doi.org/10.2112/03-0063.1>
- Lana, P.C., Marone, E., Lopes, R.M., 2001. The Subtropical Estuarine Complex of Paranagua Bay , Brazil. *Ecological Studies* 144, 131–145.
- Lastras, G., Canals, M., Urgeles, R., Hughes-Clarke, J.E., Acosta, J., 2004. Shallow slides and pockmark swarms in the Eivissa Channel, western Mediterranean Sea. *Sedimentology* 51, 837–850. <https://doi.org/10.1111/j.1365-3091.2004.00654.x>
- Le Mer, J., Roger, P., 2001. Production, oxidation, emission and consumption of methane by soils: A review. *Eur J Soil Biol* 37, 25–50.
- Lee, G., Kim, D., Yoo, D., Yi, H., 2014. Stratigraphy of late Quaternary deposits using high resolution seismic profile in the southeastern Yellow Sea 1–16. <https://doi.org/10.1016/j.quaint.2014.07.023>
- Lee, G.H., Kim, D.C., Kim, H.J., Jou, H.T., Lee, Y.J., 2005. Shallow gas in the central part of the Korea Strait shelf mud off the southeastern coast of Korea. *Cont Shelf Res* 25, 2036–2052. <https://doi.org/10.1016/j.csr.2005.08.008>
- Lee, S.H., Chough, S.K., Back, G.G., Kim, Y.B., 2002. Chirp (2 ^ 7-kHz) echo characters of the South Korea Plateau , East Sea : styles of mass movement and sediment gravity flow. *Mar Geol* 184, 227–247.
- Lessa, G.C., Angulo, R.J., Giannini, P.C., A.D. Araújo, 2000. Stratigraphy and Holocene evolution of a regressive barrier in south Brazil. *Marine Geology* 165, 87–108. [https://doi.org/10.1016/S0025-3227\(99\)00130-9](https://doi.org/10.1016/S0025-3227(99)00130-9)
- Lessa, G.C., Marone, E., Meyers, S.R., 1998. Holocene stratigraphy in the Paranagua Bay estuary, Southern Brazil. *Journal of Sedimentary Research* 68, 1060–1076. <https://doi.org/10.1306/D426890A-2B26-11D7-8648000102C1865D>
- Lewis, K.E., 1979. Hampton, Initial Archeological Investigations at an Eighteenth Century Rice Plantation in the Santee Delta, South Carolina. Research Manuscript Series No.151, Research Manuscript Series Archaeology and Anthropology. University of South Carolina.
- Li, Y., Zhan, L., Chen, L., Zhang, J., Wu, M., Liu, J., 2021. Spatial and temporal patterns of methane and its influencing factors in the Jiulong River estuary, southeastern China. *Mar Chem* 228. <https://doi.org/10.1016/j.marchem.2020.103909>
- Littke, R., Cramer, B., Gerling, P., Lopatin, N. V., Poelchau, H.S., Schaefer, R.G., Welte, D.H., 1999. Gas generation and accumulation in the West Siberian basin. *AAPG Bulletin* 83, 1642–1665. <https://doi.org/10.1306/e4fd4233-1732-11d7-8645000102c1865d>

- Liu, L., Wilkinson, J., Koca, K., Buchmann, C., Lorke, A., 2016. The role of sediment structure in gas bubble storage and release. *J Geophys Res Biogeosci* 121, 1992–2005. <https://doi.org/10.1002/2016JG003456>
- Lodolo, E., Baradello, L., Darbo, A., Caffau, M., Tassone, A., Lippai, H., Lodolo, A., De Zorzi, G., Grossi, M., 2012. Occurrence of shallow gas in the easternmost Lago Fagnano (Tierra del Fuego). *Near Surface Geophysics* 10, 161–169. <https://doi.org/10.3997/1873-0604.2011040>
- Lohrberg, A., Schmale, O., Ostrovsky, I., Niemann, H., Held, P., Schneider von Deimling, J., 2020. Discovery and quantification of a widespread methane ebullition event in a coastal inlet (Baltic Sea) using a novel sonar strategy. *Sci Rep* 10. <https://doi.org/10.1038/s41598-020-60283-0>
- Long, J.H., 2020. Studies of Quaternary Depositional Systems of the Coastal Plain and Inner Continental Shelf along the Georgia Bight: South Carolina and Georgia, U.S.A. Coastal Carolina University, Conway.
- Loyd, S.J., Berelson, W.M., Lyons, T.W., Hammond, D.E., Corsetti, F.A., 2012. Constraining pathways of microbial mediation for carbonate concretions of the Miocene Monterey Formation using carbonate-associated sulfate. *Geochim Cosmochim Acta* 78, 77–98. <https://doi.org/10.1016/j.gca.2011.11.028>
- Maher, D.T., Cowley, K., Santos, I.R., Macklin, P., Eyre, B.D., 2015. Methane and carbon dioxide dynamics in a subtropical estuary over a diel cycle: Insights from automated in situ radioactive and stable isotope measurements. *Mar Chem* 168, 69–79. <https://doi.org/10.1016/j.marchem.2014.10.017>
- Marani, L., Alvalá, P.C., 2007. Methane emissions from lakes and floodplains in Pantanal, Brazil. *Atmos Environ* 41, 1627–1633. <https://doi.org/10.1016/j.atmosenv.2006.10.046>
- Martens, C.S., Albert, D.B., Alperin, M.J., 1998. Biogeochemical processes controlling methane in gassy coastal sediments-Part 1. A model coupling organic matter flux to gas production, oxidation and transport. *Cont Shelf Res* 18, 1741–1770.
- Martins, C., Doumer, M.E., Gallice, W.C., Lúcia, A., Dauner, L., Caroline, A., Cardoso, F.D., Dolci, N.N., Camargo, L.M., Ferreira, P.A.L., Figueira, R.C.L., Mangrich, A.S., 2015. Coupling spectroscopic and chromatographic techniques for evaluation of the depositional history of hydrocarbons in a subtropical estuary. *Environmental Pollution journal* 205, 403–414. <https://doi.org/10.1016/j.envpol.2015.07.016>
- Matoušů, A., Osudar, R., Šimek, K., Bussmann, I., 2017. Methane distribution and methane oxidation in the water column of the Elbe estuary, Germany. *Aquat Sci* 79, 443–458. <https://doi.org/10.1007/s00027-016-0509-9>
- Mayerle, R., Narayanan, R., Etri, T., Abd Wahab, A.K., 2015. A case study of sediment transport in the Paranagua Estuary Complex in Brazil. *Ocean Engineering* 106, 161–174. <https://doi.org/10.1016/j.oceaneng.2015.06.025>
- McCarney-Castle, K., Voulgaris, G., Kettner, A.J., 2010. Analysis of fluvial suspended sediment load contribution through anthropocene history to the South Atlantic Bight Coastal Zone, U.S.A. *Journal of Geology* 118, 399–416. <https://doi.org/10.1086/652658>

- Meister, P., Liu, B., Ferdelman, T.G., Jørgensen, B.B., Khalili, A., 2013. Control of sulphate and methane distributions in marine sediments by organic matter reactivity. *Geochim Cosmochim Acta* 104, 183–193. <https://doi.org/10.1016/j.gca.2012.11.011>
- Merckelbach, L.M., Kranenburg, C., 2004. Determining effective stress and permeability equations for soft mud from simple laboratory experiments. *Géotechnique* 54, 581–591. <https://doi.org/10.1680/geot.54.9.581.56940>
- Migliarese, J. v., Sandifer, P.A., 1982. An ecological characterization of South Carolina wetland impoundments. Charleston.
- Missiaen, T., Murphy, S., Loncke, L., Henriët, J.P., 2002. Very high-resolution seismic mapping of shallow gas in the Belgian coastal zone. *Cont Shelf Res* 22, 2291–2301. [https://doi.org/10.1016/S0278-4343\(02\)00056-0](https://doi.org/10.1016/S0278-4343(02)00056-0)
- Myllykangas, J.P., Hietanen, S., Jilbert, T., 2020. Legacy Effects of Eutrophication on Modern Methane Dynamics in a Boreal Estuary. *Estuaries and Coasts* 43, 189–206. <https://doi.org/10.1007/s12237-019-00677-0>
- Nikaido, M., 1977. On the relation between methane production and sulfate reduction in bottom muds containing sea water sulfate. *Geochemical Journal* 11, 199–206. <https://doi.org/10.2343/geochemj.11.199>
- Noernberg, M., Lautert, L., Araújo, A., Marone, E., Angelotti, R., Netto Jr, J., Krug, L., 2006. Remote sensing and GIS integration for modelling the Paranaguá estuarine complex-Brazil. *J Coast Res* 1627–1631.
- Noernberg, M.A., 2002. Processos morfodinâmicos no complexo estuarino de paranaguá-pr, brasil: um estudo a partir de dados “in situ” e landsat-tm. *Boletim Paranaense de Geociências* 51, 142. <https://doi.org/10.5380/geo.v51i0.4190>
- Noernberg, M.A., 2001. Processos Morfodinâmicos No Complexo Estuarino De Paranaguá-Pr, Brasil: Um Estudo a Partir De Dados “in Situ” E Landsat-Tm. Universidade Federal do Paraná. <https://doi.org/10.5380/geo.v51i0.4190>
- Nooraiepour, M., Mondol, N.H., Hellevang, H., 2019. Permeability and physical properties of semi-compacted fine-grained sediments – A laboratory study to constrain mudstone compaction trends. *Marine and Petroleum Geology* 102, 590–603. <https://doi.org/10.1016/j.marpetgeo.2019.01.019>
- Okyar, M., Ediger, V., 1999. Seismic evidence of shallow gas in the sediment on the shelf off Trabzon, southeastern Black Sea. *Continental Shelf Research* 19, 575–587. [https://doi.org/10.1016/S0278-4343\(98\)00111-3](https://doi.org/10.1016/S0278-4343(98)00111-3)
- Paladino, Í.M., Mengatto, M.F., Mahiques, M.M., Noernberg, M.A., Nagai, R.H., 2022. End-member modeling and sediment trend analysis as tools for sedimentary processes inference in a subtropical estuary. *Estuar Coast Shelf Sci* 278. <https://doi.org/10.1016/j.ecss.2022.108126>
- Pantin, H.M., 1969. The appearance and origin of colours in muddy marine sediments around New Zealand. *New Zealand Journal of Geology and Geophysics* 12, 51–66. <https://doi.org/10.1080/00288306.1969.10420226>

- Payne, M.W., 1970. *Geomorphology and Sediments of the Santee Delta*. University of South Carolina, Columbia.
- Pezza Andrade, J.F., Noernberg, M.A., Nagai, R.H., 2021a. Shallow gas high-resolution seismic signatures in a subtropical estuary. *Geo-Marine Letters* 41. <https://doi.org/10.1007/s00367-021-00705-8>
- Pezza Andrade, J.F., Noernberg, M.A., Nagai, R.H., 2021b. Shallow gas high-resolution seismic signatures in a subtropical estuary. *Geo-Marine Letters* 41. <https://doi.org/10.1007/s00367-021-00705-8>
- Rao, G.D., Sarma, V.V.S.S., 2016. Variability in Concentrations and Fluxes of Methane in the Indian Estuaries. *Estuaries and Coasts* 39, 1639–1650. <https://doi.org/10.1007/s12237-016-0112-2>
- Raymond, P.A., Cole, J.J., 2001. Technical Notes and Comments Gas Exchange in Rivers and Estuaries: Choosing a Gas Transfer Velocity, *Estuarine Research Federation Estuaries*.
- Reeburgh, W.S., 2007. Oceanic methane biogeochemistry. *Chem Rev.* <https://doi.org/10.1021/cr050362v>
- Ribeiro, C.G., Berenice, M., Steffens, R., Etto, R.M., Galvão, C.W., De, C., Martins, C., de Oliveira Pedrosa, F., Kolm, H.E., 2013. Ardra Profiles Of Bacteria And Archaea In Mangrove Sediments With Different Levels Of Contamination In The Estuarine Complex Of Paranaguá, Brazil. *Arch. Biol. Technol.* v 56, 275–281.
- Rice, D.D., Claypool, G.E., 1981. Generation, accumulation, and resource potential of biogenic gas. *American Association of Petroleum Geologists Bulletin* 65, 5–25. <https://doi.org/10.1306/2f919765-16ce-11d7-8645000102c1865d>
- Robert H. Meade, 1969. Landward Transport of Bottom Sediments in Estuaries of the Atlantic Coastal Plain. *SEPM Journal of Sedimentary Research* Vol. 39. <https://doi.org/10.1306/74D71C1C-2B21-11D7-8648000102C1865D>
- Rogers, J.N., Kelley, J.T., Belknap, D.F., Gontz, A., Barnhardt, W.A., 2006. Shallow-water pockmark formation in temperate estuaries: A consideration of origins in the western gulf of Maine with special focus on Belfast Bay. *Mar Geol* 225, 45–62. <https://doi.org/10.1016/j.margeo.2005.07.011>
- Rooney, M.A., Claypool, G.E., Moses Chung, H., 1995. Modeling thermogenic gas generation using carbon isotope ratios of natural gas hydrocarbons. *Chem Geol* 126, 219–232. [https://doi.org/10.1016/0009-2541\(95\)00119-0](https://doi.org/10.1016/0009-2541(95)00119-0)
- Rosentreter, J.A., Borges, A. v., Deemer, B.R., Holgerson, M.A., Liu, S., Song, C., Melack, J., Raymond, P.A., Duarte, C.M., Allen, G.H., Olefeldt, D., Poulter, B., Battin, T.I., Eyre, B.D., 2021. Half of global methane emissions come from highly variable aquatic ecosystem sources. *Nat Geosci* 14, 225–230. <https://doi.org/10.1038/s41561-021-00715-2>
- Rosentreter, J.A., Maher, D.T., Erler, D. v., Murray, R., Eyre, B.D., 2018. Factors controlling seasonal CO₂ and CH₄ emissions in three tropical mangrove-dominated estuaries in Australia. *Estuar Coast Shelf Sci* 215, 69–82. <https://doi.org/10.1016/j.ecss.2018.10.003>

- Sansone, F.J., Rust, T.M., Smith, S. V, 1998. Methane Distribution and Cycling in Tomales Bay, California 1. *Estuaries* 21, 66–77.
- Sass, R.L., Fisher, F.M., Wang, Y.B., Turner, F.T., Jund, M.F., 1992. METHANE EMISSION FROM RICE FIELDS: THE EFFECT OF FLOODWATER MANAGEMENT, GLOBAL BIOGEOCHEMICAL CYCLES.
- Sawicka, J.E., Brüchert, V., 2017a. Annual variability and regulation of methane and sulfate fluxes in Baltic Sea estuarine sediments. *Biogeosciences* 14, 325–339. <https://doi.org/10.5194/bg-14-325-2017>
- Sawicka, J.E., Brüchert, V., 2017b. Annual variability and regulation of methane and sulfate fluxes in Baltic Sea estuarine sediments. *Biogeosciences* 14, 325–339. <https://doi.org/10.5194/bg-14-325-2017>
- Schoell, M., 1988. Multiple origins of methane in the Earth. *Chemical Geology* 71, 1–10. [https://doi.org/10.1016/0009-2541\(88\)90101-5](https://doi.org/10.1016/0009-2541(88)90101-5)
- Schubel, J.R., 1974. Gas bubbles and the acoustically impene- trable, or turbid, character of some estuarine sediments, in: Kaplan, I.R. (Ed.) (Ed.), *Marine Science*. Plenum Press, New York, pp. 275–298.
- Serra, M.C.C., Pessoa, F.L.P., Palavra, A.M.F., 2006. Solubility of methane in water and in a medium for the cultivation of methanotrophs bacteria. *Journal of Chemical Thermodynamics* 38, 1629–1633. <https://doi.org/10.1016/j.jct.2006.03.019>
- Settlemyre, J.L., Gardner, L.R., 1977. Suspended Sediment Flux Through a Salt Marsh Drainage Basin.
- Sobek, S., Delsontro, T., Wongfun, N., Wehrli, B., 2012. Extreme organic carbon burial fuels intense methane bubbling in a temperate reservoir. *Geophys Res Lett* 39. <https://doi.org/10.1029/2011GL050144>
- Song, H., Liu, X., 2016. Anthropogenic Effects on Fluxes of Ecosystem Respiration and Methane in the Yellow River Estuary, China. *Wetlands* 36, 113–123. <https://doi.org/10.1007/s13157-014-0587-1>
- Stocker, T.F., Qin, D., Plattner, G.K., Tignor, M.M.B., Allen, S.K., Boschung, J., Nauels, A., Xia, Y., Bex, V., Midgley, P.M., 2013. *Climate change 2013 the physical science basis: Working Group I contribution to the fifth assessment report of the intergovernmental panel on climate change*, *Climate Change 2013 the Physical Science Basis: Working Group I Contribution to the Fifth Assessment Report of the Intergovernmental Panel on Climate Change*. Cambridge University Press. <https://doi.org/10.1017/CBO9781107415324>
- Stranne, C., O’regan, M., Jakobsson, M., Brüchert, V., Ketzer, M., 2019. Can anaerobic oxidation of methane prevent seafloor gas escape in a warming climate? *Solid Earth Discussion*. <https://doi.org/10.5194/se-2019-50>
- Sturm, K., Grinham, A., Werner, U., Yuan, Z., 2016. Sources and sinks of methane and nitrous oxide in the subtropical Brisbane River estuary, South East Queensland, Australia. *Estuar Coast Shelf Sci* 168, 10–21. <https://doi.org/10.1016/j.ecss.2015.11.002>

- Taylor, D.I., 1992. Nearshore shallow gas around the U.K. coast. *Cont Shelf Res* 12, 1135–1144. [https://doi.org/10.1016/0278-4343\(92\)90074-T](https://doi.org/10.1016/0278-4343(92)90074-T)
- Thang, N.M., Brüchert, V., Formolo, M., Wegener, G., Ginters, L., Jørgensen, B.B., Ferdelman, T.G., 2013. The Impact of Sediment and Carbon Fluxes on the Biogeochemistry of Methane and Sulfur in Littoral Baltic Sea Sediments (Himmerfjärden, Sweden). *Estuaries and Coasts* 36, 98–115. <https://doi.org/10.1007/s12237-012-9557-0>
- Thießen, O., Schmidt, M., Theilen, F., Schmitt, M., Klein, G., 2006. Methane formation and distribution of acoustic turbidity in organic-rich surface sediments in the Arkona Basin, Baltic Sea. *Cont Shelf Res* 26, 2469–2483. <https://doi.org/10.1016/j.csr.2006.07.020>
- Torres, R., 2017. Channel geomorphology along the fluvial-tidal transition, Santee River, USA. *GSA Bulletin*. <https://doi.org/10.1130/b31649.1>
- Torres-Alvarado, M.D.R., Fernández, F.J., Ramírez Vives, F., Varona-Cordero, F., 2013. Dynamics of the methanogenic archaea in tropical estuarine sediments. *Archaea* 2013, 1–13. <https://doi.org/10.1155/2013/582646>
- Tóth, Z., Spieß, V., Jensen, J.B., 2014. Seismo-acoustic signatures of shallow free gas in the Bornholm Basin, Baltic Sea. *Cont Shelf Res* 88, 228–239. <https://doi.org/10.1016/j.csr.2014.08.007>
- Treude, T., Krüger, M., Boetius, A., Jørgensen, B.B., 2005. Treude, Tina, Martin Krüger, Antje Boetius, and Bo Barker Jørgensen. Environmental control on anaerobic oxidation of methane in the gassy sediments of Eckernförde Bay (German Baltic). *Limnol. Oceanogr* 50, 1771–1786.
- Upstill-Goddard, R.C., Barnes, J., 2016. Methane emissions from UK estuaries: Re-evaluating the estuarine source of tropospheric methane from Europe. *Mar Chem* 180, 14–23. <https://doi.org/10.1016/j.marchem.2016.01.010>
- Valentine, D.L., Chidthaisong, A., Rice, A., Reeburgh, W.S., Tyler, S.C., 2004. Carbon and hydrogen isotope fractionation by moderately thermophilic methanogens. *Geochim Cosmochim Acta* 68, 1571–1590. <https://doi.org/10.1016/j.gca.2003.10.012>
- Vardar, D., Alpar, B., 2016. High-resolution seismic characterization of shallow gas accumulations in the southern shelf of Marmara Sea, Turkey. *Acta Geophysica* 64, 589–609. <https://doi.org/10.1515/acgeo-2015-0059>
- Visnovitz, F., Bodnár, T., Tóth, Z., Spiess, V., Kudó, I., Timár, G., Horváth, F., 2015. Seismic expressions of shallow gas in the lacustrine deposits of Lake Balaton, Hungary. *Near Surface Geophysics* 13, 433–446. <https://doi.org/10.3997/1873-0604.2015026>
- Wallenius, A.J., Dalcin Martins, P., Slomp, C.P., Jetten, M.S.M., 2021. Anthropogenic and Environmental Constraints on the Microbial Methane Cycle in Coastal Sediments. *Front Microbiol*. <https://doi.org/10.3389/fmicb.2021.631621>
- Wang, F., Ding, J., Tao, C., Lin, X., 2021. Sound velocity characteristics of unconsolidated sediment based on high-resolution sub-bottom profiles in Jinzhou Bay, Bohai Sea of China. *Cont Shelf Res* 217. <https://doi.org/10.1016/j.csr.2021.104367>

- Wang, Q., An, S.Q., Ma, Z.J., Zhao, B., Chen, J.K., Li, B., 2006. Invasive *Spartina alterniflora*: Biology, ecology and management. *Acta Phytotaxonomica Sinica* 44, 559–588. <https://doi.org/10.1360/aps06044>
- Weber, T., Wiseman, N.A., Kock, A., 2019. Global ocean methane emissions dominated by shallow coastal waters. *Nat Commun* 10. <https://doi.org/10.1038/s41467-019-12541-7>
- Weems, R.£, Lewis, W.C., 1997. Detailed Geologic Sections from Auger Holes in Northeastern Charleston County, South Carolina, east of 79° 45' West Longitude. Openfile Report 97-712-A. Reston, VA.
- Wells, N.S., Chen, J.J., Maher, D.T., Huang, P., Erler, D. v., Hipsey, M., Eyre, B.D., 2020. Changing sediment and surface water processes increase CH₄ emissions from human-impacted estuaries. *Geochim Cosmochim Acta* 280, 130–147. <https://doi.org/10.1016/j.gca.2020.04.020>
- Weschenfelder, J., Corrêa, I.C.S., 2018. Shallow gas features and distribution in the patos lagoon: A coastal trap for gas-generator sediments. *Pesquisas em Geociencias* 45. <https://doi.org/10.22456/1807-9806.91385>
- Weschenfelder, J., Klein, A.H.F., Green, A.N., Aliotta, S., de Mahiques, M.M., Ayres Neto, A., Terra, L.C., Corrêa, I.C.S., Calliari, L.J., Montoya, I., Ginsberg, S.S., Griep, G.H., 2016. The control of palaeo-topography in the preservation of shallow gas accumulation: Examples from Brazil, Argentina and South Africa. *Estuar Coast Shelf Sci* 172, 93–107. <https://doi.org/10.1016/j.ecss.2016.02.005>
- West, W.E., Coloso, J.J., Jones, S.E., 2012. Effects of algal and terrestrial carbon on methane production rates and methanogen community structure in a temperate lake sediment. *Freshw Biol* 57, 949–955. <https://doi.org/10.1111/j.1365-2427.2012.02755.x>
- Whelan, T., Coleman, J.M., Suhayda, J.N., Roberts, H.H., 1977. Acoustical penetration and shear strength in gas-charged sediment. *Marine Geotechnology* 2, 147–159. <https://doi.org/10.1080/10641197709379776>
- Wiesenburg, D.A., Guinasso, N.L., 1979. Equilibrium Solubilities of Methane, Carbon Monoxide, and Hydrogen in Water and Sea Water. *J Chem Eng Data* 24, 356–360.
- Wilhelm, E., Battino, R., Wilcock', R.J., 1977. Low-Pressure Solubility of Gases in Liquid Water. *Chemical Review* 77, 219–262.
- Wilson, C.A., Hughes, Z.J., FitzGerald, D.M., 2012. The effects of crab bioturbation on Mid-Atlantic saltmarsh tidal creek extension: Geotechnical and geochemical changes. *Estuar Coast Shelf Sci* 106, 33–44. <https://doi.org/10.1016/j.ecss.2012.04.019>
- Yamamoto, S., Alcauskas, J.B., Crozie, T.E., 1976. Solubility of Methane in Distilled Water and Seawater. *J Chem Eng Data* 21, 78–80.
- Ye, W., Zhang, G., Zheng, W., Zhang, H., Wu, Y., 2019. Methane distributions and sea-to-air fluxes in the Pearl River Estuary and the northern South China sea. *Deep Sea Res 2 Top Stud Oceanogr* 167, 34–45. <https://doi.org/10.1016/j.dsr2.2019.06.016>

- Zander, F., Heimovaara, T., Gebert, J., 2020. Spatial variability of organic matter degradability in tidal Elbe sediments. *J Soils Sediments* 20, 2573–2587. <https://doi.org/10.1007/s11368-020-02569-4>
- Zeikus, J.G., 1977. The biology of methanogenic bacteria. *Bacteriological Reviews* 41, 514–541. <https://doi.org/10.1128/membr.41.2.514-541.1977>
- Zem, R.C., Patchineelam, S.M., Guerra, J.V., 2007. Fluxos residuais de material particulado em suspensão na Zona de Máxima Turbidez da Baía de Paranaguá, Paraná. Residual fluxes of suspended particulate matter in the turbidity maximum zone of Paranaguá Bay, Paraná, in: Associação Brasileira de Estudos Do Quaternário (ABEQUA).
- Zhang, G., Zhang, J., Liu, S., Ren, J., Xu, J., Zhang, F., 2008. Methane in the Changjiang (Yangtze River) Estuary and its adjacent marine area: Riverine input, sediment release and atmospheric fluxes. *Biogeochemistry* 91, 71–84. <https://doi.org/10.1007/s10533-008-9259-7>
- Zhang, J., 2011. Pore pressure prediction from well logs: Methods, modifications, and new approaches. *Earth Sci Rev.* <https://doi.org/10.1016/j.earscirev.2011.06.001>
- Zhang, X., Lin, C.M., 2017. Characteristics and accumulation model of the late Quaternary shallow biogenic gas in the modern Changjiang delta area, eastern China. *Pet Sci* 14, 261–275. <https://doi.org/10.1007/s12182-017-0157-2>
- Zhou, Y., Wojtanowicz, A.K., Li, X., Miao, Y., Chen, Y., 2018. Improved model for gas migration velocity of stagnant non-Newtonian fluids in annulus. *Journal of Petroleum Science and Engineering* 168, 190–200. <https://doi.org/10.1016/j.petrol.2018.05.025>